THE KINETICS OF LIME HYDRATION AND ITS CONTROL BY SUPERFICIAL RECARBONISATION

By

A. Maciel-Camacho

A THESIS SUBMITTED TO THE COUNCIL FOR NATIONAL ACADEMIC AWARDS IN PARTIAL FULFILMENT OF THE REQUIREMENTS FOR THE DEGREE OF **DOCTOR OF PHILOSOPHY** AT SHEFFIELD CITY POLYTECHNIC IN COLLABORATION WITH BRITISH STEEL CORPORATION, SWINDEN LABORATORIES.

July 1991

ACKNOWLEDGEMENTS

The author would like to acknowledge Professor A W D Hills and Dr R Jackson for their constructive supervision and advice during the course of this research. The author wishes to express his gratitude to his industrial supervisor Dr D Engledow, from British Steel Corporation, Swinden Laboratories. Thanks are also expressed to all the technicians at Metals and Materials Department for their helpful suggestions and comments at various stages of this work. Especial thanks go to Mr. D Latimer for his friendship. I am grateful to the National Council of Science and Technology of México and the Technological Institute of Morelia for their financial support. Finally I would like to thank my wife Silvia for her patience and understanding through it all.

PREFACE

This thesis is submitted in part fulfilment of the requirements for the degree of **DOCTOR OF PHILOSOPHY** of the Council for National Academic Awards. The research was carried out during the period March 1988 to July 1991 at the Department of Metals and Materials Engineering, Sheffield City Polytechnic, in collaboration with British Steel Corporation, Swinden Laboratories.

Post-graduate courses were attended at Sheffield City Polytechnic during the above period on Process Metallurgy, Advanced Thermodynamics, Computational Methods and Numerical Analysis.

The Author attended two seminars on "Hydrogen in Steel" and "Control of Oxygen during Steelmaking Processes and Production of Ultra-clean Steel" at The Institute of Metals, London.

A. Maciel-Camacho.

July 1991.

KINETICS OF LIME HYDRATION AND ITS CONTROL BY SUPERFIAL RECARBONISATION

By

Arquimiro Maciel-Camacho

ABSTRACT

The hydration of calcium oxide and its control by superficial recarbonisation have been investigated by suspending a single pellet into an atmosphere of controlled humidity or carbon dioxide content for hydration and recarbonisation respectively. The reaction rate was monitored using a computer aided gravimetric method. The computerised system allowed the simultaneous measurement of the temperature and weight of a reacting pellet. It has been shown that the hydration reaction takes place on a sharp definite interface between the product layer and the unreacted core. A theoretical model for the hydration rate has been derived on the basis of the unreacted core model by introducing the effect due to the sample swelling.

The model was solved and compared to experimental results data. Quite reasonable values were obtained for the chemical reaction rate constant and the effective diffusion coefficient through the product shell. Results suggested that gas phase mass transfer, pore

diffusion, and chemical reaction were all contributing resistances in the model, that is, the process was under mixed control. On the other hand, the results obtained clearly indicate that the recarbonated film increases the hydration resistance of the lime core.

TABLE OF CONTENTS

NOMENCLATURE

A, A_1, A_2 = Constants

A = Surface area, $[m^2]$

A = Gaseous reactant.

A_o = Knudsen diffusion parameter

a = Activity.

B = Constant.

B = gaseous reactant.

B_o = Viscous flow parameter, [-]

C = Water capacity of the slag.

C = Constant defined in Eq.(6.1).

C_i = Concetration of species i, $[kmol.m^3]$.

C_j= Concentration of species j, $[kmol.m^{-3}]$

$C_{j,b}$= Concentration of j in the bulk gas, $[kmol.m^{-3}]$

$C_{j,o}$ = Concentration of j at the exterior surface of the solid, $[kmol.m^{-3}]$

$C_{j,i}$ = Concentration of j at the reaction front, $[kmol.m^3]$

C_o = Molecular diffusion parameter.

Cp = Molar specific heat of pellet, $[J.kg^{-1}.K^{-1}]$

D = Diffusion coefficient, $[m^2.s^{-1}]$.

D_e = Effective diffusion coefficient defined in Eqs.(6.12) and (6.14).

D_{ij} = Molecular binary diffusion coefficient, $[m^2.s^{-1}]$

$D_{ij,eff}$ = Effective molecular diffusion coefficient, $[m^2.s^{-1}]$

$D_{i,eff}$ = Effective combined diffusivity, $[m^2.s^{-1}]$

$D_{A,efl}$ = Effective diffusivity in the carbonated layer $[m^2.s^{-1}]$.

$D_{i,k}$ = Knudsen diffusion coefficient, $[m^2.s^{-1}]$

D_s = Interparticle diffusivity defined in Eq.(2.59).

e = Emissivity, [-]

e^- = Electron.

e_H^x = Interation parameter of hydration with a x element.

f = Relative reacted layer thickness , [-]

f_x = Activity coefficient of x element in the liquid steel.

H = Enthalpy, $[kJ.kmol^{-1}]$

h = Heat transfer coefficient, $[W.m^{-2}.K^{-1}]$

K = Equilibrium constant.

k = Boltzman constant, $[J.K^{-1}.kmol^{-1}]$

k = Constant defined in Eq.(2.49).

k = Liquid mass transfer coefficient, $[m.s^{-1}]$

k = Rate reaction constant, $[m.s^{-1}]$.

k_H = Mass transfer parameter defined by Eq.(2.18).

k_o = Knudsen flow parameter.

L = Pellet diameter, [m]

L_H = Hydrogen partition coefficient.

M = Molecular weight, $[kg.kmol^{-1}]$

m = mass, [kg]

$\dot{N}_i$ = Molar flux of solute i, $[kmol.m^{-2}.s^{-1}]$

$\dot{N}_k$ = Knudsen flux, $[kmol.m^{-2}.s^{-1}]$

$\dot{N}_{vis}$ = Viscous flux, $[kmol.m^{-2}.s^{-1}]$.

$\dot{n}_i$ = Molar flow rate of solute i, $[kmol.s^{-1}]$.

$\dot{n}_o$ = Initial flow rate, [kmol.s^{-1}].

n = gas concentration, [kmol.m^{-3}]

P = Total pressure, [Pa].

p = Partial pressure, [Pa]

$p_{A,b}$ = Partial pressure of species A in the bulk gas, [Pa]

$p_{A,e}$ = Partial pressure of species A at the equilibrium, [Pa].

$p_{A,i}$ = Partial pressure of species A at the reaction interface, [Pa].

$p_{A,o}$ = Partial pressure of species A at the exterior surface of the pellet, [Pa].

Q = Activation energy, [J.kmol^{-1}]

R = Universal gas constant, [J.kmol^{-1}.K^{-1}]

R = Grain radius, [m]

r = Radius, [m]

r_c = Unrecarbonated core radius, [m].

r_o = Pellet radius, [m].

r_o' = Modified pellet radius due to swelling, [m].

r_i = Radius of the unreacted core, [m]

r* = Normalized radius, [-]

S = Internal surface area, [m^2.kg^{-1}]

S = Shape factor, [m]

T = Temperature, [K]

t = Time, [s]

t_c = Time for complete reaction, [s].

t = Tonne, [10^{3}kg]

U = Linear velocity, $[m.s^{-1}]$

V = Volume, $[m^3]$

V = Voltage, [v]

v_M = Mass centre velocity, $[m.s^{-1}]$.

W = Mass of metal, [kg]

w = Probability factor.

X = Fraction mole.

X = Fractional hydration

X_{CaO} = Mass fraction of CaO in the CaO/Al_2O_3 mixture.

Y = Fractional recarbonisation.

GREEK LETTERS

α = Gas phase mass transfer coefficient, $[m.s^{-1}]$

β = Constant defined by Eq.(2.39).

γ = Constant defined by Eq.(2.37).

Γ = Rate of disappearance of gas reactant per mole of initial solid reactant.

Δ = Difference between values.

δ = Constant defined by Eq.(2.50).

δ = Thickness of the layer recarbonated, [m]

ϵ = Energy of interaction between molecules.

ϵ = Porosity, [-]

ϵ_o = Initial porosity, [-].

κ = Parameter diffined in Eq.(2.49).

μ = Viscosity, [Pa.s]

ν = Mean molecular velocity, [$m.s^{-1}$]

Φ = Swelling ratio, [-]

ρ = Density, [$kg.m^{-3}$]

ρ_s = Apparent molar density, [$kmol.m^{-3}$]

ρ_t = True density, [$kg.m^{-3}$]

σ = Collision diameter, [A]

σ = Stefan-Boltzman constant, [$W.m^{-2}.K^{-4}$]

τ = Tortuosity factor.

τ = Function defined in Eq.(6.4)

ψ = Parameter defined in Eq.(2.38), [-].

Ω = Collision integral, [-]

ω = Permiability of a gas through a porous solid, [$m^2.s^{-1}$]

SUBSCRIPT

A,B = Reactants.

b = In the gas bulk.

c = For complete reaction

D = Diffusive flow.

e = Equilibrium.

eff = Effective.

f = final.

g = gas.

H_2 = Hydrogen.

ij = Diffusing pair.

i = At the reaction interface.

i = Instantaneous.

i = Constituent i.

j = Constituent j.

k = Knudsen diffusion.

o = Initial

o = At the gas-solid interface.

s = solid.

s = steel.

s = molar

t = True

t = Total

u = Surrounding.

vis = Viscous flow.

SUPERSCRIPT

x = Any chemical element.

BRACKETS

{ } = Gaseous phase.

( ) = Dissolved in slag.

[ ] = Dissolved in steel.

[ ] = Concentration.

DIMENSIONLESS GROUPS

Nu = Nusselt number for heat transfer.

Pr = Prandtl number.

Re = Reynolds number.

Sc = Schmidt number.

Sh = Sherwood number.

1. INTRODUCTION

The increasing demand for better steel quality by the end users, in respect of cleanness, low gas content, narrow analytical range makes it necessary to develop new metallurgical technologies.

For many years steelmakers have studied methods of reducing the level of dissolved hydrogen in a variety of steel products. Dissolved hydrogen is particularly troublesome in heavy plates, rails and large forgings. In these cases, the steel must be largely free of hydrogen (< 2 ppm) before casting to avoid hydrogen assisted cracking or stress corrosion cracking in certain service environments.

Vacuum degassing and inert gas injection are two methods commonly employed to reduce the hydrogen level in liquid steel. At present, the possibility of using halide gases is being investigated with hopeful results [1]. Slow or controlled cooling of semifinished steel is used to reduce the hydrogen content in the solidified steel. However, slow cooling is not a panacea because it requires inventory management for long periods and can produce unpredictable results.

Vacuum degassing processes, such as DH, RH and RH-OB [2,3] can reduce the hydrogen content by half. The ferroalloys and other materials added in these processes introduce hydrogen to the liquid steel thus increasing the treatment time. Injection processes such as TN, LF and ASEA-SKF require large quantities of inert gas to achieve low hydrogen contents. These processes, largely used to desulphurise, deoxidise and for inclusion shape control, need large amounts of lime (10 kg/tonne) which can introduce hydrogen into the system though combined water of hydration. Owing to the metallurgical conditions prevailing the removal of this hydrogen is difficult. There is therefore need for a reliable method of controlling the moisture level in the lime, and in other slag making materials.

This thesis describes a study of the mechanism and kinetics of moisture absorption by lime and an examination of a method for increasing the hydration resistance of lime. If the concentration of water in flux making materials can be minimised by a method of this type, the inert gas consumption and the treatment time to achieve a particular hydrogen level will be decreased considerably.

The next chapter of this thesis presents a literature survey of the role played by moisture in lime and other slag making materials in causing detrimental hydrogen levels in

liquid steel, and of gaseous diffusion and reactions involving porous solids, particularly where they relate to the production and hydration of lime. The third chapter in the thesis describes the experimental techniques that have been developed for preparing lime pellets from calcium carbonate powder, as well as the experimental that have been developed to study hydration and depassivation of these lime pellets. The fourth chapter contains the experimental results and the fifth presents a theoretical model for the hydration of lime. The sixth chapter discusses the results and the last chapter presents the conclusions.

2. LITERATURE SURVEY.

2.1. INTRODUCTION.

The literature survey is centred on the main hydrogen sources during secondary steelmaking processes; the effect of hydrogen on the mechanical properties of steel; the transfer mechanism of gaseous phases through the metallic bath, and metallurgical problems related to the production of low hydrogen steels (below 1 ppm) particularly in secondary steelmaking processes which use great amounts of lime. The physical and chemical properties of lime and its ability to absorb moisture also are considered. Since the hydration of slagmaking materials is a gas-solid reaction, gas-solid reactions with particular emphasis on gaseous diffusion in reactions involving porous solids are also considered.

2.2. HYDROGEN IN STEEL

2.2.1. THE EFFECT OF HYDROGEN ON THE MECHANICAL PROPERTIES OF STEEL.

It is well known that hydrogen has a deleterious effect on the mechanical properties of steel; it can cause hairline cracking, shatter or flaking [4-6], especially in low alloy NiCr, NiCrMo, NiCrMoV steels [7]. A flake may be

defined as a tight crack formed by the combined action of hydrogen and stress. Flaking is common in large forgings. The simultaneous presence of hydrogen and stress provide the basic conditions conductive to hydrogen cracking and embrittlement.

For cracking to occur, the hydrogen must normally be concentrated at the embrittlement location such as a crack tip by diffusion. A number of mechanism have been suggested [8] to explain how hydrogen causes embrittlement: i) the pressure of recombined hydrogen acts with the applied stress to propagate the crack; ii) the precipitation of hydrogen on the crack surface lowers the surface energy of the crack; iii) the accumulation of hydrogen in front of the crack reduces the lattice strength.

It would appear that no one mechanism is correct to the exclusion of the others, and that each can be shown to operate under appropriate circumstances. It may suffice to say that each mechanism probably assists in hydrogen crack initiation and propagation [8].

The presence of hydrogen in steel decreases ductility, reduction in area, elongation, fracture toughness and fatigue resistance[8-10]. It would appear that hydrogen has little effect on mechanical properties in compression [11].

The development of linepipe steel resistant to sulphide

cracking has generated many studies in this area; the research was mainly concerned with hydrogen induced cracking in the absence of external stress (HIC). Over the past few years, however some guarantees of resistance to sulphide stress cracking (SSC) have been demanded by the consumers [4,12].

Charbonnier et al[13], reported that, when external stresses are low or nonexistent, (HIC), the initial crack direction is imposed by metallurgical factors, such as elongated inclusions. When the steel is free from inclusions and submitted to high external stress (SSC), initiation occurs in zones of high hardness, the crack direction depending only on the imposed stress field.

Combining metallographic observations and a simplified mechanical analysis, Charbonnier et al suggest that hydrogen embrittlement is governed by a critical normal stress and not by a critical shear stress as is the case in ductile fracture. Not only does this analysis explain the orientation of cracks around inclusions but also the orientation of secondary cracks in blistering, path changes when cracks interact and crack initiation in the absence of inclusions (SSC). The way in which fracture occurs depends on the amount of dissolved hydrogen.

Hydrogen is assumed to limit the shear processes and thus promote fracture by separation of atomic planes. Depending

on the combination between time dependent diffusional and mechanical parameters, the two modes of cracking HIC and SSC can operate simultaneously.

Charbonnier and his coworkers have also explained the influence of rolling conditions. The lower is the temperature at the end of rolling, the higher is the HIC susceptibility. This is because, the dislocation density is higher in this case so that the trapping of hydrogen is enhanced and the critical hydrogen concentration leading to cracking is more easily reached.

When external stress is applied in the longitudinal or transverse direction, the local plasticity of the metal governs the SSC resistance. The SSC resistance increases with the finishing temperature of rolling.

Coundreuse and Charles [14] reported that hydrogen induced cracking of steel occurs when the amount of hydrogen is greater than a critical concentration (Ck) and they reported values for Ck from 0.7 to 1.5 ppm. This Ck value depends on metallurgical parameters such as chemical composition, inclusions (number, distribution), segregation, and microstructure defects (dislocations, grain boundaries).

Other researchers [15-21] have reported that a number of defect sites interact significantly enough with hydrogen in ferrous alloys to act as traps under circumstances in which the material exhibits hydrogen-induced loss of ductility.

These sites include point defects, dislocations, interfaces and surfaces and volume defects. It is now well established that hydrogen embrittlement of steels correlates closely with hydrogen-defect interaction processes.

Steelmakers have understood the deleterious effects that hydrogen has upon the bulk properties of steel, and the costly solid state diffusion treatments which are required to avoid these effects. Manufacturers of steel have therefore been directed efforts towards more practical solutions such as reducing the hydrogen content of liquid steel.

2.2.2. SOURCES OF HYDROGEN IN STEELMAKING.

In all the reports analysed [22-31] it is possible to see that the main hydrogen sources are humidity in the air, water in the raw materials and in the refractories.

According to Zuliani et al [22] most hydrogen problems can be related to post-furnace operations which involve tapping and teeming steel through humid atmospheres; the use of improperly dried alloy additions, synthetic slag components and refractories; hydrocarbon lubricants and mould washes.

Pocklington et al [23] reported that large quantities of lime added, in order to achieve good desulphurization, are the major potential source of hydrogen pick-up. They recommend the preheating of ladle additions or the use of

sealable containers for the transport of lime directly to the plant, followed by careful storage prior to use.

Okamoto et al [24] concluded that the prevention of hydrogen absorption at each stage is as important as vacuum degassing in order to decrease hydrogen in molten steel. They reported that hydrogen absorption during tapping is 1.0 to 2.0 ppm in 50 kg/mm^2 grade steel to which large amount of ferro-alloys are added. Water adhering to the ferro-alloys and to the fluxes is considered to be the main factor for this. During Ca-Si treatment, hydrogen content increases considerably, more or less in proportion to the amount of burnt lime added to control the slag basicity. This is because of the water content of the burnt lime so that hydrogen absorption can be reduced by proper control of the lime after burning.

Riboud and Gatellier[25] reported that secondary steelmaking slags can dissolve appreciable quantities of water which can decrease the apparent overall efficiency of the vacuum treatment. When low hydrogen contents are aimed for, it is therefore essential to use clean additions before and after treatment.

Fruehan[26] reported that hydrogen is a major concern in the ladle treatment of steels. In these clean steels there are fewer inclusions on which hydrogen can accumulate, so that the hydrogen concentration in the inclusions that do exist may be high enough to cause the hydrogen induced cracking.

The ladle treatment itself, furthermore, can cause the hydrogen content to increase: typically the hydrogen content will increase by 1 to 1.5 ppm during the ladle treatment. This hydrogen pick-up can be attributed to the water associated with the materials used (lime, CaSi and other fluxes).

Haida and his coworkers [27] reported that atmospheric hydrogen can be absorbed from the furnace atmosphere, during pouring and casting. In this case the most critical aspect the humidity of the atmosphere. The slag also plays an important role, since it can be a strong transmitter of hydrogen from atmospheric humidity. Atmospheric moisture is typically in the range 5 to 15 grams of water per cubic metre. The amount of air entrained into the steel during processing is very variable but can be of the order of 0.5 m^3/tonne. Hence the contribution of hydrogen from moisture in air entrained in the steel could be as high as 0.8 ppm in the steel. Slag, moreover can contain 40 ppm or more of hydrogen and may therefore serve as a reservoir of hydrogen which can be transferred to the steel during the turbulent mixing that occurs on tapping.

Okamoto and et al[24] found that high carbon ferromanganese has the highest moisture content. A one per cent addition of this ferromanganese would result in a pick-up of 0.5 ppm of hydrogen if 50% of the moisture is retained as hydrogen in the steel.

Harvey [28] mentions in his paper that the moisture in raw materials is as follows: FeSi and FeCr 0.2%, FeMn 0.1-0.8%, lime 1.5% and CaF_2 2.0%. The preheating of ladle additions has obvious advantages in minimising pick-up from such sources.

Jaeger et al [29] reported that there are three sources of hydrogen in the ESR process: flux containing hydroscopic lime, moisture in the atmosphere and hydrogen in the electrode. The hydrogen level in flux containing solid lime was found to be in between 30 and 60 ppm. Among the different components of the flux, CaO was found to be the major contributor to the adsorption of moisture. They suggested that the fluxes should be calcined in electric furnaces with a neutral atmosphere containing a minimum of water vapour. Other sources of hydrogen are tundish refractories continuous casting and the runner bricks in bottom poured ingots.

Harvey [28] reports in his paper that it is difficult to produce bulk lime with a moisture content less than 0.5% and yet this content is significant in terms of its potential contribution to hydrogen in the steel.

Hills [30] suggested that the hydration resistance of lime could be increased by coating it with a film of calcium carbonate and in this way the absorption of hydrogen into liquid steel could be minimised. This same approach was

proposed by Harvey, who also considers a further advantage: decomposition of the carbonate would generate gas within the bath which could flush hydrogen from the system.

Borisov etal[31] studied the thermodynamics of the reactions of lime hydration and recarbonisation in a sinter bed. They concluded that lime hydration and recarbonisation can occur at room temperature, but that the hydration of calcium carbonate is insignificant at temperatures less than 1050 K. The standard free energy change of the reaction at the given temperature, T, was found from the equation

$$\Delta G_T = -8.314T\ln K \qquad \text{(joules/mol)}$$

and they reported the following values.

REACTION EQUATION	ΔG_T VALUES, kJ/Mol			
	TEMPERATURE, K			
	298	350	373	1050
$CaO + CO_2 = CaCO_3$	-130.0	-121.6	-117.8	-14.2
$CaO + H_2O_{(g)} = Ca(OH)_2$	-64.4	-56.5	-50.4	-30.5
$CaCO_3 + H_2O_{(g)} = Ca(OH)_2 + CO_2$	65.3	65.1	64.9	44.7

Thus the literature survey reported above points to lime as the strongest potential source of hydrogen during secondary steelmaking. However, taking into account the suggestions of Hills, Harvey and Borisov it might be possible to minimise this potential. The work reported in this thesis has been undertaken to examine this possibility in some detail.

2.2.3. DISSOLUTION OF HYDROGEN IN STEEL

The solubility of a gas in a metal bath depends on the partial pressure of the gas over the liquid metal. At a specific temperature, for a given steel the solubility is proportional to the square root of the gas partial pressure Sieverts' Law [32].

Sieverts' Law arises because, when a diatomic gas dissolves in a metal, it does so in the atomic form. Thus for hydrogen:

$$1/2\{H_2\}_{(g)} = [H] \qquad (2.1)$$

If it is assumed that hydrogen activity in the liquid steel follows Henry's Law, then the equilibrium constant of reaction 2.1 is:

$$K_{[H]} = [\%H]/\sqrt{p_H} \qquad (2.2)$$

rewriting

$$[\%H] = K_{[H]}\sqrt{p_H} \qquad (2.3)$$

Water vapour is also an important source of hydrogen. The dissolution reaction is:

$$\{H_2O\}_{(g)} = 2[H] + [O] \qquad (2.4)$$

the equilibrium constant of reaction (2.4) is:

$$K_{H_2O} = [\%H]^2.[\%O]/p_{H_2O} \qquad (2.5)$$

rewriting

$$[\%H] = \sqrt{K_{H_2O} \cdot p_{H_2O}/[\%O]} \qquad (2.6)$$

At any given partial pressure of hydrogen or of water vapour there is an equilibrium content of hydrogen in steel proportional to $\sqrt{p_H}$ or to $\sqrt{p_{H_2O}}$. To get very low hydrogen contents, then, these pressures must be kept low. Furthermore, for rapid elimination of hydrogen, the pressure in the system should be significantly less than the equilibrium pressure of the hydrogen.

Thus, the solubility of hydrogen in steel depends on the partial pressures of the hydrogen or water vapour and on the bath temperature and steel composition.

PARTIAL PRESSURE. The Eqs. (2.3) and (2.6) show that the hydrogen content is directly proportional to the square root of gaseous species (H_2, H_2O) partial pressure, this is in agreement with Sieverts' Law.

TEMPERATURE. The Eqs. (2.3) and (2.6) give a relationship between hydrogen solubility and temperature, since that K_H and K_{H_2O} depend on temperature. The hydrogen content of liquid steel is considerably more than the solid solubility. As a result, gross porosity in steel casting can results from hydrogen expulsion during solidification [33].

STEEL COMPOSITION. Elements dissolved in iron affect hydrogen solubility [34-37]. Gatellier and Gaye [34] report the following relationship for a low alloy steel:

$$\log [\%H] = \log a_H - e_H^x[\%X] \qquad (2.7)$$

Oxygen is dissolved simultaneously with hydrogen, during reaction of water vapour with liquid steels reaction (2.4). From Eq.(2.6), it is possible to see that the equilibrium hydrogen content depends on the oxygen content in the bath.

For this reason, hydrogen elimination in secondary steelmak-

ing processes, where the oxygen content is low, is difficult. One again, it must be concluded that the best technological solution is to reduce the moisture content of the raw materials used.

2.2.3.1. SOLUBILITY OF HYDROGEN IN SLAG.

The molten slags used in steelmaking operations can have a substantial solubility for water vapour and also provide an immediate source of hydrogen to the molten steel bath. All of the investigators[22,34-51] agree that the hydrogen content of the slag is a function of both slag basicity and of the square root of the partial pressure of water vapour.

Structural models have been suggested: at high basicity the water is assumed to be present in slags as free hydroxyl ions (OH^-) whereas in acid slags the water may be bound to silicon forming -Si-OH groups. Some investigations have shown, however, that slag cover prevents hydrogen transfer from dry atmosphere, in contact with the slag, to the liquid steel. It appears that hydrogen itself is not soluble in the slag. The take up of hydrogen in the slag is essentially in the form of OH^- ions [34].

In the literature consulted [34-40] there is agreement that the transfer of hydrogen from water vapour takes place in two steps:

At the gas/slag interface

$$1/2\{H_2O\}_{(g)} + 1/2(O^{2-}) = (OH^-) \quad (2.8)$$

At the slag/metal interface

$$(OH^-) = [O] + [H] + e^- \quad (2.9)$$

The electron, e^-, is consumed by a slag/metal reaction of the form $[S]+2e^-=(S^{2-})$. The equilibrium constant relative to water vapour dissolution in the slag is of the form[34]:

$$K_{(H_2O)} = (OH^-)/\sqrt{(O^{2-})}\cdot p_{H_2O} \quad (2.10)$$

Using a formalism identical to that developed for the sulphur content of slags, it is possible to characterise a slag of given composition at a definite temperature, by its "WATER CAPACITY". Gatellier[34] define the water capacity of a slag, C_{H_2O}, as the amount of water that a slag can dissolve at a given temperature and one atmosphere partial pressure of water vapour.

$$C_{(H_2O)} = K_{(H_2O)}\cdot\sqrt{(O^{2-})} = (H_2O \text{ ppm})/\sqrt{p_{H_2O}} \text{ atm} \quad (2.11)$$

The water capacity depends on the slag composition, mainly the basicity, see Figure 1. . In general, secondary steelmaking slags have a water capacity in the range of 1500 to 2000 $ppm/atm^{1/2}$ [34].

At the metal/slag interface the equilibrium depends on the Composition of the phases. The equilibrium constant of reaction (2.4) can be rewritten in the following form:

$$K_{[H_2O]} = a^2_{[H]} \cdot a_{[O]} / p_{H_2O} \qquad (2.12)$$

and the water capacity of the slag can be rewritten in the form:

$$C_{(H_2O)} = \sqrt{\{K_{[H_2O]} \cdot (H_2O \text{ ppm})\}} / a_{[H]} \cdot \sqrt{a_{[O]}} \qquad (2.13)$$

From Gatellier and Gaye [34]

$$\text{Log } K_{[H_2O]} = -10778/T - 0.026$$

at 1550 °C

$$C_{(H_2O)} = 10.7(\%H_2O) / a_{[H]} \cdot \sqrt{a_{[O]}} \qquad (2.14)$$

in low alloy steels the hydrogen activity obeys Henry's law, and in the infinitely dilute solution standard state, it is approximately equal to [%H], so that, a partition coefficient between slag and steel can be defined as:

$$L_H = 1/9 \cdot (\%H_2O) / [\%H] = 0.0104 C_{(H_2O)} \cdot \sqrt{a_{[O]}} \qquad (2.15)$$

The partition coefficient, L_H, depends on the oxygen content in the steel and the water capacity of the slag.

Zuliani and coworkers[45] reported that temperature has a negligible effect on water vapour solubility in slag, their work was carried out in the range 1500 to 1550 ^{o}C. Iguchi et al [46] reported a modest temperature effect over the 200 ^{o}C range from 1400 to 1600 ^{o}C.

Zuliani et al [45] reported that the replacement of the lime by magnesia had a negligible effect on the hydrogen solubility in the slag. Iguchi and Fuwa[46] found that, at a given basicity, the water vapour solubility increased with increasing magnesia content. Sosinsky[42] found that water solubility in the system CaMgO-SiO_2 is a negative function of silica activity. Since MgO decreases the silica activity, at constant basicity, then the MgO increases the water solubility.

On the basis of this literature survey it is possible to conclude that:

i) The hydrogen content in steel depends not only on the partial pressure of water vapour but also on slag basicity and oxygen activity.

ii) Lime contributes to the formation of (O^{2-}) ions. Thus hydrogen contents will be higher in high basicity slags.

iii) Temperature has a negligible effect on water vapour solubility at steelmaking temperatures.

iv) The effect of MgO in the slag on water solubility is not clear yet.

2.2.4. CONTROL OF HYDROGEN IN STEELMAKING.

In most secondary steelmaking processes the hydrogen is removed by vacuum. There are three basic types of degassing systems:

1) Stream Degassing
2) Recirculation
3) Ladle Processes

Stream Degassing. Stream degassing processes, such as ladle to ladle and ladle to mould, are good for removing hydrogen. However, due to limitations, not capable of removing inclusions or decarburisation, they are not practised [52].

Recirculating. Recirculating systems include RH, RH-OB (oxygen blowing) and DH. RH and RH-OB are the most widely practised recirculating degassing processes. They can generally reduce the hydrogen content by half during a treatment lasting 25 to 30 minutes. RH-PB (powder blowing) has been developed in conjunction with the RH-OB process. In the RH-PB process, a $CaO-CaF_2$ flux is blown and hydrogen removal being carried out simultaneously with powder blowing. If this flux is dried before use the hydrogen removal level is similar to RH and RH-OB. The hydrogen removal in DH units is similar to RH.

Ladle Processes. Ladle processes include VOD (vacuum oxygen decarburization), VAD (vacuum argon degassing) and ladle furnaces (ASEA, TN, Daido, Standard Messo, SAFE, and others). These units combine vacuum processes, ladle heating and possibly oxygen injection. These processes produce steels with hydrogen levels of about 1.5 ppm.

A disadvantage of ladle processes in regard to hydrogen is the pick-up of this gas from injected fluxes or top slagmaking fluxes; these fluxes being $CaO-CaF_2-Al_2O_3$ based mixtures with CaO contents higher than 50%. To obtain lower hydrogen contents these processes can be used in conjunction with RH or RH-OB units or stream degassing. Nevertheless, subsequent degassing treatment introduces additional problems such as higher tapping temperatures and increased refractory wear.

In ladle degassing the hydrogen removal rate is controlled by liquid phase mass transfer [53-62], the rate equation being given as:

$$d[\%H]/dt = -kA\rho[\%H]/W \qquad (2.16)$$

separation of variables and integrating yields

$$\ln\{([\%H]-[\%H_e])/([\%H_o]-[\%H_e])\} = -kA\rho t/W \qquad (2.17)$$

where, $[\%H_o]$, $[\%H_e]$ and $[\%H]$ are the initial, in equilibrium and instantaneous hydrogen content respectively, k is the mass transfer coefficient, A the surface area, ρ is the density and W is the mass of the steel. If the pressure is low Eq.(2.17) simplifies to:

$$\ln\{[\%H]/[\%H_o]\} = -k_H t \qquad (2.18)$$

where, k_H is an overall constant for the process. However, Eq.(2.17) is more general and should be used for accurate control.

Hydrogen removal can be improved by increasing stirring, which increases both k and A. Therefore, in most operations gas stirring is also used.

Choudhury et al [62] reported that heats with top addition contained 4.2 ppm of hydrogen as a result of the humidity of the lime. These hydrogen contents are lowered to 1.5 ppm and less than 1 ppm by application, respectively, by 360 kJ/tonne and 760 kJ/tonne circulation energy. These authors have also shown that the stirring energy depend on the amount of stirring gas.

It should be noted that lower gas flow rates are required in systems at reduced pressure to give stirring energies equivalent to those produced by gas stirring at atmospheric pressure. Under a pressure of 1-5 torr the stirring

energy is a factor of two higher than it is under atmospheric pressure, but is concentrated in the upper part of the bath. The higher stirring energy under vacuum results from greater expansion of gas [61].

When there is a significant quantity of slag on top of the metal during vacuum treatment the rate of hydrogen removal will be reduced. The slag reduces the metal-vacuum surface area and the slag must also be degassed to achieve low hydrogen levels. Hydrogen must diffuse through the slag which decreases the overall rate of hydrogen removal [60].

Lefebure et al[63] reported that the average dehydrogenation with the DH process is greater than 50%. For some grades and thicknesses, this content is still too high and it is necessary to resort to slow cooling after rolling. The 2 ppm level easily achievable with DH operation is adequate in most cases where this can be done. For very thick plates, alloyed grades, or plates thicker than 50 mm rolled from continously cast slabs for "on line" accelerated cooling after rolling, however, a hydrogen content of less than 1.5 ppm or even 1 ppm would be advisable.

Binder et al[64] reported that hydrogen levels of 1 ppm were achieved after 20 to 25 minutes with the introduction of Ar into a nozzle at a rate of 400 l/min. Riboud and Gatellier [25] maintain that, operating under optimum conditions for vessel pressures below 2 mbar, hydrogen contents of about

1.5 ppm are reached after 30 minutes of treatment, whether the process used is RH, DH or a ladle vacuum treatment.

Hence, on the basis of the literature reviewed, it can be concluded that, long treatment times or large amounts of stirring gas are required to reduce hydrogen contents below 1.5 ppm. These times or amounts of gas can be reduced by reducing the humidity content of the raw materials used.

The objective of this work is to study the rate of lime hydration and then to be able to increase the hydration resistance of this slagmaking material, since it is the main source of hydrogen during secondary refining.

2.3. PHYSICAL AND CHEMICAL PROPERTIES OF LIME.

The lime used in steelmaking is obtained by calcination of calcium carbonate. Hills [65] studied the calcination of limestone and how it is affected by temperature and CO_2 partial pressure, concluding that the decomposition of calcium carbonate is controlled by heat and mass transfer.

Calcium carbonate in its most widespread mineral form calcite, has a varying density of 2.72-2.93 g/cm^3 corresponding with a medium molar volume of 35.5 cm^3 [66]. Muller [67] reported that the true unit cell is a rhombohedron containing $2(CaCO_3)$. The cell parameter is a=b=c= 6.32 Å.

Calcium oxide, as produced by oxidation of the metal, crystallises in cubic units cells of ionic type, with cell parameter a= 4.82 Å, a density of 3.34 g/cm^3 and the corresponding molar volume is 16.8 cm^3 [66].

Burnt lime is generally considered to be thermodynamically identical with CaO made from the metal, although differing strongly in structure and properties. Structurally, a specimen of burnt lime, carefully calcined, will maintain the same shape, dimensions, and molar volume as it had as carbonate. This means that 52.5% of its volume should be present as internal pores and voids, with a correspondingly enlarged inner surface. The extraordinary high reactivity of burnt lime in various chemical reactions is generally ascribed to this internal surface area [67].

Continued heating of lime after its calcination leads to sintering and aggregation of the crystals comprising the lump. The lump consequently shrinks, becoming progressively denser, or hard-burned, less porous, and less reactive to water [68]. The time and the temperature of calcination are important process variables in the calcination of limestone. Natalie and Evans[69] and Slater[70] reported that increasing the temperature at which the lime is formed from limestone, or increasing the time at this temperature, results in a decline in pore surface area and water reactivity. Some sintering of the outer lime layer

may occur even while a limestone lump is decomposing, since the surface of the lump may be at a high temperature and consequently there is an apparent density gradient within a freshly decomposed lump of lime from the outside inwards. The rate of sintering of lime is also dependent on the presence of impurities such as iron, alumina, and silica which promote liquid formation at the surface of the calcium oxide crystals during the lime burning process [68].

Various investigators [71-75] have reported that increasing the reactivity of the lime improves its rate of dissolution in a steelmaking slag, (the reactivity of a lime to water has been used as a standard test to asses the performance of the lime in oxygen steelmaking processes, ASTM C110). Greater lime reactivity has important benefits in terms of more rapid refining rates and thus greater productivity. Lime of high reactivity is, however, extremely susceptible to hydration, and also recarbonization, if it is exposed to the atmosphere for any length of time. The rate of reaction of lime with water depends, among other factors, upon the area of the calcium oxide surface available to water molecules. In the case of a highly porous, low-density lime, it is not only the external surfaces that are readily accessible to water molecules. The rate of reaction is then a function of the total specific surface area of the lime. Because its internal surfaces are large in relation to its

external surface, reactive low-density lime has a specific surface area as high as 2 m^2/g.

Calcium hydroxide, $Ca(OH)_2$, is hexagonal crystalline, with a density of 2.24 g/cm^3 and its molar volume is 33.1 cm^3 slightly less than that of burnt lime [66].

2.4. GASEOUS DIFFUSION AND REACTIONS INVOLVING POROUS SOLIDS

2.4.1. INTRODUCTION

The rates of gas-solid reactions have long been of interest in process metallurgy as well as in other fields of engineering and science. In most cases of practical interest, the rates of such reactions are determined by transport of gaseous reactants and products rather than by the intrinsic chemistry of the reaction. In some instances, mass transport is by the diffusion of gases within the pores of a solid, while viscous flow of gases under pressure gradients can also be important.

A quantitative description of the progress of a reaction must then depend on a knowledge of the transport properties of the gas and how these properties are affected by the pore structure of the solid.

A common feature of all gas-solid reaction systems is that the overall process may involve several intermediate steps [76-78].

Typically, these intermediate steps involve the following:

i). Convective transport of the gaseous reactant from the bulk gas to the particle surface.

ii). Diffusion of the gaseous reactant through the product layer to the reaction interface.

iii). Chemisorption of at least one of the reactants at the

solid exterior and interior surface followed by surface chemical reaction and subsequent desorption of the product of the surface reaction.

iv). Diffusion of the gaseous product through the product layer to the particle surface, and

v). Transport of gaseous products through the gas film back into the main body of the fluid.

Not all of these steps are involved in all reactions. For example, if no gaseous products are formed, or if the shell product is not formed, steps iv and v do not contribute directly to the reaction resistance. The resistances of the different steps usually differ greatly in which case the step with highest resistance is rate controlling.

2.4.2. PHENOMENOLOGICAL DESCRIPTION OF FLOW AND DIFFUSION

In the absence of conditions causing turbulence, there are three main types of isothermal gas transport in free space or porous media.

MOLECULAR DIFFUSION , in which the different species of a mixture undergo relative movement under the influence of composition gradients, the resistance to this movement arising from molecule-molecule collisions. When molecular diffusion occurs within a porous solid, the solid does no more than restrict the space available for the gas to occupy and constrain the directions in which it can diffuse.

VISCOUS FLOW , in which the gas acts as a continuum fluid driven by a pressure gradient. Once again, in a porous solid, molecule-molecule collisions dominate over molecule to wall collisions when viscous flow is occurring.

FREE MOLECULE OR KNUDSEN DIFFUSION , here the pore size is very much smaller than the mean free path of the gas mixture so that almost all of the collisions will be between gas molecules and the pore walls. This diffusion process is known as Knudsen Diffusion and the actual progress of gas molecules through the porous solid is an amalgamation of the geometry of the pores and the geometry of the random motion of gas molecules.

In the bulk of the technical processes in which gaseous diffusion in porous solids is important, the process is "mixed", that is, it involves both molecule to molecule collisions and molecule to wall collisions, and hence both molecular and Knudsen diffusion are important.

Corresponding to these three mechanisms there are three transport coefficients: The molecular diffusion coefficient D_{ij} (for a binary mixture of species i and j), the viscosity coefficient μ, and the Knudsen diffusion coefficient D_{ik} (for species i). There are also three corresponding parameters that characterise the solid medium through which the gas moves: the porosity-tortuosity ratio ϵ/τ for

molecular diffusion, the viscous flow parameter B_o, and the Knudsen flow parameter k_o. These three parameters are unknown, and are usually found from experiment rather than by calculation from an assumed geometry.

2.4.2.1. MOLECULAR DIFFUSION

To analysing molecular diffusion it is necessary to define a diffusion coefficient for a mixture in which the net flux is zero and in which there is also no pressure gradient. In this case the purely diffusive fluxes $\dot{N}_{1D}$ and $\dot{N}_{2D}$ of a binary mixture are

$$\dot{N}_1 = -D_{12}\nabla n_1 \qquad (2.19)$$
$$\dot{N}_2 = -D_{21}\nabla n_2$$

It is easy to see that $D_{12} = D_{21}$ since

$$\dot{N}_1 + \dot{N}_2 = \dot{N}_D = 0 \quad \text{for no net flux}$$

and

$$\nabla(n_1 + n_2) = \nabla n = 0 \quad \text{for no pressure gradients.}$$

where

$\dot{N}_1$, $\dot{N}_2$ = Flux, $[kmol.m^{-2}.s^{-1}]$

D_{12}, D_{21} = Diffusivity coefficient, $[m^2.s^{-1}]$

n_1, n_2 = Concentration [kmol.m^{-3}]

$\dot{N}_D$ = Net flux diffusive [kmol.m^{-2}.s^{-1}]

Unfortunately, a situation such as this is very difficult to produce experimentally, since a small pressure gradient is necessary to keep $\dot{N}_D = 0$ [79] due to interaction with the walls of the experimental vessel. It is, However, still possible to describe this diffusion by the same diffusion coefficient D_{12}, including an extra term that apportions the net flux contribution to each species,

$$\dot{N}_{1D} = -D_{12}\nabla n_1 + X_1\dot{N}_D$$
$$\dot{N}_{2D} = -D_{21}\nabla n_2 + X_2\dot{N}_D \qquad (2.20)$$

where

$X_i = n_i/n$ is the mole fraction.

Equations (2.20) thus define pure diffusive transport in the continuum region; the key point is that the pressure is uniform so that the viscous transport is zero.

The diffusion in porous media can be described by transport equations of the same form as Eqs. (2.20), provided D_{12} is replaced by an effective diffusion coefficient $D_{12,eff}$, whose value depends of the geometry of the medium.

$$D_{12,eff} = D_{12}\cdot(\epsilon/\tau) \qquad (2.21)$$

where the constant ϵ/τ is called the porosity-tortuosity factor. From geometric considerations of the random model suggested by Wheeler [80], $\tau \approx 2$. The binary effective diffusion coefficient is less than the binary diffusion coefficient, D_{12}, because transport can only occur in the voids of the porous solid and must follow a tortuous path. Both $D_{12,eff}$ and D_{12} are inversely proportional to pressure.

Graham cited by Mason and Marrero[81] discovered experimentally that the fluxes in Eqs. (2.20) within a porous solid under iso-baric conditions are related by the equation:

$$\dot{N}_{1D}/\dot{N}_{2D} = (M_2/M_1)^{1/2} \qquad (2.23)$$

The simplest physical explanation of this relationship is based on an equality between the momentum transferred to the walls by the diffusing molecules of each species, as suggested by Hoogschagen [82].

2.4.2.2. VISCOUS FLOW

Viscous flow is caused by a pressure gradient, the behaviour of the gas being described by the coefficient of viscosity. Moreover, a mixture behaves the same as a single gas, since bulk viscous flow does not cause a gaseous mixture to separate into its components.

Applying Poiseuille's law for liquids, but remembering that a gas is compressible, the result has the form

$$\dot{N}_{vis} = \text{Flow/Area} = - (nB_o/\mu)\nabla P \qquad (2.23)$$

where

$\dot{N}_{vis}$ = Viscous flux [kmol.m^{-2}.s^{-1}]

B_o = Constant characteristic of the hole geometry [m^2]

μ = Viscosity [Pa.s]

P = pressure [Pa]

For mixtures, the viscous flux of species i is proportional to its mole fraction, since the flow is nonseparative,

$$\dot{N}_{ivis} = X_i\dot{N}_{vis} \qquad (2.24)$$

2.4.2.3. FREE-MOLECULE DIFFUSION

This type of diffusion was studied by Knudsen [83], and is called Knudsen diffusion. The flux of molecules through a pore channel is equal to the number of molecules passing into the entrance of the channel multiplied by the probability that a molecule that enters will get all the way through the channel and not bounce back out of the entrance. This probability depends on the geometry of the channel and the

law of reflection for molecules hitting the inner walls of the hole.

If there is a gas of molecular density n at one end of the hole and a vacuum at the other, the effusive flux, $\dot{N}_k$, is

$$\dot{N}_k = w \cdot n \cdot \nu \qquad (2.25)$$

where

w = probability factor

ν = mean molecular speed

If there is a gas mixture instead of a single gas, each species acts independently of the other species, and the total flow is a sum of terms,

$$\dot{N}_k = \sum_{i=1}^{n} w_i n_i \nu_i \qquad (2.26)$$

For gas on both sides of the channel, the net flux is proportional to the difference between the gas concentrations at the two ends. In differential form this gives:

$$\dot{N}_k = -D_{ik} \nabla n_i \qquad (2.27)$$

for one species of a mixture, where D_{ik} is defined as the Knudsen diffusion coefficient. Comparing Eqs.(2.25) and (2.27), it is possible to see that D_{ik} is proportional to ν; it is therefore customary to write

$$D_{ik} = (4/3)k_o \nu_i \qquad (2.28)$$

where k_o is called the Knudsen permeability constant and is characteristic of the pore geometry. It is evident that D_{ik} is independent of pressure and increases with temperature as $T^{1/2}$.

For different gases at the same pressure on the two sides of the hole, Eqs.(2.27) and (2.28) give

$$\dot{N}_{1k}/\dot{N}_{2k} = D_{1k}/D_{2k} = \nu_1/\nu_2 = (M_2/M_1)^{1/2} \qquad (2.29)$$

2.4.2.4. COMBINED TRANSPORT

The diffusion of a gas molecule through a porous solid is impeded by collisions both with the pore walls and with other molecules present in the pores. The resistances to gaseous diffusion arising from molecular and Knudsen diffusion are thus additive. Viscous and diffusive flows, on the other hand, contribute independently to the total transport, of a gas species so that the total flux is just the sum of the diffusive and viscous fluxes, being no extra terms due to coupling between the two mechanisms. This principle of combination has simple electrical analogue: Diffusive flows combine like resistors in series (voltage drops add, as do

resistances to flow); diffusive and viscous flows combine like resistors in parallel (currents add, as do fluxes) [84].

Considering the diffusive flows first, the momentum transferred by species i is proportional to the gradient of the partial pressure of that species ($p_i = n_i RT$). Rearrange Eqs.(2.20) for continuum diffusion and Eq.(2.27) for free-molecule diffusion to emphasise the momentum transfer rather than the flux:

$$-(1/RT)\nabla p_1 = (1/D_{12})(\dot{N}_{1D} - X_1\dot{N}_D) \qquad (2.30)$$

and

$$-(1/RT)\nabla p_1 = (1/D_{1k})\dot{N}_{1k} \qquad (2.31)$$

with similar equations for species 2. Thus it is the ∇p_1 terms which add; moreover $\dot{N}_{1D}$ and $\dot{N}_{1k}$ are the same, just as the current through two series resistors is the same. Combining Eqs. (2.30) and (2.31) in this way yields

$$-(1/RT)\nabla p_1 = (1/D_{1k})\dot{N}_{1D} + (1/D_{12})(\dot{N}_{1D} - X_1\dot{N}_D) \qquad (2.32)$$

with similar equations for species 2. This equation describes the diffusion of one component of a binary mixture

at uniform total pressure throughout the entire pressure range from free-molecule to the continuum limits.

If a gradient of the total pressure exists, the viscous fluxes must be added to the diffusive fluxes,

$$\dot{N}_1 = \dot{N}_{1D} + \dot{N}_{1vis}, \qquad \dot{N}_2 = \dot{N}_{2D} + \dot{N}_{2vis} \tag{2.33}$$

and the total flux is

$$\dot{N} = \dot{N}_1 + \dot{N}_2 = \dot{N}_D + \dot{N}_{vis} \tag{2.34}$$

the viscous fluxes being given by Eqs.(2.23) and (2.24). The easiest way to do this is to replace each diffusive flux in Eq.(2.32) by

$$\dot{N}_{iD} = \dot{N}_i - X_i\dot{N}_{vis} \tag{2.35}$$

which leads to

$$-(1/RT)\nabla p_1 = [(1/D_{1k}) + (1/D_{12})]\dot{N}_1 - (X/D_{12})\dot{N} - (X_1/D_{1k})\dot{N}_{vis} \tag{2.36}$$

substituting for $\dot{N}_{vis}$ from Eq.(2.23) and rearranging, we can obtain the following neat form:

$$\dot{N}_1 = -D_1\nabla n_1 + X_1\delta_1\dot{N} - X_1\gamma_1(nB_o/\mu)\nabla p \qquad (2.37)$$

where

$$\delta_1 = D_1/D_{12} = D_{1k}/(D_{1k}+D_{12})$$
$$\gamma_1 = D_1/D_{1k} = D_{12}/(D_{1k}+D_{12}) = 1-\delta_1$$

The diffusivity D_1 for the mixed region where Knudsen diffusion and molecular diffusion have to be considered together was derived by Evans et al [85] as:

$$\frac{1}{D_1} = \frac{1}{(1-\psi X_1)/D_{12} + 1/D_{1k}} \qquad (2.38)$$

where $\psi = 1 + \dot{N}_2/\dot{N}_1$. In the special case of equimolar counterdiffusion $\dot{N}_1 = -\dot{N}_2$ and the Eq.(2.38) simplifies to Bosanquet's[86] equation:

$$1/D_1 = (1/D_{1k}) + (1/D_{12})$$

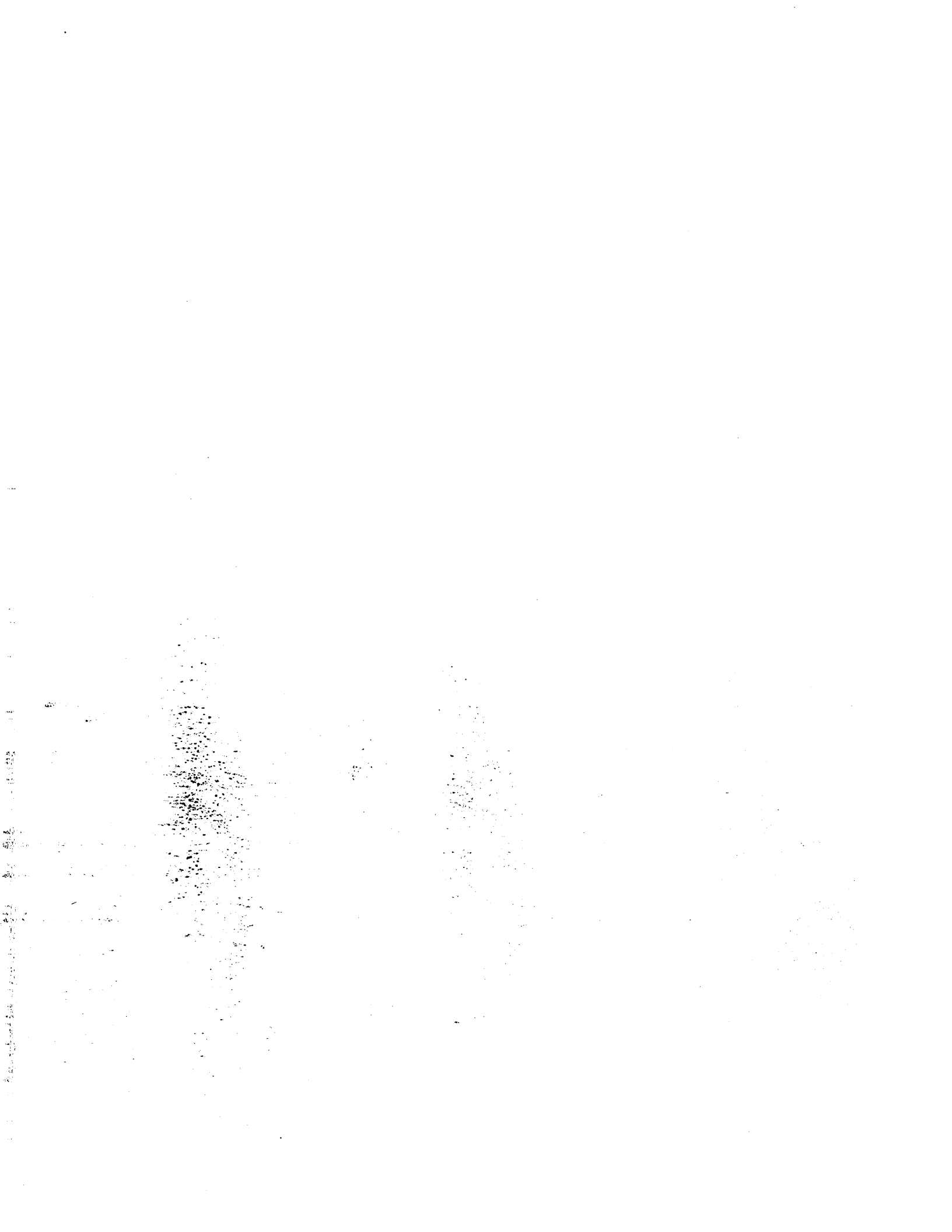

A similar equation holds for $\dot{N}_2$, with corresponding definitions of D_2, δ_2, and γ_2.

The complete phenomenological description of diffusion and flow in a binary mixture over the whole pressure range is given by Eq.(2.37) plus the corresponding equation for the second component. The interesting thing about this form of the equation is that it clearly exhibits both the free-molecule and continuum limits, as well as the behaviour in the transition region, through the pressure dependece of D_1, δ_1, and γ_1. These dependencies follow from the fact that D_{1k} is independent of pressure and D_{12} is inversely proportional to pressure. Thus at very low pressures $D_1 = D_{1k}$, $\delta_1 = 0$, and $\gamma_1 = 1$, so that Eq.(2.27) for free molecule diffusion is recovered. At high pressures $D_1 = D_{12}$, $\delta_1 = 1$, and $\gamma_1 = 0$ (but $n\delta_1 = nD_{12}/D_{1k} =$ constant), so that Eqs.(2.20) for continuum diffusion are recovered if the pressure gradient is zero.

Although the two independent fluxes $\dot{N}_1$ and $\dot{N}_2$ are completely described by Eq.(2.37) and its analog for component 2, it is often convenient to take one of the independent fluxes to be the total flux $\dot{N}$. That is, instead of having two diffusion equations in which the pressure appears in subsidary role, we would like to have one diffusion equation, plus one flow equation in which the pressure gradient appears in a primary

role. This flow equation can be obtained by adding Eq.(2.36) and its analog for component 2, eliminating $\dot{N}_2$ by $\dot{N}_2 = \dot{N}-\dot{N}_1$, and substituting for N_{vis} from Eq.(2.23). The result is

$$\dot{N}-\beta_1\dot{N}_1 = -(D_{2k}/RT)[1+(BoP/\mu D_k)]\nabla p \qquad (2.39)$$

where

$$\beta \equiv 1-(D_{2k}/D_{1k}) = 1-(M_1/M_2)^{1/2}$$

$$1/D_k = (X_1/D_{1k}) + (X_2/D_{2k})$$

Here $\beta_1\dot{N}_1$ is the portion of the net flux that is driven by diffusion alone, and $(\dot{N}-\beta_1\dot{N}_1)$ is thus the portion driven by the pressure gradient alone. Eqs.(2.37) and (2.39) furnish an alternative complete description of combined diffusion and viscous flow in a binary mixture.

To obtain the extension to multicomponent mixtures, we first combine momentum transfers for continuum diffusion, add on the free molecule momentum transfer, then include the viscous flux by way of Eq.(2.35), and finally substitute for $\dot{N}_{visc}$ from Eq.(2.23). For the first step we go back to Eq.(2.30) and its analog for component 2, and eliminate the total diffusive flux $\dot{N}_D$ between the two equations, obtaining

$$-(1/RT)\nabla p_1=(1/D_{12})(X_2\dot{N}_{1D}-X_1\dot{N}_{2D})=(n_1n_2/nD_{12})(V_{1D}-V_{2D}) \tag{2.40}$$

where V_{iD} is an average diffusion velocity for species i and the relation $\nabla p_2 = -\nabla p_1$ was used. A similar equation exists for ∇p_2, but with reversed signs. The extension to multicomponent mixtures is now plausible: For each new species there is another momentum-transfer term on the right hand side of the equation,

$$\begin{aligned}
-(1/RT)\nabla p_1 &= (n_1n_2/nD_{12})(V_{1D}-V_{2D})+(n_1n_3/nD_{13})(V_{1D}-V_{3D})+\cdots,\\
-(1/RT)\nabla p_2 &= (n_2n_1/nD_{21})(V_{2D}-V_{1D})+(n_2n_3/nD_{23})(V_{2D}-V_{3D})+\cdots,\\
&\ \ \vdots\\
&\text{etc.}
\end{aligned} \tag{2.41}$$

For a mixture of n species, there is a total of n equations, of which only n-1 are independent. This set of equations usually called the Stefan-Maxwell equations, is valid for continuum diffusion at constant total pressure.

Adding in the free-molecule and viscous contributions, yields the general result,

$$-\nabla n_1 = (1/D_{1k})[\dot{N}_1 + X_1(nBo/\mu)\nabla p] + (1/D_{12})(X_2\dot{N}_1 - X_1\dot{N}_2) + \\ + (1/D_{13})(X_3\dot{N}_1 - X_1\dot{N}_3) + \ldots\ldots,$$

$$-\nabla n_2 = (1/D_{2k})[\dot{N}_2 + X_2(nBo/\mu)\nabla p] + (1/D_{21})(X_1\dot{N}_2 - X_2\dot{N}_1) + \\ + (1/D_{23})(X_3\dot{N}_2 - X_2\dot{N}_3) + \ldots\ldots,$$

.

.

etc. (2.42)

Equations (2.42) must be regarded as phenomenological description of the problem because there is no assurance that the D_{ij} in Eqs.(2.42) are the same as the ones in the corresponding binary mixture equations. Some authors [87-89] reported that this is nearly true. This is an important simplification in the treatment of multicomponent gaseous diffusion.

2.4.3. DETERMINATION OF THE TRANSPORT COEFFICIENTS

The effective diffusivity, the Knudsen diffusivity and the parameters that characterise the solid medium, ϵ/τ, B_o, A_o, are important when considering the kinetics of gas-solid reactions involving porous solids. This is because the overall reaction rate is, in general, controlled simultaneously by gaseous diffusion and by chemical reaction rates at solid surfaces.

There are two ways of obtaining the diffusion coefficients. The first is to calculate them from the overall reaction rate on the basis of a mathematical model. However, if the assumptions adopted in the model are not adequate, the results lose their physical significance. The second way is by direct measurement, which has the advantage of not being reliant on an assumed mathematical model. Direct measurements of effective diffusvity have been made by a canister method [90-92]. The most common method currently in use, however, is the Wicke and Kallenbach method [93] which has been modified constantly for use on specific systems and under various experimental conditions [94-97].

Staia and Hills [97] made direct measurements of gaseous diffusion coefficients in porous lime using one such modification. The diffusion cell consisted of a hollow sphere of the solid under investigation sealed onto a

"diffusion shaft". This had been manufactured from hypodermic tubing to contain three separate passages for the supply and removal of a gas stream to and from the central cavity of the sphere and for the measurement of the total pressure in the cavity. A gas stream of one composition was supplied to the central cavity and a stream of a different composition was passed over the outer surface of the sphere.

The diffusion flux across the sphere can be determined from the flow rate and change in composition of either gas stream. The partial pressure conditions on either side of the sample could also be determined from the compositions of the gases and the measured total pressures inside and outside the sphere. Permeability experiments could be conducted on the same sample.

The principles underlying the method will be discussed briefly. First of all they used the Dusty Gas Model developed by Evans, Watson and Mason [98]. The model shows how permeability measurements can be combined with the diffusion measurements to separate molecular and Knudsen effects.

The three parameters that determine the behaviour of gases within the porous solid are:

(i) the Knudsen diffusion parameter, A_o

$$D_{A,k} = A_o(T/M_A)^{1/2} \tag{2.43}$$

where $D_{A,k}$ is the Knudsen diffusion coefficient;

(ii) the viscous flow parameter, B_o

$$v_M = -(B_o n/\mu)\nabla P \tag{2.44}$$

where v_M is the mass centre velocity of the gas mixture; and

(iii) the molecular diffusion parameter, C_o

$$D_{AB,eff} = C_o D_{AB} \tag{2.45}$$

where $D_{AB,eff}$ is the effective binary molecular diffusion coefficient in the porous solid and D_{AB} is the binary molecular diffusion coefficient in the free gas.

The three parameters, A_o, B_o, C_o, are properties of the porous solid, and can be determined from the method developed by Hills and Staia.

The first two parameters can be determined from measurements of the permeability of a single gas through the porous solid made at a number of different total pres-

sures. The permeability of gas A through the porous solid is described in terms of a permeability constant, ω_A, defined by the following equation:

$$\dot{N}_A = -(\omega_A/RT)\nabla p_A \qquad (2.46)$$

Rearranging the Eq.(2.37) for a single gas A it becomes

$$\dot{N}_A = \frac{D_{Ak} + B_o P/\mu}{RT}\nabla p_A \qquad (2.47)$$

Comparison between Eqs.(2.46) and (2.47) can be deduced that the permeability of the porous solid is given by the following equation:

$$\omega_A = D_{Ak} + B_o P/\mu$$

or

$$\omega_A = A_o\,(T/M_A)^{1/2} + B_o P/\mu \qquad (2.48)$$

Plotting measured values of ω_A against the total pressure yields a straight line, A_o being obtained from the intercept and B_o from the slope.

The molecular diffusion parameter, C_o, can be determined from the measurement of binary diffusion rates under

isobaric conditions, using an iterative solution of the two equations.

$$C_o = \frac{N_A RT(\kappa-1)}{\kappa D_{AB} SP \ln\left\{\frac{\kappa P-\delta(1-\kappa)[p_A]_e}{\kappa P-\delta(1-\kappa)[p_A]_i}\right\}} \qquad (2.49)$$

and

$$\delta = \{1 + (C_o/A_o) D_{AB} (M_A/T)^{1/2}\}^{-1} \qquad (2.50)$$

where S is the shape factor and κ the square root of the ratio of the relative molar masses of the two gases in a binary mixture.

The method was used to determine diffusion coefficient in porous lime, and these results will be used in the calculations of the present work.

2.4.4. MODELLING OF HETEROGENEOUS GAS-SOLID REACTIONS

The mathematical modelling of gas-solid reactions is helpful for the planning of experiments, for the interpretation of measurements and for the synthesis of informa-

tion obtained on single grain or single particle kinetics into a description of multi-particle, macro systems. Within this context the mathematical model of a gas-solid reaction system could be defined as a set of differential equations which express the conservation of the gaseous and the solid reactants as well as that of thermal energy.

Up to the present, many models of gas-solid reactions have been developed and compared with experimental data. These models can be classified into three categories:

1) Models with geometrically undefined interfaces which are applied to very porous materials or slow chemical reaction rates. In this case, the reaction takes place in the whole volume, or a major part of it. These models are called "The Homogeneous Reaction Model"[99] or "The Continuous Reaction Model"[79,100], since the reaction proceeds homogeneously or continuously throughout the pellet.

2) Models with one interface which is geometrically well-defined where the reaction takes place. The unreacted core model [79,99,100], in which the reaction proceeds only at the interface between the inner unreacated core and the outer reacted shell. This model is also called the shell model [101], the interface reaction model [102], or the topochemical model [103]. When the unreacted core is

dense, this model becomes the prominent mechanism because the reacting gas can not penetrate into the unreacted core.

3) Mixed models with a reaction zone. Certain porous pellets do not follow the unreacted core model because the reacting gases can penetrate into the unreacted core giving rise to a reaction zone of finite extent. Models incorporating a finite reaction zone are called intermediate models [99,104,105], the reaction zone model [101], or the grain model [78,102,106-109].

This section will discuss the unreacted core model and the zone model, since the lime hydration was found to show an interface well defined macroscopically.

UNREACTED CORE MODEL

The analysis presented below will be restricted to the gaseous reaction of a dense particle as this is the simplest case. Consider a spherical particle suspended in a gas stream of specified temperature and composition. The reaction proceeds topochemically at the interface between the reactant and product solids.

GAS-FILM DIFFUSION. If the gas composition in the bulk gas phase outside the film is assumed to be uniform, the

rates of transfer of reactant gas A and product gas B through the gas -film are respectively given by

$$-\dot{n}_{g,A} = 4\pi r_o^2 \alpha (C_{A,b} - C_{A,o}); \quad [kmol/s] \qquad (2.51)$$

$$+\dot{n}_{g,B} = 4\pi r_o^2 \alpha (C_{B,o} - C_{B,b}) \quad [kmol/s] \qquad (2.52)$$

where,

α: gas-film mass transfer coefficient, [m/s]

$C_{j,b}$: concentration of species j in the bulk gas phase, [$kmol/m^3$]

$C_{j,o}$: concentration of species j at the exterior surface of the pellet, [$kmol/m^3$]

r_o: external radius of the pellet, [m]

The mass transfer coefficient is correlated in terms of the Sherwood number, which in the case of combined diffusion and convection is a function of the Reynolds and the Schmidt numbers. For convection mass transfer to or from the surface of a sphere Bird, Stewart and Lightfoot [110] recommend the following correlation:

$$Sh = 2.0 + 0.6(\rho UL/\mu)^{1/2}(\mu/\rho D_{AB})^{1/3} \qquad (2.53)$$

where,

$Sh = \alpha L/D_{AB}$ = Sherwood number

D_{AB} = Binary molecular diffusivity [m^2/s]

L = characteristic length dimension of system [m]

U = velocity of the fluid [m/s]

ρ = fluid density [kg/m^3]

μ = fluid viscosity [Pa.s]

At low flow rates the Sherwood number approaches an asymptotic limit of two for a sphere in motionless fluid. Thus the extent of kinetic control exerted by the boundary layer is a function of the fluid dynamics of the gas phase. However, for flow rates above a certain level, the reaction rate is found to be relatively independent of the gas flow rate [103,111].

INTERPARTICLE DIFFUSION. The molar flow of reactant or product gas across any spherical surface in the ash layer is given by

$$\dot{n}_j = -4\pi r^2 . D_{j,eff}(\partial C_j/\partial r) \quad (j=A \text{ or } B) \qquad (2.54)$$

If the Eq.(2.54) is integrated with respect to r between the reaction interface at r_i and the external surface at r_o, the rates of transfer of reactant and product gases through the product layer are respectively given by

$$-\dot{n}_A = D_{A,eff}[4\pi r_o r_i/(r_o-r_i)](C_{A,o}-C_{A,i}) \qquad (2.55)$$

$$+\dot{n}_B = D_{B,eff}[4\pi r_o r_i/(r_o-r_i)](C_{B,i}-C_{B,o}) \qquad (2.56)$$

where,

$D_{j,eff}$: effective diffusivity of species j in the product layer, [m^2/s]

$C_{j,i}$: concentration of species j at the reaction interface, [$kmol/m^3$]

r_i: radius of the reaction interface, [m].

In the integration above, the effective diffusivites of gases A and B were assumed to be independent of the position in the layer.

INTERFACE CHEMICAL REACTION. If the interface reaction is assumed to be first-order, the rate of the reaction is given by

$$\dot{n}_c = 4\pi r^2 k(C_{A,i} - C_{B,i}/K), \text{ [kmol/s]} \qquad (2.57)$$

where,

k: specific rate constant for the forward reaction [m/s]

K: equilibrium constant for the reaction

OVERALL RATE EQUATION. Under a steady state, the reaction proceeds as follows:

$$-\dot{n}_{g,A} = -\dot{n}_A = \dot{n}_C = \dot{n}_B = \dot{n}_{g,B} \tag{2.58}$$

Upon substitution of Eqs.(2.51),(2.52),(2.55),(2.56) and (2.57) into the Eq.(2.58), the interface and surface concentration terms cancel out, yielding the following overall rate equation:

$$\dot{n}_C = \frac{(C_{A,b} - C_{A,e})}{\frac{1}{4\pi r_o^2 \alpha} + \frac{r_o - r_i}{4\pi r_o r_i D_s} + \frac{K}{4\pi r_i^2 k(1-K)}} \tag{2.59}$$

where,

$C_{A,e}$: concentration of A at equilibrium under the same total pressure as in the gas bulk phase.

D_s: interparticle diffusivity, [m^2/s], defined by

$1/D_s = [K/(1+K)][(1/D_{A,eff}) - (1/KD_{B,eff})]$

$\dot{n}_C$ is related to $-dr_i/dt$ by

$$\dot{n}_C = -d(4\pi r^3 \rho_s/3)/dt = -4\pi r^2 \rho_s (dr_i/dt) \tag{2.60}$$

where,

ρ_s= apparent molar density of solid reactant [kmol/m^3]

Equating the right-hand sides of Eqs.(2.59) and (2.60) and rewriting the resultant equation using the relative thickness of reacted layer f defined by

$$f = (r_o - r_i)/r_o \tag{2.61}$$

the following overall rate equation in terms of f is obtained

$$\frac{df}{dt} = \frac{(C_{A,b}-C_{A,e})/r_o \rho_s}{(1-f)^2/\alpha+r_o(f-f^2)/D_s+K/k(1-K)} \tag{2.62}$$

The relative importance of the gas film, product layer and chemical reaction resistances will vary as conversion progresses. For example, for a constant size particle the gas film resistance remains unchanged, the resistance to reaction increases as the surface of unreacted core decreases, while the ash layer resistance is nonexistent at the start because no ash is present, but becomes progressively more and more important as the ash layer builds up.

When one of these resistances is much greater than the other resistances, that resistance controls the progress of the reaction. However, it may not be reasonable to consider that just one step controls throughout reaction.

The assumptions made in this model may not match reality precisely. For example, reaction may occur within a diffuse front rather than along a sharp interface giving behaviour intermediate between the shrinking core and the continuous reaction models. Also, for a fast reaction, the rate of heat release may be high enough to cause significant temperatures gradients within the particles or between the particles and its surroundings. This problem was treated in detail by Wen et al [112] and Hills [113]. Despite these complications Wen [105] and Ishida and coworkers [114,115], on the basis of studies of numerous systems, concluded that the shrinking core model is the best simple representation for the majority of reacting gas-solid systems.

Kasama and coworkers [116] analyzed the liquid phase hydration kinetics of calcium oxide by using the model above discussed. Their equation derived in this way has the following form:

$$-\frac{dr}{dt} = \frac{1}{\frac{1}{k_s} + \frac{R-r}{D_e}} \cdot \frac{C_A}{d_B} \qquad (2.63)$$

were,

r = radius of unreacted core; [cm]

R = radius of initial grain; [cm]

C_A = Concentration of water ; [$mol.cm^{-3}$]

d_B = molar density of lime; [$mol.cm^{-3}$]

k_s = reaction rate constant; [$cm.s^{-1}$]

D_e = effective diffusivity; [$cm^2.s^{-1}$]

Kasama and coworkers found that the rate of hydration was of the type of mixed control of chemical reaction and diffusion of water through the hydrated layer, and at the last stage of hydration , it is controlled by diffusion of water. They also concluded that the hydration rate increases with temperature increase or decrease in the grain size, and that the activation energy of the reaction is 8.68 kcal/mol.

ZONE REACTION MODELS

Recently, some improved models [99,102,104-106,109] have been proposed in order to correct the simplifications of the unreacted core model for the reaction of porous solid and gas. The unreacted core model may be acceptable, however, if the reaction zone is very narrow in comparison with the diameter of the pellet.

The following major assumptions are made to derive the basic equations [102,106-117] for these models involving

an extended reaction region.

i) The pellet is considered to be spherical, having a uniform porosity ϵ_o before reaction and composed of dense grains having a constant radius R_o.

ii) The reaction of the grains proceeds topochemically.

iii) During reaction, there is no change in pellet diameter and no cracks are formed.

iv) Temperature and pressure are uniform in and around the pellet during the reaction.

Under the above assumptions, the basic equations for the concentration of gaseous reactants and products are obtained as outlined below:

A mass balance on reactant A yields the following differential equation describing diffusion of A between the grains:

$$\frac{D_{A,eff}}{r^2}\cdot\frac{\partial}{\partial r}(r^2\partial C_A/\partial r)-(1-\epsilon_o)\,\rho_t\Gamma = 0 \qquad (2.64)$$

where,

ρ_t = true molar density of reactant solid

Γ = rate of disappearance of gaseous reactant per mole of initial solid reactant

A similar equation may be written for the gaseous product:

$$\frac{D_{B,eff}}{r^2}\cdot\frac{\partial}{\partial r}\left(r^2\frac{\partial C_B}{\partial r}\right)+(1-\epsilon_o)\rho_t\cdot n_s\cdot\Gamma = 0 \qquad (2.65)$$

where, n_s is the moles of B formed by the reaction of one mole of A. Subsequently, n_s will be taken as unity, but the modification to account for other values of n_s is straight forward.

Eqs.(2.64) and (2.65) are valid for equimolar counter diffusion or where diffusion between the grains is purely of the Knudsen type. It is to be noted that no accumulation terms appear in the two equations, the 'quasi-steady' assumption thus being implicit in the formulation.

Before proceeding further, the reaction term, Γ, has to be related to the concentration of the reactants and products and also to the rate of progress of the reaction front, within the grains any particular localisation, r.

$$dR/dt = -k/\rho_s\cdot(C_A - C_B/K) \qquad (2.66)$$

where k is the chemical reaction rate constant and K is the equilibrium constant.

Γ, the reaction term, is related to the advancement of the reaction front within a grain, as shown below:

For the case where one mole of A reacts with one mole of solid, we have:

$$4\pi R^2 (dR/dt)\rho_S = 4\pi R^2 k(C_A - C_B/K) \qquad (2.67)$$

Thus, upon integration, the reaction term is defined:

$$\Gamma = (3R^2 k/\rho_s R_o^3)(C_A - C_B/K) \qquad (2.68)$$

On substituting for Γ from Eq.(2.68) into Eq.(2.64) and (2.65) yields

$$\frac{D_{A,eff}}{r^2}\cdot\frac{\partial}{\partial r}\left(\frac{r^2\partial C_A}{\partial r}\right) - 3(1-\epsilon_o)(R^2k/R_o^3)(C_A - C_B/K) = 0 \qquad (2.69)$$

$$\frac{D_{B,eff}}{r^2}\cdot\frac{\partial}{\partial r}\left(\frac{r^2\partial C_B}{\partial r}\right) - 3(1-\epsilon_o)(R^2k/R_o^3)(C_A - C_B/K) = 0 \qquad (2.70)$$

The initial and boundary conditions for the governing Eqs. (2.66), (2.68) and (2.70) have to express the following physical constraints:

a) the initial position of the reaction front within each grain, i.e., that no reaction had taken place before t=0

b) the fact that the concentration profiles are symmetrical about the centre of the pellet, and

c) the continuity of the molar fluxes at the outer surface of the pellet, i.e., diffusive flux across the outer surface of the pellet = convective flux through the gas film surrounding the pellet. These boundary conditions are given in Eqs.(2.71) through (2.75):

$$R = R_o \text{ for all } r \text{ at } t = 0 \qquad (2.71)$$

$$\partial C_A/\partial r = 0 \text{ at } r = 0 \qquad (2.72)$$

$$\partial C_B/\partial r = 0 \text{ at } r = 0 \qquad (2.73)$$

$$D_{A,eff}\,\partial C_A/\partial r = \alpha(C_{Ab} - C_A) \quad \text{at} \quad r=r_o \qquad (2.74)$$

$$D_{B,eff}\,\partial C_B/\partial r = \alpha(C_{Bb} - C_B) \quad \text{at} \quad r=r_o \qquad (2.75)$$

In general, the temperature of the pellet will differ from that of the gas stream, because of the heat generated or absorbed by the chemical reaction. For relatively small heats of reaction ready allowance may be made for non-isothermality, by assuming that the pellet is at uniform temperature at any given time [104]; then the unsteady state heat balance yields the following:

$$\frac{dT}{dt} = \frac{H}{Cp}\cdot\frac{dX}{dt} - [3/r_o(1-\epsilon_o)\rho_s\cdot Cp][h(T-T_u)+e\sigma(T^4-T_u^4)] \quad (2.76)$$

with

$$T = T_u \qquad \text{at} \qquad t=0$$

where, T and T_u are the pellet and environment temperatures in absolute units, H is the heat of reaction, Cp is the molar specific heat of the pellet, e is the total emissivity of the pellet, X the overall extent of reaction and σ the Stefan-Boltzmann constant.

From the knowledge of dX/dt the pellet temperature may thus be computed and the property values may then be evaluated at this correct temperature.

Eqs.(2.66), (2.69), (2.70) and (2.76), together with the boundary conditions contained in Eqs.(2.71) through (2.75) represent a complete statement of the problem.

CHAPTER 3

EXPERIMENTAL APPARATUS AND PROCEDURES

3. EXPERIMENTAL APPARATUS AND EXPERIMENTAL PROCEDURE.

3.1. EXPERIMENTAL APPARATUS.

The first part of the experimental work was to develop experimental techniques to study the rate at which lime absorbs humidity and to determine the factors that affect its hydration rates. In order to carry out this work, certain items of equipment were designed and built: a gas train, reaction furnace and steel dies to produce the calcium carbonate pellets.

3.1.1. GAS TRAIN AND FURNACE.

A schematic diagram of the furnace and the associated gas train is shown in Figure 2. The gas train comprised three streams, two of which carried CO_2 and air straight to the reaction furnace, the remaining stream carrying air to the water vapour saturator, and then to the reaction furnace. This latter stream provided mixture of air and water vapour of controlled composition. Both CO_2 and air streams were dried with anhydrous magnesium perclorate.

The volumetric flow rates of the dry gases were measured using Gallenkamp orifice meter size No.3 with di-n-butyl phthalate as the manometric fluid. Calibration data were supplied by Gallenkamp for air at one atmosphere and 15 °C. No calibration data were supplied for CO_2 and hence a

calibration curve was obtained with the aid of an Alexander-Wright total volume meter. The calibration data are presented in Fig. 3. One point in the air calibration curve shows scatter which can be attributed to an error in the calibrations reading.

To ensure that the air was at the same temperature as the thermostatically controlled water bath, it was first passed through a coil copper tubing 10 m long and 3.125 mm in internal diameter immersed in the water bath. The calculations to determine the coil length are shown in appendix A. After this coil, the air flowed through a plastic cube, which contained distilled water, and the air was made to bubble through a ceramic porous plug. The extent of saturation achieved is shown in Figure 4 for a range of water bath temperatures. The experimental points illustrated in Figure 4 were determined using a Dew Point Meter, installed between the water bath and the reaction furnace, the results showed good reproducibility. To prevent condensation of water vapour, the remainder of the gas train, consisting of 3.125 mm internal diameter copper tubing, was maintained at a temperature higher than the condensation temperature of the water by means of a heating tape.

The furnace was constructed from an alumina tube of internal diameter of 40 mm, heated by a 25 ohm resistance of Kanthal wire (0.128 ohms per yard). The ends of

the alumina tube were sealed by water cooled aluminium end assemblies with copper cooling coils.

The furnace temperature was controlled using a Gardsman controller, model JP, with Pt/Pt 13%Rh sensor. A chromel-alumel thermocouple was installed inside the furnace near the sample, the output from this thermocouple being fed to a potentiometric recorder, and a second chromel-alumel thermocouple was placed inside the sample, its leads, 0.15 mm diameter, being contained in a twin bore alumina sheath of 2 mm external diameter.

The reaction system allowed the reacting mass and the temperature of the sample to be monitored under controlled conditions of temperature, gas composition and gas mass transfer rate. This reaction system was used to monitor the calcination of the calcium carbonate pellets, the vapour phase hydration of the resulting lime pellets, the controlled partial recarbonisation of the lime pellets and the vapour phase hydration of these partially recarbonised pellets.

The reaction rates were determined using a Micro-Force Transducer which was connected to an IBM compatible Microcomputer, one slot of which was filled by a "Multi-Lab" analogue to digital card model PCL-712. The sample thermocouple and sample weight transducer being connected to this. Routines to determine the temperature and mass of

the sample from the resulting digital signals, have been written in BASIC and are listed in Appendix C. The transducer was installed on the upper part of the furnace and connected to the channel 0 of the Multi-Lab Card via a voltage amplifier.

3.1.2. THE PRODUCTION OF THE CALCIUM CARBONATE PELLETS.

The spherical pellets were prepared from "Analar" grade calcium carbonate powder of about 5-8 μm particle size, obtained from BDH Chemicals Ltd, by compaction under pressure in a three part mould made from gel-flex hot melt compound. This is a castable material based on vinyl resin which behaves as a liquid under high pressures thus producing isostatic pressing conditions.

The three part moulds were cast in a steel die previously heated to approximately 120 °C in order to avoid shrinkage. The gelflex was heated to 180 °C; at which temperature it is molten and then can be poured into the die. The steel die and mould are shown in Figure 5. The calcium carbonate spheres were compacted in a steel die, which was constructed from three concentric rings and a plunger, these are shown in Figure 6. This die was designed by Staia [118] and machined by workshop staff within the Department of Metals and Materials Engineering at the Sheffield City Polytechnic.

The taper bore of the outer ring, made from EN25 steel,

was machined in its hardened state, first by turning, using a tungsten carbide tool and finally by cylindrical grinding. The intermediate sleeve made from H13 and the inner sleeve made from D2 KE 970 steel were first rough turned both externally leaving approximately 1.5 mm of material on both faces. Machining stresses were removed at this stage by thermal stress relieving treatment in order to avoid distortion during the subsequent hardening treatment. Both items were then turned to within 0.2 mm of their final dimensions. The components were then hardened and tempered in order to develop their maximum hardness. After hardening and tempering, the intermediate and inner sleeves were precisely ground to give the correct interference and mating angle. A 2 mm radius was ground on the leading outer edge of both the intermediate and inner sleeves in order to reduce the chance of tearing when the components were pressed together. The intermediate sleeve was pressed into the outer one and finally the inner sleeve pressed into position.

In order to make the spheres, the bottom part of the gelflex mould was filled with calcium carbonate powder and the upper part was then placed over the bottom part. The two halves were aligned using metals pins and then the upper half of the mould was filled with powder. A circular disc of gelflex, 20 mm high, was finally placed on top of the mould to produce a uniform distribution of gelflex mould around the sphere, see Figure 5.

At this stage the thermocouple was placed inside the sample.

The mould and its contents were introduced into the bore of the powder compacting die. A compacting pressure of 250 MN/m^2 was applied to the plunger for five minutes and almost perfect spheres of $CaCO_3$ were obtained, see Plate 1.

3.2. EXPERIMENTAL PROCEDURE

The experimental procedure which was carried out in four main steps, is described below, the four steps are:-

i) Sintering of calcium carbonate
ii) Calcination of calcium carbonate
iii) Hydration of calcium oxide
iv) Recarbonisation of calcium oxide

3.2.1. SINTERING.

The samples were sintered at 850 °C for 120 minutes in an atmosphere of pure CO_2 in order to eliminate any trace of volatile material and to increase their strength so that they could be handled. The $CaCO_3$ samples were then cooled to room temperature to obtain their weight and diameter. Several diameters were measured in different directions using a micrometer screw gauge, and the mean found.

The samples made in this way had an apparent density of 2.0 g/cm^3 and a porosity of 0.29. After the sample had been weighed the thermocouple tails were welded onto the ends of the thermocouple leads using oxy-acetylene welding with a stainless steel flux.

The sample porosity was derived by using the following relationship:

$$\epsilon = 1 - \rho / \rho_t \qquad (3.1)$$

3.2.2. CALCINATION.

The calcium carbonate pellets were hung from the Micro-Force Transducer arm using the thermocouple leads. The thermocouple wires were 0.15 mm diameter, so that their effect on the Transducer sensitivity was negligible. The samples were heated to the calcination temperature in an atmosphere of CO_2 and kept at this temperature until a uniform temperature throughout the sample had been obtained. Once these conditions were established the CO_2 flow was changed to air to begin the calcination process, and the sample weight change periodically monitored by the computerised system.

Calcination was carried out at 750, 850, 1010 and 1100 °C in order to produce pellets with different properties.

The flow rate of air was 1.0 Nl/minute for each of the runs. The end of calcination was determined when successive X (fraction reacted) readings were the same and approximately equal to unity. The samples were held at the calcination temperature for 30 minutes after calcination had been finished in order to obtain uniform porosity throughout the whole sample.

The samples were then cooled in dry air down to the temperature for recarbonisation or hydration experiments.

The calcium oxide resulting from these calcination treatments had densities in the range of 1.155 to 1.450 g/cm^3 giving porosities between 0.65 and 0.54 respectively depending of the calcination temperature.

3.2.3. HYDRATION OF THE CALCIUM OXIDE.

When the sample was at the predetermined hydration temperature the flow of dry air was changed to the desired air/water vapour mixture and the sample weight change was continuously monitored by the computerised system. The water vapour in the gas mixture was controlled by passing the air through the water saturator, held in the water bath at the given temperature, and the temperature of the water bath was thermostatically controlled within ±0.5 °C. A layer of plastic balls on the

surface of the water bath reduced the heat and evaporation losses from the water bath. The experimental procedure allowed information to be collected covering the effect of temperature, partial pressure of water vapour, and gas flow rate.

Preliminary runs were carried out at flow rates in the range from 0.5-2.0 Nl/minute in order to determine the flow rates that should be used. At flow rates in the range of 0.5-1.5 Nl/minute the hydration reaction rates were similar, but, at higher flow rates the speed of the hydration reaction slowed down. This was thought to be because the gas mixture did not have time to come to equilibrium in the saturator at these flow rates. Consequently a flow rate of 1 Nl/minute was chosen as the optimum flow rate and the extent of saturation was determined for a range of water bath temperatures at this flow rate.

The temperature of the gas pipe line from the saturator to the reactor was maintained at 80 °C in order to avoid condensation.

3.2.4. RECARBONISATION OF CALCIUM OXIDE.

Recarbonisation was carried out to obtain a layer of calcium carbonate around the pellet of calcium oxide in order to reduce the lime hydration rate. After calcination, the sample was cooled in dry air down to the recar-

bonisation temperature. The flow of dry air was then changed to the desired air/CO_2 mixture, and the sample weight was continuously monitored by the computerised system.

The composition of the air/CO_2 mixture was controlled using two, previously calibrated, Gallenkamp orifice meters size No. 3, the flow rate being maintained at 1 Nl/minute.

Recarbonisation was carried out under different conditions of temperature and CO_2 partial pressure.

3.2.5. DISCLOSURE OF REACTION INTERFACE

The hydration and recarbonisation of calcium oxide by water vapour and carbon dioxide respectively, are heterogeneous reactions which take place at the interface between the solid and the gaseous reactants. The area of this interface and its position should be precisely known, in order to be able to approach the kinetics correctly. If there is a product layer it is also important to know its physical characteristics.

The position of the reaction interface was made visible by sectioning and polishing partially reacted samples, using SiC papers and cleaning them with alcohol. The sectioned

phenolpthalein. Phenolphalein, a colourless indicator, turns pink in the presence of alkali. The pink lime core contrasted strongly with the white calcium hydroxide or carbonate layer, see plates 2 and 3. This was due to an electrochemical reaction taking place between the different phases.

3.2.6. COMPUTER AIDED GRAVIMETRY

A computer aided gravimetric method was developed to follow the kinetics of the reactions. The spherical samples were suspended into atmospheres of controlled humidity or CO_2 partial pressure. The weight loss or gain of a pellet due to calcination, hydration or recarbonisation being measured using a micro force transducer type LB-1. The load beam type LB-1 transducer is designed to be used for the measurement of very small weights or forces, permitting measurements to be made at positions remote from the indicating equipment. It provides a permanent record when used with a chart, digital print out, or other recording instrument. It also allows a number of channels to be monitored continuously when employed in conjunction with data logging equipment.

The load type LB-1 beam consists of a crossed leaf spring hinge to which is affixed a four arm active strain gauge bridge. It has a sensitivity of 170 microV/g/V, a linearity deviation of ±0.21% and a hysteresis of 0.12%.

This transducer was connected to an IBM compatible micro-computer, one slot of which was filled by a "Multi-Lab" analogue to digital card to which the pellet thermocouple and the sample weight transducer were connected.

The PCL-712 multi-lab card is a multifunction analog/digital input/output card, its functions include 16 single ended analog inputs, 16 digital outputs and a programmable timer/counter. This full size card offers 12 bit resolution for both D/A and A/D conversions and turns the IBM PC into a powerful data acquisition instrument. The PCL-12 has an input bipolar range of ±5 V, an accuracy of ±0.2% and, < 30 microseconds of conversion time.

In order to perform the A/D conversion, the A/D converter can be triggered by internal sources or by external source. In the present work it was triggered by internal sources, including direct trigger by software and pacer trigger using the programmable timer/counter. Temperature and mass monitoring routines, incorporating the digital signals, have been written in BASIC and are listed in Appendix C.

4. EXPERIMENTAL RESULTS

The weight loss or gain, ΔW, at any time, t, was determined from the difference of the instantaneous weight of the sample, W_i, and the initial weight, W_o. These ΔW measurements were converted into fractional reaction, X, using the relationship;

$$X = \Delta W/\Delta W_t \qquad (4.1)$$

where

ΔW_t = Change of weight corresponding to complete reaction

$\Delta W_t = 0.44*W_o$ for calcination

$\Delta W_t = (18/56)*W_o$ for hydration

$\Delta W_t = (44/56)*W_o$ for recarbonisation

These relationships were included in the computer routine and the print out, which included the reaction time, sample temperature, sample weight, and fractional conversion was tabulated using a parallel printer.

4.1. HYDRATION RESULTS

The hydration results are listed in Tables I-XVI, the column heading, X, refers to overall solid conversion. Each table specifies the experimental conditions, such as

partial pressure of reactant gas, reaction temperature, pellet calcination temperature, and pellet size.

The experimental results are presented in the form of X-t plots. The effect of water vapour partial pressure, calcination temperature, and hydration temperature on the reaction kinetics are shown in Figures 7,8 and 9 respectively.

Figure 7 shows the effect of partial pressure of water vapour on hydration rates, this figure was plotted by using values from Tables II, V and XIII. It is evident from the graph that increasing the partial pressure of water vapour increases the rate of hydration when the other parameters, i.e. porosity and hydration temperature, are kept constant.

In the plots there is a marked change of slope at the 0.50/0.60 fractional hydration level. Up to this point, the rate of hydration is characterised by a steady decrease. At the 0.50/0.60 level there is an inflexion in the curves to a steeper rate. It is also evident that at the lower partial pressure of water vapour the point at which the change of slope is observed is at the longer time spans.

Visual examination of these samples at the end of the tests revealed extensive cracking in all samples. In most cases the experiment had to be terminated because the

samples disintegrated.

The calcination temperature has a strong effect on reaction rates, as shown in Figure 8 which was drawn using data from Tables II,X,XIV and XV. The figure shows two sets of graphs. In each case there are samples calcinated at different temperatures but reacted at two different partial pressures of water vapour, 2.8 kPa and 1.2 kPa. The plots confirm the previous effect of increasing water vapour on reaction rates as shown in Fig.7. However, at each partial pressure of water vapour, the sphere with the lower calcination temperature shows the greater hydration rate.

The spheres hydrated at the higher partial pressure of water vapour also show the "breakaway" phenomenon observed in the previous set of samples. At the higher partial pressure the change in slope is observed again at ± 0.50 fraction hydrated. However at the 1.2 kPa partial pressure value the change of slope is observed at about the 0.4 fractional hydration level and for the lower water vapour partial pressures it would appear that the change in slope occurs at lower levels of fractional hydration but at very much longer test times.

The hydration temperature has a weak effect on the hydration rates, as shown in Figure 9. The plot shows the results of two experiments carried out at 50 °C and 100 °C

and 2.8 kPa of water vapour partial pressure. It is clear from the graph that increasing the hydration temperature increases the rate of reaction, but its effect is not as strong as the effect of the partial pressure of water vapour and the sample calcination temperature. The experimental results were tabulated in Tables II and XVI.

During the hydration process there was a small increase in temperature inside the sample of the order of 2 to 12 °C, depending on the hydration rate. This effect is shown in the temperature of the sample in Tables I-XVI.

4.2. RECARBONISATION

As shown in section 4.1, the lime calcination temperature, which is related to the porosity of the sample, plays an important role on hydration rates, thus if the surface porosity is reduced it can become a powerful barrier to the water vapour diffusing into the sample. With this hypothesis in mind the surface of the sample was recarbonated. The main aim of this step was to determine the thermodynamic and kinetic conditions necessary to obtain a controlled layer thickness of calcium carbonate.

Sixteen runs were carried out to obtain information on the effect of temperature, partial pressure of CO_2, calcination temperature and sample size on the reaction rates

and extent of reaction. The results are listed in Tables XVII-XXXII, again each table specifies the experimental conditions.

The effect of temperature on recarbonisation rates and fractional recarbonisation is shown in Figure 10, the experimental data were taken from Tables XVII - XX and XXII. In all cases, the recarbonisation rate is fast during the initial stage, but it slows down as the reaction progresses. The recarbonisation rate of lime increases as temperature increases, reaching its maximum rate at around 500 °C. On further increasing the temperature to 700 °C, however, the recarbonisation rate falls. The extent of reaction also depends on recarbonisation temperature, as can be seen in the same figure; at temperatures less than 700 °C all the curves show a similar pattern and the maximum fractional recarbonisation is reached at 500 °C and the minimum at 400 °C. The curve obtained from the results of the experiment carried out at 850 °C shows the slowest reaction rate and the highest recarbonisation level. The time required to reach the plateau part of the curve was around nine minutes in most of the cases, however at the higher temperature of 850 °C this time was around 45 minutes.

The effect of CO_2 partial pressure and calcination temperature on recarbonisation rates and fractional recarbonisation are summarised in Figures 11 and 12 respectively.

On increasing the carbon dioxide partial pressure, the rate of the recarbonisation process and the extent of recarbonisation are increased. Both the reaction rate and the extent of reaction at one atmosphere partial pressure of CO_2 were substantially higher than those at lower CO_2 partial pressures. The lowest fractional recarbonisation (0.07) was obtained at 0.22 atm of CO_2 partial pressure. However, all the curves show similar behaviour at any partial pressure of CO_2 reaching the plateau at around the same time. Figures 11 and 12 were drawn taken the data from Tables XX,XXIII-XXV,XXIX,XXX and XXV,XXXI-XXII respectively.

The initial calcination temperature of the pellet is an important parameter during the recarbonisation reaction. Increasing the calcination temperature allows a very thin and dense product layer to be produced. Two sets of results of kinetic experiments performed at 500 °C and one atmosphere of CO_2 partial pressure and at 400 °C and 0.5 atmosphere of CO_2 partial pressure are depicted in Figure 12. At the low partial pressure of CO_2, where the lime was initially calcined at 1100 °C the maximum extent of reaction achieved was 0.06 while in lime calcined initially at 850 °C the reaction extent was 0.18. At the higher partial pressure of CO_2 the same behaviour was observed; the recarbonisation rate and extent of recarbonisation were greater when the sample was calcined at the lower temperature. The sample size is another important

parameter during lime recarbonisation, the extent of recarbonisation will be higher in smaller samples; Figure 13 shows the results of experiments carried out at 500 °C and one atmosphere partial pressure of CO_2. Again all cases show a similar behaviour; a fast first stage followed by a plateau.

During the recarbonisation process there was an increase in temperature inside the sample, that fact is depicted in Figure 14 which shows an initial quick increase followed by a plateau and then a decrease.

The recarbonated layer and the unreacted core showed a sharp interface when viewed macroscopically, see plate 2. The calcium carbonate layer thickness, δ, was obtained using the following relationship:

$$\delta = r_o - r_i \qquad (4.2)$$

where,

$$r_i = \{3m_o(1-X)/4\pi\rho_s\}^{1/3}$$

m_o = initial mass of the solid

The presence of a sharp interface reinforced the arguement for adopting this relationship.

4.3. HYDRATION WITH RECARBONATED LAYER

To test whether the recarbonated film increases the hydration resistance, nine runs were carried out, the results obtained being listed in Tables XXXIII-XLI.

The effects of layer thickness, δ, and calcination of the initial pellet on hydration rates are depicted in Figures 15 and 16. Figure 15 shows the results of six experiments carried out with samples with different layer thickness. It is clear from this figure that the hydration rate decreases as calcium carbonate layer thickness increases. The sample with 0.1 mm layer thickness behaves in a similar manner to the sample without a layer of calcium carbonate. There is a steady fractional hydration which is followed by a marked change in slope, the hydration rate, however, being lower than the unrecarbonated sample. The samples with greater carbonate layer thickness show a very low hydration rate for about 200 minutes which is then followed by a steady increase.

On the other hand, the hydration rate tends to decrease as the initial calcination temperature of the pellet is increased. This effect is shown in Figure 16, where a comparison is made between samples calcined at different temperatures, it is evident that the sample calcinated at

the higher temperature has the greater hydration resistance.

Visual examination of these pellets revealed extensive cracking. The time to achieve the critical extent of reaction before the calcium carbonate layer started to crack depended of the layer thickness and calcination temperature.

4.4. BEHAVIOUR OF INERT MATERIAL

The effect of inert material on CaO hydration reaction rates was studied by mixing $CaCO_3$ and Al_2O_3 powder, the hydration resistance of Al_2O_3 being much higher than that of CaO. The mixture of $CaCO_3/Al_2O_3$ was compacted using the method described in chapter 3 and the mixture was later sintered and calcined to obtain a mixture of CaO/Al_2O_3. The calcination temperature was 850 °C which is much lower than the melting point of the mixture, therefore it did not form a solid solution. The weight fraction of Al_2O_3 in the final CaO pellet were 10, 15, and 22% by weight. Experiments were also carried out on specimens with a layer of $CaCO_3$ of different thickness to evaluate its effect on hydration rate. The results obtained from this set of experiments are tabulated in Tables XLII-LIII.

The effects of the fraction of Al_2O_3 on hydration rate of samples which had not been recarbonised are shown in Figure 17. At the beginning of the reaction, the hydration rate decreases with increasing alumina content of the mixture. Upon further exposure to water vapour a point is reached where the curves cross each other and show marked change of slope; the fractional hydration where this change of slope occurs decreases as the Al_2O_3 content increases.

When the sample was covered with a film of $CaCO_3$ the hydration rate was considerably slower. The hydration rate decreases with increasing alumina content and the rate also decreases with increasing thickness of carbonate layer. These results are plotted in Figures 18, 19 and 20 for pellets with 10, 15 and 22% of alumina respectively and different levels of recarbonisation. The runs were carried out in an atmosphere of 2.8 kPa of water vapour partial pressure.

A common steel refining flux mixture is 70%CaO-20%Al_2O_3-10%CaF_2, therefore this mixture was tested using the same procedure cited above.

This mixture has a low melting point, so that it softened at the calcination temperature and this was shown by the change in shape of the sample from spherical to oval under its own weight. When this sample was suspended in

a Air-CO_2 stream the maximum recarbonisation extent reached was 0.005, that is a very thin film of $CaCO_3$ was formed. After that the sample was cooled and the flow was changed to an air-water vapour mixture and kept in this atmosphere for 1500 minutes, during this period of time the weight gain was 13 mg, that is, a negligible amount of hydration. In this case the $CaCO_3$ film made the mixture completely inert to hydration.

CHAPTER 5

THEORETICAL MODEL FOR HYDRATION

5. THEORETICAL MODEL FOR HYDRATION.

An approximate theoretical model has been derived, in order to examine the effect of the parameters involved in the hydration reaction of calcium oxide. In this model the mass transfer and chemical reaction processes are analysed in terms of the unreacted core model. The model is described below.

The gas phase hydration of calcium oxide

$$H_2O + CaO_{(s)} = Ca(OH)_{2(s)} + HEAT \qquad (5.1)$$

is thought to proceed topochemically in accordance with the statements illustrated in Figure 21. The interface between the hydrated shell and the unreacted core is relatively sharp in a macroscopic sense, see plate 3. The interface was seen to remain spherical and sharply defined until the calcium hydroxide layer began to crack.

On the basis of the description mentioned above the overall reaction rate can be determined using the unreacted core model, assuming that the following steps occur successively during the reaction.

1. Transport of water vapour from the bulk gas phase to the outer surface of the pellet.
2. Diffusion of water vapour through the calcium hydroxide layer to the reaction interface.
3. Chemical reaction of the gas with solid oxide to form solid product plus heat.

Step 1 is conveniently referred to as gas-film resistance. Similarly step 2 is identified as shell layer resistance and step 3 as an interface resistance. The theoretical model will be developed following the unreacted core model described in the literature survey chapter, equating it to the lime hydration in particular.

The 3 steps offer resistance in series to the overall chemical reaction. The rate equation for each step is written in terms of a molar flow of reactant gas, a partial pressure gradient driving force, and a resistance. The algebraic combination of the two transport and reaction steps is simply handled by the classical Ohm's law treatment of series resistances, eliminating intermediate concentration terms, and yielding a relationship for the rate of reaction with the driving force expressed in terms of bulk phase and equilibrium concentrations. Total resistance to the reaction is the sum of the resistances of the individual steps.

The partial pressure of water vapour in the bulk phase, at the exterior surface, at the interface, and at equilibrium are identified by subscripts b, o, i, and e respectively. The reactant gas is identified as "A" and the solvent gas (dry air) as "B".

The rate of consumption of CaO [kmol.s^{-1}] is equal to the apparent molar density of the calcium oxide core multiplied by the rate of consumption of the core volume. Simple conservation considerations show that the following identity applies:

$$\dot{n}_A = -\rho_s(dV/dt) = -\rho_s 4\pi r_i^2(dr_i/dt) \qquad (5.2)$$

For every mole of CaO reacting at the interface, 1 mole of water vapour is consumed, so that at steady state Eq.(2.55) can be rewritten as:

$$-\dot{n}_{A,g} = -\dot{n}_{A,s} = -\dot{n}_{A,c} = -\dot{n}_A \qquad (5.3)$$

Where the suffices g, s and c means in gas phase, shell layer and reaction interface respectively.

5.1. GAS-FILM DIFFUSION

If the gas composition in the bulk gas phase outside the film is assumed to be uniform, the molar flow of water vapour from the bulk gas phase to the exterior surface of the sample is given by:

$$n_{A,g} = 4\pi r_o^2 \alpha C_T \{\ln(1-[C_A^*]_b) - \ln(1-[C_A^*]_o)\} \qquad (5.4)$$

Since the experiments were carried out at very low water vapour concentrations, C_A^*, the following approach can be done:

$$\lim_{C_A^* \to 0} \{\ln(1-[C_A^*])\} = C_A^* \qquad (5.5)$$

Thus the Eq.(5.4) can be rewritten using the partial pressure of water vapour instead of concentration in the following form:

$$n_{A,g} = -4\pi r_o^2 \alpha (p_{A,b} - p_{A,o})/RT \qquad (5.6)$$

The molar flow is proportional to a conductance term and

to a driving force equal to the partial pressure difference across the film.

The mass transfer coefficient α can be obtained using Eq.(2.53).

5.2. SHELL-LAYER DIFFUSION

The rate of water vapour diffusion through the shell of hydrated lime is:

$$\dot{n}_{A,s} = -4\pi r_i^2 D_{A,eff}(\partial p_A/\partial r)/RT \qquad (5.7)$$

Since the area across which diffusion occurs is not a constant, Eq.(5.7) is integrated with respect to r between the reaction interface at r_i and the external surface at r_o under the usual quasi steady state assumption. The flow is proportional to a conductance term and to the partial pressure gradient existing across the shell layer.

$$\dot{n}_{A,s} = -[4\pi r_i r_o D_{A,eff}/(r_o-r_i)](p_{A,o}-p_{A,i})/RT \qquad (5.8)$$

where, $D_{A,eff}$ is the effective diffusion coefficient in the porous calcium hydroxide layer given by Eq.(2.21)

For the intermediate pressure range where Knudsen diffusion and molecular diffusion have to be considered together Eq.(2.38) must be used instead Eq(2.21). In the case of lime hydration ψ=1 because the water vapour diffuses in stagnant air, therefore $\dot{N}_B = 0$, and the mol fraction of the reactant gas, X_A is very small . Thus the Eq.(2.38) becomes:

$$D_{A,eff} = \{1/D_{AB,eff} + 1/D_{A,k}\}^{-1} \qquad (5.9)$$

5.3. INTERFACE CHEMICAL REACTION

The rate of consumption of reactant gas and formation of solid product due to chemical reaction is proportional to the area of the receding interface. There is no a priori method for predicting the correct kinetic expression for the interface reaction. The simplest possibility is that the surface reaction may be adequately described by simple, first order, reversible kinetics. If this is accepted as a working hypothesis, which must be tested in detail later by comparison with experimental data, the rate of the reaction is given by:

$$\dot{n}_{A,c} = -4\pi r_i^2 k(p_{A,i} - p_{A,e})/RT \qquad (5.10)$$

The specific rate constant k for the first order surface reaction has the units [$m.s^{-1}$]. The group k'=k/RT may be used as an alternative form of the rate constant having the units [$kmol.m^{-2}.Pa^{-1}.s^{-1}$].

5.4. OVERALL RATE EQUATION

Three molar current equations have been obtained describing the flow of water vapour inward for each step. In each case the flow is proportional to a partial pressure gradient providing the driving force for mass transfer or chemical reaction. At steady state all of the current equations are related by simple stoichiometry as expressed in Eq.(5.3), thus the equations may be converted into terms of water vapour molar flow and rearranged:

$$(RT/4\pi r_o^2\alpha)(-\dot{n}_A) = (p_{A,b} - p_{A,o}) \qquad (5.6')$$

$$[RT(r_o-r_i)/4\pi r_i r_o D_{A,eff}](-\dot{n}_A) = (p_{A,o} - p_{A,i}) \qquad (5.8')$$

$$(RT/4\pi r_i^2 k)(-\dot{n}_A) = (p_{A,i} - p_{A,e}) \qquad (5.10')$$

Upon algebraic addition of these equations the interface and surface concentration terms cancel out, yielding an Ohm's law type of relation for the rate of reaction with

the driving force expressed in terms of known bulk phase and equilibrium concentrations:

$$n_A = - \frac{(p_{A,b}-p_{A,e})/RT}{(1/4\pi r_o^2\alpha)+[(r_o-r_i)/4\pi r_i r_o D_{A,eff}]+(1/4\pi r_i^2 k)} \quad (5.11)$$

Viewing the overall reaction rate as the absorption rate of water vapour as determined by weight gain, the total resistance to the overall reaction is expressed by the denominator of Eq.(5.11), whose terms may be identified respectively as the gas film, shell layer, and interface resistances. The gas film resistance decreases due to the calcium oxide swelling during the hydration reaction, this will be discussed later. The shell layer resistance begins at zero and increases continuously as the shell thickens, and the chemical reaction resistance has its minimum value at zero time. The shell layer, chemical, and overall resistances all tend toward infinity as the unreacted core radius approaches zero. Thus the rate of water vapour absorption becomes very slow and approaches zero as the unreacted core is consumed.

Combining the continuity equation, Eq.(5.2), with Eq. (5.11) yields the differential expression for the rate of change of the core radius.

$$dr_i/dt = - \frac{(p_{A,b}-p_{A,e})/RT\,\rho_s}{(r_i^2/r_o^2\alpha)+[r_i(r_o-r_i)/r_o D_{A,eff}]+(1/k)} \quad (5.12)$$

The terms in the denominator may be identified as the resistances to the rate of advance of the reaction interface for spherical geometry. These terms differ from the corresponding resistances to water vapour absorption by the factor $4\pi r_i^2$. Hence, the penetration resistances either take on zero values or remain finite as reaction proceeds.

Since the sample swells during the reaction, from r_o to r_o', the Eq.(5.12) can be rewritten as,

$$dr_i/dt = - \frac{(p_{A,b}-p_{A,e})/RT\,\rho_s}{(r_i^2/r_o'^2\alpha)+[r_i(r_o'-r_i)/r_o'D_{A,eff}]+(1/k)} \qquad (5.13)$$

A useful mathematical function is obtained when the relative position of the interface, $r^* = (r_i/r_o)$, is used as the measure of reaction rate. Rearranging of Eq.(5.13) in terms of r*, gives the following overall rate equation:

$$dr^*/dt = - \frac{(p_{A,b}-p_{A,e})/RTr_o\,\rho_s}{\frac{r_o^2 r^{*2}}{r_o'^2\alpha} + \frac{r_o}{D_{A,eff}}\left[r^* - \frac{r_o r^{*2}}{r_o'}\right] + \frac{1}{k}} \qquad (5.14)$$

The ratio between r_o' and r_o, is assumed to obey the following relationship:

$$\frac{r_o'}{r_o} = \frac{1 - \Phi}{1 - \Phi/r^*} \tag{5.15}$$

were Φ is the swelling ratio. The substitution of the (r_o/r_o') value into Eq.(5.14) yields:

$$\frac{dr^*}{dt} = - \frac{(p_{A,b}-p_{A,e})/RTr_o\rho_s}{\frac{(1-\Phi/r^*)^2 r^{*2}}{(1-\Phi)^2\alpha} + \frac{r_o}{D_{A,eff}} \cdot \frac{r^*-r^{*2}}{1-\Phi} + \frac{1}{k}} \tag{5.16}$$

Integrating Eq.(5.16) between limits ($r^*=1$ at $t=0$ and $r^*=0$ at the end of reaction), gives the integrated rate equation as follows:

$$\frac{1-r^{*3}-3\Phi+3\Phi r^{*2}+3\Phi^2-3\Phi^2 r^*}{3(1-\Phi)^2\alpha} + \frac{r_o}{6D_{A,eff}} \cdot \frac{3-3r^{*2}-2+2r^{*3}}{1-\Phi} + \frac{1-r^*}{k} = \frac{(p_{A,b}-p_{A,e})}{RTr_o\rho_s} \cdot t \tag{5.17}$$

The position of the interface, r^*, can be related to the relative layer thickness, f, by means of the relationship $r^*=1-f$. Thus substituting of the r^* value into Eq.(5.17) yields:

$$\frac{3f-3f^2+f^3+3(\Phi^2-2\Phi)f+3\Phi f^2}{3(1-\Phi)^2\alpha} + \frac{r_o}{6D_{A,eff}}\cdot\frac{3f^2-2f^3}{1-\Phi} + \frac{f}{k} = \frac{(p_{A,b}-p_{A,e})}{RTr_o\rho_s}\cdot t \qquad (5.18)$$

Thus, Eq.(5.18) becomes the integrated rate equation for lime hydration. Therefore the time required for reach any hydration extent can be expressed as follows:

$$t = \left[\frac{3f-3f^2+f^3+3(\Phi^2-2\Phi)f+3\Phi f^2}{3(1-\Phi)^2\alpha} + \frac{r_o}{6D_{A,eff}}\cdot\frac{3f^2-2f^3}{1-\Phi} + \frac{f}{k}\right]\cdot \left[\frac{RTr_o\rho_s}{p_{A,b}-p_{A,e}}\right] \qquad (5.19)$$

And the time required for complete reaction is obtained by letting f=1 in Eq.(5.19):

$$t_c = \left[\frac{1+3(\Phi^2-\Phi)}{3(1-\Phi)^2\alpha} + \frac{r_o}{6D_{A,eff}}\cdot\frac{1}{(1-\Phi)} + \frac{1}{k}\right]\cdot\left[\frac{RTr_o\rho_s}{p_{A,b}-p_{A,e}}\right] \qquad (5.20)$$

5.5. OVERALL EQUATION FOR LIME HYDRATION WITH A RECARBONATED FILM

The analysis was carried out based on the steps described in sections 5.1 to 5.4, for a pellet without a layer of calcium carbonate, in which were developed three equations for the molar flow of reactant in the gas-film, product layer and interface chemical reaction. In this section a fourth equation is developed for the flow in the calcium carbonate layer, that is:

$$\dot{n}_{A,l} = -(4\pi r^2 D_{A,efl}/RT)(\partial p_A/\partial r) \qquad (5.21)$$

Eq.(5.21) is to be integrated with respect to r between the $CaCO_3/CaO$ interface at r_c and the external surface at r_o. The uncarbonated core radius, r_c, is illustrated in Figure 21.b. Plate 2 shows that the interface between the carbonated and uncarbonated layers is very sharp, so that it is mathematically valid to carry out the integration of equation (5.21) between a definite radius, r_c, and the other radius of the pellet. The rate of transfer of reactant gas through the calcium carbonate layer is thus given by:

$$n_{A,l} = - \frac{4\pi r_o r_c D_{A,efl}}{r_o - r_c} \cdot \frac{p_{A,o} - p_{A,l}}{RT} \qquad (5.22)$$

where,

$D_{A,efl}$ = Effective diffusivity in the $CaCO_3$ layer

$p_{A,l}$ = Partial pressure of gas A at the $CaCO_3/CaO$ interface, and

$r_o - r_c = \delta$ can be identified as the thickness of the calcium carbonate layer.

Following the procedure used in section 5.4 to eliminate the surface, $CaCO_3/Ca(OH)_2$ and $Ca(OH)_2/CaO$ interfaces concentration terms the following overall rate equation is obtained:

$$n_A = - \frac{(p_{A,b} - p_{A,e})/RT}{\frac{1}{4\pi r_o^2 \alpha} + \frac{\delta}{4\pi r_o r_c D_{A,efl}} + \frac{r_c - r_i}{4\pi r_c r_i D_{A,eff}} + \frac{1}{4\pi r_i^2 k}} \qquad (5.23)$$

The terms of the denominator of Eq.(5.23) may be identified respectively as the gas film, calcium carbonate layer, calcium hydroxide shell, and interface resistances. The relative importance of the gas film and interface resistances depend on the porosity of the calcium carbonate and calcium hydroxide layers, at very low porosities they can be neglected.

Equating the right-hand sides of Eqs.(5.2) and (5.23) and rewriting the resultant equation using the relative thickness of carbonated and hydrated layers, the following overall equations in terms of f, defined as $(1-r_i/r_c)$, is obtained:

$$\frac{df}{dt} = \frac{(p_{A,b}-p_{A,e})/RTr_c\rho_s}{\frac{r_c^2(1-f)^2}{r_o^2\alpha} + \frac{\delta r_c(1-f)^2}{r_o D_{A,efl}} + \frac{r_c(f-f^2)}{D_{A,eff}} + \frac{1}{k}} \qquad (5.24)$$

Integrating Eq.(5.24) and further rearrangement gives the integrated rate equation as follows:

$$\frac{r_c^2(3f-3f^2+f^3)}{3r_o^2\alpha} + \frac{\delta r_c(3f-3f^2+f^3)}{3r_c D_{A,efl}} + \frac{r_c(3f^2-2f^3)}{6D_{A,eff}} + f/k = \frac{(p_{A,b}-p_{A,e})}{RTr_c\rho_s}\cdot t \qquad (5.25)$$

6. DISCUSSION

6.1. EXPERIMENTAL ACCURACY

TRANSDUCER CALIBRATION. The transducer was calibrated measuring the voltage change due to the increase or decrease in weight using standard calibration weights in the range of 0 to 12 g. The results are drawn in the form of weight-volts plot in Figure 22. These values were used to develop an equation to obtain the sample weight change as a function of voltage using the Principle of Least Squares.

$$WEIGHT = 9.1683*V(0) + 2.7337 - C \qquad (6.1)$$

where

V(0) = voltage output, channel 0

C = Thermocouple sheath weight

Tests were performed to ensure that the Micro-Force Transducer was accurately calibrated and to prove the applicability of Equation 6.1. Standard calibration weights were used. One hundred readings were made for each point and the mean found; the transducer accuracy can be improved by increasing the number of readings. Increasing the number o f readings beyond 100 would mean,

however that the monitoring system would expend too much time performing the operation and the mean would be the average of readings at different times. For example, one hundred readings could be made in 6 seconds while one thousand would take 18 seconds - too long a time to follow a rapid reaction. A 6 seconds sampling period, however, does not introduce any serious error in the experiments carried out in this work and the accuracy obtained with 100 readings is of acceptable standard. The results are presented in the form of reading weight against standard weight plot in Figure 23 which shows the high degree of accuracy that was attained.

If the gas stream is changed for a denser or less denser gas an apparent weight increase or decrease of the sample occurs. This phenomenon is due to buoyancy forces. The effect of buoyancy resulting from density differences between dry air and moist air or carbon dioxide, was evaluated using the relationship developed by Zuliani et al [45].

$$\Delta W_b = W_s (\rho' - \rho)/\rho_s \qquad (6.2)$$

where

ΔW_b = Weight change due to buoyancy force

W_s = sample weight

ρ = density of dry air

ρ' = density of moist air or carbon dioxide

ρ_s = Apparent density of the sample

The calculations are given in appendix B which yield -0.035 mg and 0.598 mg for hydration and recarbonisation respectively. The minus sign means a decrease in weight, these values were found to be negligible.

THERMOCOUPLE CALIBRATION. The thermocouple placed inside the sample was calibrated following a procedure similar to that used for the transducer. Voltage changes due to increasing or decreasing temperature were measured and referenced against a standard thermocouple with a digital output. The values obtained are drawn in Figure 24, each point represents the mean of 100 readings. These values were used to develop a equation to obtain the sample temperature as a function of the voltage output, again using the Principle of Least Squares.

$$TEMP = 502.01*V(1) + 511.79 \qquad (6.3)$$

Where V(1) = voltage output, channel 1.

The accuracy obtained using Eq.(6.3) is ± 1 °C in the temperature range of 16 to 850 °C and ±5 in the temperature range of 850 to 1100 °C.

PARTIAL PRESSURE OF WATER VAPOUR. The partial pressure of water vapour in the gas flow was measured using a Dew Point Meter, several readings were carried out for each water bath temperature and the average found. The water vapour saturation also was determined by weighing a glass bulb containing anhydrous magnesium perclorate before and after exposure to the moist gas delivered from the water bath. The data were plotted against bath temperature in Figure 4 and compared with equilibrium saturation values reported in the literature [66].

The degree of gas saturation was sensitive to the flow rate, so that it was important to control the flow rate closely. The flow rate was measured using Gallenkamp orifice meters which were calibrated using an Alexander-Wright total volume meter, the results were in agreement with the data supplied by Gallenkamp. The values obtained for CO_2 and air were reported in the Figure 3.

PARTIAL PRESSURE OF CARBON DIOXIDE. The partial pressure of CO_2 was controlled using the Gallenkamp orifice meters to measure the flow rate of each gas, air and CO_2. The density of CO_2 was calculated from the ratio of Air/CO_2 flow rates. Since the flowmeters were accurately calibrated and since the gas mixtures were approximately 50%CO_2/50%Air the density of CO_2 calculated in this way would have the same order of accuracy as the flow measurements (±5% error). The total flow rate of the mixture air/CO_2 was controlled to 1 Nl/minute.

6.2. PERFORMANCE AND VALIDITY OF THE MODEL

A generalised mathematical model has been developed assuming that the gas film, calcium hydroxide layer and interface resistances play an important role during the hydration reaction of calcium oxide. The effect of superficial recarbonisation on hydration rates was also modelled mathematically by adding a fourth resistance, for the $CaCO_3$ layer, to the overall reaction rate equation developed for hydration of unrecarbonated lime.

By using the relations developed in section 5.4 and the previous experimental results, the chemical reaction rate constant and the interparticle effective diffusion coefficient have been evaluated and the validities of these values are discussed below.

All the physical property values and constants involved in this discussion are reported in Appendix D, together with all necessary calculations.

6.2.1. HYDRATION OF UNRECARBONATED SAMPLES

As was mentioned before the lime hydration rate for an unrecarbonated sample shows two stages. In the first stage, the reaction takes place at a sharp interface which maintains its spherical shape and in the second stage the reaction interface shows an irregular front. Where a crack had penetrated the outer reaction zone, access to the

unreacted material was made easier. In these areas the reaction front proceeded at a faster rate and the resulting interface appeared irregular. When the cracks were deep two or more concentric reaction interfaces were formed. The cracks become new penetration fronts and reaction within the core now proceeded from the cracked zone as well as from the original interfaces, the new cores reacting to the water vapour by the same mechanism as before. In this section the first stage will be analysed only, comparison between theory and experiment being made in relation to the main parameters involved.

Since $p_{A,e}$, estimated in Appendix D, is very small at low temperatures, it can be neglected and the overall rate equation may be simplified to a function of partial pressure of the water vapour in the bulk gas.

The chemical reaction rate constant k and the interparticle effective diffusion coefficient $D_{A,eff}$ can be evaluated using the method proposed by Warner [111] and latter by Yagi and Ono [119].

The overall rate equation, Eq.(5.18), can be rearranged to the following form:

$$\tau(t) = \frac{r_o}{6D_{A,eff}} \cdot \frac{3f-2f^2}{1-\Phi} + \frac{1}{k} \qquad (6.4)$$

where

$$\tau(t) = \frac{p_{A,b}}{RTr_o \rho} \cdot \frac{t}{f} - \frac{3-3f-f^2+3(\Phi^2-2\Phi)+3\Phi f}{3(1-\Phi)\alpha} \quad ; \quad [s/cm]$$

If the values of $\tau(t)$ calculated from the experimental data are plotted against the corresponding values of $\{(3f-2f^2)/(1-\Phi)\}$ a straight line would be obtained. The effective diffusivity $D_{A,eff}$ is calculated from the slope of this line and the rate constant k from the intercept of the line with ordinate axis.

The relative thickness of the hydrated shell is related to the fractional hydration, X, by

$$f = 1 - (1 - X)^{1/3} \qquad (6.5)$$

Typical plots of $\tau(t)$ vs $\{(3f-2f^2)/(1-\Phi)\}$ are shown in Figure 25. The values of $D_{A,eff}$ derived from these plots are compared with those calculated for an ideal pore structure in Table D.I, Appendix D. This table also shows the experimental conditions. In order to calculate the effective diffusivity the sample porosity was derived using Eq.(3.1). Since the Knudsen diffusion coefficient was greater than the molecular diffusion coefficient, in all the experiments using unrecarbonated samples, the effective diffusion coefficient of $H_2O_{(v)}$ through the calcium hydroxide was estimated from Eq.(2.38), see Appen-

dix D. As can be seen in Table D.I there are only small differences among the estimated diffusion coefficients and those derived graphical.

The reaction rate constant k has an Arrhenius dependence on temperature as shown in Figure 26, this plot was obtained drawing the values of ln (k), obtained graphically from plots similar to Fig.25, against 1/T using the Principle of Least Squares.

The experimental activation energy of 19.85 kJ/mol was obtained from the slope of the graph shown in Figure 26. This value is half that reported by Kasama and coworkers [116] who studied the reaction of lime immersed in liquid water. However, they did not consider that water would evaporate at the higher temperatures on the sample surface and that the reaction kinetics increase due to higher water vapour diffusivity in the product layer, so in effect their results were not simply due to chemical rate constant increasing with temperature. Their equation was reported in the literature survey chapter, section 2.4.4.

The experimental activation energy also can be calculated at the start of the reaction, assuming that no product layer has formed so that $r_i = r_o$. Under these conditions, Eq.(5.11) takes the form:

$$\dot{n}_o = \text{initial rate} = \frac{p_{A,b}/RT}{\frac{1}{4\pi r_o^2 \alpha} + \frac{1}{4\pi r_o^2 k}} \qquad (6.6)$$

The first term in the denominator is slightly temperature sensitive while the second term is very much so indeed. Therefore, by measuring the initial rates at different temperatures one should be able to determine the activation energy. At low temperatures k is small and α is comparatively large and for flow rates above the critical flow rate the gaseous boundary layer resistance is negligible. Eq.(6.6) thus simplifies to :

$$\dot{n}_o = 4\pi r_o^2 k p_{A,b}/RT \qquad (6.7)$$

or approximately:

$$\dot{n}_o = A_1 k = A_2 \text{Exp}(-Q/RT) \qquad (6.8)$$

where A_1 and A_2 are constants and Q the activation energy for the reaction. Thus a Plot of $\ln(\dot{n}_o)$ against 1/T will yield a straight line, see fig.27, and Q can be derived from its slope, which was found to be 4.35 kJ/mole. The lower activation energy value obtained using this procedure confirms that the gas film resistance can not be neglected.

The variation of transport (gas-film and shell layer), chemical and total resistances over the normalised core radius (r_i/r_o) is illustrated in Figure 28. The figure shows that the three individual resistances are important, and the process must be considered to be under mixed control for its entire duration. Particular importance of the gas-film is observed in the initial stages.

The linearity of the plots following equation (6.4), (eg Figure 25) and the agreement between the measured values and calculated values for $D_{A,eff}$, constitute strong evidence that the reaction is under mixed control. Further evidence is provided by the accuracy with which the theoretical model based on this mechanism predicts the actual course of the reaction.

The theoretical and experimental data are presented in the form of f-t plots to assess the theoretical model; Figures 29 and 30 show respectively the effect of water vapour partial pressure and the sample calcination temperature on the reaction rate. The $D_{A,eff}$ derived graphically was used to determine the theoretical plots.

The results of three runs carried out at water vapour partial pressures of 1.5 kPa, 2.8 kPa and 3.6 kPa and at 50 °C are plotted in Figure 29, the samples having been calcined at 850 °C. The corresponding theoretical values calculated under these conditions are shown as full lines in the diagrams. The experimental and theoretical data

coincide well until 0.5/0.6 of fractional hydration has occurred. Thereafter the experimental values deviate towards higher values than the predicted values. This behaviour is attributed to the cracking phenomenon described previously. The effective diffusion coefficient within the cracks is greater than that in the porous product layer so the reaction rate accelerates.

The cracking of the sample is due to the stresses that result from the expansion that occurs when lime hydrates. These stresses can be accommodated within the porous layer during the early stages of the reaction, but eventually become greater than the calcium hydroxide layer strength, causing it to crack.

The hydration rate increases with the partial pressure of water vapour. The experimental results show that a 18 mm diameter lime lump calcined at 850 °C achieves a hydration extent of 0.50 in 900 minutes at 1.5 kPa of water vapour partial pressure, while the same extent of hydration is achieved at 3.6 kPa in 380 minutes. That means, the level of hydration of the lime will be higher in the season with higher atmospheric humidity. The variation of hydrogen in steel with the variation of atmospheric moisture, reported by Plocklington [23] and Harvey [28], can be attributed among other factors to the level of moisture in the lime.

The temperature at which the sample was calcined has a strong influence on the hydration rate; samples calcined at higher temperatures show lower hydration rates. This effect is attributed to the decrease in porosity and internal surface area that occurs with increasing calcination temperature. This effect is more pronounced at higher partial pressures of water vapour. Because the reaction driving force is proportional to the partial pressure of the reactant gas and the porosity is the free space that allows gas flow inwards into the pellet; that is, there are two factors acting simultaneously . Figure 30 compares the experimental results with the theoretical model in relation to calcination temperature. It can be seen that there is good agreement especially up to 50% hydration (f=0.2).

The Eq.(5.38) states that the effective diffusion coefficient is directly proportional to the sample porosity, because the reactant gas can diffuse easily through the product layer. The results confirm that lime having a denser structure has an increased hydration resistance. Lime with low porosity can be obtained by increasing the calcination temperature up to about 1300 °C or by keeping it at a lower temperature, of the order of 1000 °C, for longer times [120,121,].

The sample size has a strong effect on the hydration kinetics, the rate increases as the lime lump radius decreases due to the greater specific surface area ($S\alpha 3/r$) and higher mass transfer coefficient.

The reaction rate increases with the hydration temperature, in the temperature range of the present study (20-100 °C), since the effective diffusion coefficient and the chemical rate constant increase with temperature, Eq.(D.3) states that $D_{A,eff}$ is proportional to $T^{1.75}$. For this reason the lime can become very reactive to water vapour during the cooling down period after its calcination, this would have harmful effects in use.

6.2.2. RECARBONISATION

Recarbonisation of lime is strongly dependent on temperature. The reaction rate has two contrary effects, one thermodynamic and the other kinetic. At high and low temperatures chemical reaction is the controlling step, thus the reactant gas has enough time to penetrate into the sample to react in the whole sample or in a wide reaction zone, and the extent of reaction achieved is very high. However, in the temperature range, 400 to 700 °C, where the gas diffusion is the controlling step, the reaction is carried out in a narrow reaction zone, and the extent of reaction is much less. This was thought to be

because the carbonate layer becomes more and more dense, so increasing the gas diffusion resistance through this external carbonate layer. In order to produce a narrow calcium carbonate layer the reaction should be carried out at the temperature where the chemical reaction is the fastest, that is, at the middle of the temperature range cited above.

The partial pressure of CO_2 also affects the carbonate layer thickness. The layer is thinner the lower the partial pressure of CO_2, when the reaction is carried out in the temperature range 400 to 700 °C. This was thought to be because the reactant gas is consumed in a narrow external film and it could not reach further solid reactant after the recarbonated film became denser. The temperature at which the sample had been calcined, which as we have seen, is related to the porosity of the sample, also plays an important role on the final layer thickness. Since a sample calcined at a high temperatures is less porous, the recarbonated layer that builds up is finer and denser as shown in Figure 12. This figure shows that the final layer thickness obtained on a sample calcined at 1100 °C was 0.2 mm, corresponding to a fractional recarbonisation of 0.07.

Summarising, the most important parameters during the lime recarbonisation process are temperature, lime porosity and partial pressure of CO_2, controlling these parameters

allows the production of any layer thickness. As Figure 14 shows; the sample is heated up during the recarbonisation process by the heat generated by the chemical reaction. A carbonated sample must therefore be cooled in an atmosphere of controlled CO_2 content in order to avoid the decomposition of the external carbonate layer.

The time to reach the maximum layer thickness at any partial pressure of CO_2 in the temperature range of 400 to 700 °C was approximately 10 minutes which is relatively short.

6.2.3. HYDRATION OF RECARBONATED LIME

On the basis of the above discussion one technical alternative to increase the hydration resistance would be to form a low porosity layer on the pellet surface keeping the inner core with the high porosity that allows slag/steel reactions to proceed without delay. The low value of $D_{A,efl}$ in the low porosity layer (see equation (5.25)) would inhibit the hydration process. The approach was to cover the sample with a film of calcium carbonate. Some runs were carried out to test the protection against hydration that this method provided, and the results are discussed below.

The main feature of the hydration rates of recarbonated lime pellets is the marked inoculation period that oc-

curred, during which there was virtually no weight gain. In run 36, for example, there was little or no weight gain by the sample for the first 200 minutes of the reaction time. In other runs, delays of up to 500 minutes could occur. It is apparent that two different processes are occurring, and these will be discussed separately.

6.2.3.1 STEADY REACTION PERIOD

During the steady reaction period, it is assumed that a definite front between hydrated and non-hydrated lime is progressing inwards towards the centre of the pellet inside the carbonated layer. The pellets in these experiments did not swell, so that it appears that the carbonated layer is exerting a compressive force on the pellet. As a consequence, the porosity of the hydrated lime will be low and, since the water vapour must diffuse through this layer, the rates of diffusion will be low. It is during this period of the reaction that equation (5-25) will apply, with low values of the water vapour diffusion coefficients in both the carbonated and hydrated layers. Thus we can rearrange the equation in the following form:-

$$\frac{r_c}{3D_e}\left[\frac{\delta}{r_o}(3f-3f^2+f^3) + \frac{3f^2-2f^3}{2}\right] + \frac{1}{k} = \frac{p_{A,b}}{RTr_c\rho_s}\cdot t' \qquad (6.9)$$

The time in this equation, t', is measured from the end of

the inoculation period.

All the variables appearing in Eq.(6.9) could be determined from the experimental data and experimental results, therefore the diffusion coefficient can be obtained directly from this equation or using the graphical procedure described in the last section.

The equation (6.9) can be rearranged in the form:

$$\frac{p_{A,b}}{RT\rho_s}\cdot t - \frac{f}{k} = \frac{r_c}{3D_e}\left[\frac{\delta}{r_o}(3f-3f^2+f^3) + \frac{3f^2-2f^3}{2}\right] \qquad (6.10)$$

And so a graph of left hand side values of this equation calculated from the experimental data against the corresponding values of term in brackets, defined as $\tau(f)$, should be a straight line. Figure 31 shows typical plots obtained indicating that they were fairly linear.

Figure 31 shows the results of three experiments plotted in this way for three different pre-treatment calcination temperatures of the original calcium carbonate pellet. It is apparent that the curves are very close to straight lines, so the proposed process for the hydration of the interior lime sphere would appear to be reasonable. Values of the diffusion coefficient of the compressed lime

are obviously a function of the initial pre-treatment calcination temperature at which the lime was formed. The value for lime formed at 850 °C is 1.2×10^{-3} $cm^2.s^{-1}$ whereas the values for pre-treatment calcination temperatures of 1000 and 1100 °C are 2.8×10^{-4} and 2.6×10^{-4} $cm^2.s^{-1}$, respectively. These values are in keeping with the results obtained by Staia [118] for diffusion coefficients in non hydrated lime, although they are an order of magnitude smaller.

6.2.3.2 Inoculation period.

Figure 15 shows hydration experiments for a number of samples for which the pre-treatment calcination temperature was the same and which were all recarbonated at the same temperature under the same partial pressure of CO_2. The only difference was that they were re-calcined for different periods of time to produce different recarbonated shell thicknesses. It is apparent that these curves differ almost entirely due to different inoculation times. To test whether this is so, Figure 32 has been plotted using equation (6-10) but against the real time. As with figure 31, the plots give good straight lines once the reaction starts, but they also show the inoculation period to be determined from the intercept on the vertical axis.

Table LV shows the relationship between the inoculation period and the thickness of the calcium carbonate layer -

the thicker the layer, the longer the inoculation time. This suggests that the inoculation delay could be related in some way to the diffusion of water vapour through the recarbonated layer. In order to examine this suggestion further, estimated diffusion coefficients are also tabulated in Table LV, having been calculated approximately from unsteady state diffusion theory. To a rough approximation, the time, τ, taken for a concentration change to penetrate a distance δ is related to the diffusion coefficient, D, following the equation:-

$$\sqrt{(D\tau)} = \delta \qquad (6.11)$$

Estimated values determined in this way are shown in sixth column of table LV. These values show an interesting characteristic. When the thickness of the layer is about 0.1 or 0.2 mm, the coefficients are of the order of 10^{-8} $cm^2.s^{-1}$ whereas they are an order of magnitude greater when the layer thickness is about 0.5 to 0.6 mm. Literature values for the diffusion coefficient of water vapour in pure calcium carbonate could not be found, but experiments on zeolites [122] have provided values of the order of 10^{-6} $cm^2.s^{-1}$. Zeolites have an open structure that is relatively easy for water vapour to diffuse through, so that a diffusion coefficient value of 10^{-8} $cm^2.s^{-1}$ could indicate that water is diffusing through the calcium

carbonate lattice across a layer of coherent calcium carbonate.

There is some evidence in Table LV to support this suggestion since the bottom two results - for the low porosity lime originally calcined at 1000 and 1100 °C - show recarbonated layers of zero porosity, and the lowest diffusion coefficients. Here, also, the diffusion coefficient for the thinner layer is significantly lower than the coefficient for the thicker layer.

The variation of the estimated diffusion coefficient with the layer thickness could be explained if the advancing recarbonisation reaction front were under compression as the lime crystallites enlarged as they transformed into the carbonate. The compressive forces involved would have two effects. They would compress the crystallites together to form a zero porosity barrier to the diffusing CO_2 and they would place layers of the recarbonated layer outside the reaction front under tension. These layers would then open up, forming low porosity channels for the water vapour to diffuse relatively easily. As a consequence, the diffusion coefficient, estimated from the carbonated layer as a whole, would increase as the layer thickness increased. This, of course, is the tendency exhibited by the results in the table.

The same type of mechanism could explain the acceleration in the hydration rate, once the inoculation period is

completed. This acceleration occurs once the water vapour has penetrated the recarbonated layer and is starting to react with the lime. The compressive forces created in the zone of this reaction would, again, place the outer layers of the sample under tension, opening up the structure and allowing the higher diffusion coefficients, calculated from Figure 31, to be established.

Thus it appears reasonable to conclude that the hydration of the partially recarbonated lime samples occurs by the same mechanism as the uncarbonated ones. The only difference is that an inoculation period exist during which water vapour is diffusing through highly coherent layers of calcium carbonate on the outside the lime.

The hydration rate is lower as δ increases and as its porosity decreases, the layer porosity having a stronger effect than the layer thickness. This is an important finding because it suggests that the formation of a very thin carbonate layer of low porosity would be effective in inhibiting hydration without impairing the quality of the lime, and would, moreover, minimise loss of CaO.

The experimental results and those obtained using Eq.(6.9) were compared. Such comparison are made in Figure 33.a and 33.b. The experimental results are taken from runs 33-35, and 38,40 and 41, in which the partial pressure of $H_2O_{(v)}$ was 2.8 kPa for the three first runs

and 1.2 kPa for the last three runs. Values of the parameters used in the calculations were taken from the same runs. The relative product layer thickness curves predicted by the model match fairly well with the experimental results until the $CaCO_3$ layer cracks due to the swelling of the $Ca(OH)_2$ shell.

The critical extent of hydration required to carbonate layer beginning to crack depend on its thickness, and the time required to reach such extent of hydration also depends on its thickness and porosity. After the layer have been broken the sample loses its hydration impermeabilisation. Fig.15 shows that a 0.1 mm layer thickness required an extent of reaction of 0.2 for cracking. So a 18 mm pellet with calcined at 1100 °C and a recarbonated layer thickness of 0.2 mm exposure in a 1.2 kPa partial pressure of $H_2O_{(v)}$ atmosphere will require more than 150 hours to reach such level of hydration while a sample without carbonated layer will be completely hydrated in around 24 hours. The lime used in steelmaking generally is calcined in the temperature range of 1000-1200 °C and the average of atmospheric moisture is 1.2 kPa.

6.2.4. HYDRATION OF LIME/ALUMINA MIXTURES

The kinetics of hydration of pellets prepared from CaO/Al_2O_3 mixtures can be analysed using the equations (5.18) and (5.25) for unrecarbonated and recarbonated samples respectively.

UNRECARBONATED SAMPLES.- In section 4.4 it was mentioned that the CaO/Al_2O_3 did not form a solid solution at the calcination temperature, so that the role played by alumina was to close up the open pores to water vapour flow towards the reaction interface and reduce the surface area in which the reaction can be carried out. Under these conditions the chemical rate constant, k, was not affected by the alumina content, thus the k values obtained for pure lime can be used to determine the hydration rate of the mixture.

In this case the hydration rate of the mixture can be derived using Eq.(5.18). Considering that the rate of the chemical reaction is proportional to the surface area and that only a fraction of the total surface area of the sample is available for the reaction; Eq.(5.18) can be rearranged to the following form:

$$\frac{3f-3f^2+f^3+3(\Phi^2-2\Phi)f+\Phi f^2}{3(1-\Phi)^2\alpha} + \frac{r_o}{6D_{A,eff}}\cdot\frac{3f^2-2f^3}{1-\Phi} + \frac{f}{X_{CaO}k} = \frac{p_{A,b}-p_{A,e}}{RTr_o\rho_s}\cdot t \qquad (6.12)$$

where, X_{CaO} is the CaO mass fraction in the mixture.

Since f could be calculated from the continuous trace of the sample's weight, all the variables appearing in Eq.(6.13) could be determined except the effective diffusion coefficient of the $Ca(HO)_2$ layer. It can be determined directly from the equation or by using the graphical method described above. The effective diffusivity, 0.069 cm^2/s was similar for three the different mixtures with alumina contents of 10, 15 and 22% by weight. This unexpected behaviour is attributed to the following mechanism. The alumina content reduces the lime porosity, but, increases the porosity of the hydrated layer. Analysing the porosity using the Eq.(3.1) shows that the initial sample porosities were 0.61,0.60 and 0.58 for pellets with alumina contents of 10, 15, and 22% respectively while the product layer porosity was 0.59 in all the cases. The effective diffusion coefficient is thus similar in the three levels of alumina content. Therefore, the major effect of the alumina on the hydration rate is the reduction of the effective reaction surface area.

The experimental results and those derived from the Eq.(6.13) are compared in Figure 34 which shows good agreement until 0.4/0.5 of fractional hydration. From this point the experimental reaction rate is greater than that predicted theoretically due to the cracking phenomenon. It is possible to see that the mixtures behave the

same as pure lime, nevertheless, the cracks appear at a lower level of reaction, under these circumstances the alumina accelerates the lime hydration.

RECARBONATED SAMPLES.- The kinetics of hydration of recarbonated pellets made of CaO/Al_2O_3 mixtures can be studied using Eq.(5.25). In this particular case the gas film resistance was very small compared to the carbonate and calcium hydroxide layers and the interface resistances, so it can be neglected.

The surface area exposed to the gaseous reactant is reduced in proportion to the mass fraction of inert material introduced, producing an increase on the interface resistances. Thus Eq.(5.25) can be rearranged to the following form:

$$\frac{r_c\delta(3f^2-3f^2+f^3)}{3r_oD_{A,efl}} + \frac{r_c(3f^2-2f^3)}{6D_{A,eff}} + \frac{f}{X_{CaO}k} = \frac{p_{A,b}}{RTr_c\rho_s}t \qquad (6.13)$$

Again, assuming similar effective diffusion coefficients for both layers, $D_{A,efl} \approx D_{A,eff}$, thus an overall effective diffusion coefficient, D_e, can be used and Eq.(6.13) is rearranged as:

$$\frac{r_c}{3D_e}\left[\frac{\delta}{r_o}(3f-3f^2+f^3) + \frac{3f^2-2f^3}{2}\right] + \frac{f}{X_{CaO}k} = \frac{p_{A,b}}{RTr_c\rho_s}\cdot t \qquad (6.14)$$

All the parameters in this equation are known, therefore the effective diffusion coefficient is obtained directly from this equation or graphically, plotting the term in bracket against

$$\frac{p_{A,b}}{RTr_c\rho_s}\cdot t - \frac{f}{X_{CaO}k}$$

allows D_e to be obtained from the slope of the graph. The D_e values were obtained directly from the equation, various values were determined for each run and the mean found, the values were in the range of 5.5×10^{-4} to 8.5×10^{-4} cm^2/s

The addition of inert material to lime has a weak influence on the effective diffusion coefficient of the recarbonated layer, since the porosity of this layer increases as the alumina level is increased. The hydration rate, however is lowered because the interface resistance is strongly affected.

The relative layer thickness, f, is plotted against time in Figure 35. This figure compares the experimental results and those predicted by the theoretical model, the

figure shows again that the reactant gas need certain time to reach the $CaCO_3/CaO$ interface. Figure 35 also shows a good correlation with the experimental results.

6.3. POTENTIAL APPLICATION FOR HYDROGEN CONTROL IN STEELMAKING

In almost all of the secondary steelmaking processes, lime is used to control the slag composition in order to carry out slag/metal reactions. This research shows that lime could reach high levels of hydration in a few hours, at contents of water vapour as low as atmospheric, and these levels of hydration are a function of the partial pressure of the water vapour, so that it is reasonable assume that the level of humidity of the lime used in steelmaking process depend of the atmospheric moisture. Lime generally is transported and stored in open containers, so that it has enough time to reach high levels of hydration before being used. The research also shows that the hydration level achieved in any given time depends on the calcination temperature, being higher in lime calcined at the low temperature. This fact could be used to compensate the seasonal variation in the lime humidity. If all the water contained in the lime goes into the molten steel/slag system it would increases considerably the hydrogen content in the steel taking into account that is common practice add 10 kg of lime per tonne of steel.

Lime is added in two ways, to the surface of the molten steel or by injection deep into the steel bath. When it is added in the first way a part of the moisture content in this lime is evaporated and passes to the atmosphere and the other part is dissolved in the slag and transferred to the steel. On the other hand when the lime is added by injection most of the lime moisture content is dissolved into the liquid steel because there is more contact time.

If this source of hydrogen is minimised the consumption of stirring gas and the treatment time could be reduced considerably. The passivation of lime by forming a carbonate film during it cooling down should be considered as a possible solution to this problem. A fractional carbonisation of around 10% is able to reduce considerably the hydration rate, such level of recarbonisation does not represent high loss of CaO and the heat loss from liquid steel due to the thermal decomposition of the recarbonated layer is low, furthermore, the newer technologies used in secondary steelmaking have reheating facilities in order to compesate heat loss.

The kinetic parameters that govern the recarbonisation reaction have been established in this research. Any layer thickness can be produced, from a few microns to completly recarbonisation controlling carefully such parameters. The physical properties of the recarbonated

7. CONCLUSIONS

Using a computer aided gravimetric technique, the kinetics of lime hydration with water vapour have been investigated, in H_2O/Air mixtures at atmospheric pressure and temperatures between 20 and 100 °C. The results have been analysed using the unreacted core shrinking model modified to include effects due to the swelling of the sample. The only parameters to be determined experimentally were the chemical rate constant and the effective diffusion coefficient of water vapour through the $Ca(OH)_2$ product layer. The effect of superficial recarbonisation and inert material additions on the reaction rate also was investigated. Measured and calculated results showed satisfactory agreements. On the basis of the results obtained it is possible to conclude that:

1. The gaseous hydration of lime pellets proceeds through a sequence of transport and chemical steps acting in series.

2. Theoretical examination of the gas-film, product shell and interface resistances shows that at the beginning of the reaction the interparticle diffusion resistance is negligible and the gas-film and the interface resistances were the controlling steps. As the reaction progresses both the interface and the interparticle diffusion resist

ances became the controlling steps. That is, the lime hydration is controlled by mass transfer and chemical steps.

3. The gaseous hydration process occurred without an incubation period. The hydration rate was directly proportional to the partial pressure of water vapour in the reactor and the lime reactivity (porosity, surface area and grain size). The hydration rate also was affected by the reaction temperature, increasing as the temperature increase.

4. The chemical rate constant, the activation energy and the effective diffusion coefficient were determined from experimental hydration data by a graphical analysis.

5. The present research shows that covering the lime lumps with a film of $CaCO_3$ increases considerably the hydration resistance. This method of lime pasivation could be used to minimise hydrogen pick up by liquid steel from hydrated lime.

6. It was shown that additions of alumina contributed to an increase the hydration resistance. Such additions reduce the surface area exposed to gaseous reactant, nevertheless, the samples had a tendency to crack at lower levels of fractional hydration than those free of Al_2O_3

accelerating the reaction. The hydration resistance could be increased by firing the mixtures at temperatures where a solid solution can be formed.

7. It was established that the samples prepared from CaO with additions of alumina and fluorspar, calcined at 850 °C, had a high hydration resistance. In this case both the transport and chemical resistances were increased. This result could be applied to increase the hydration resistance of synthetic slags or lime-fluorspar coverings of steel welding electrodes.

R E F E R E N C E S

1. Kern, D.W., Stelts, P.D., Fioravanti, K.J., Iron & steelmaker, July 1990, 33-40.

2. Frueham R.J., Iron & steelmaker, June 1990.

3. Emi, T. and Iida, Y. Scaninject III, part I, Lulea, Swede, June 15-17, 1983.

4. Margot-Marette, H., Bardou, G., and Charbonnier, J.C., Corros. Sci., 27, (10-11), 1987, 1009-1026.

5. Salvago, G., Fumagalli, G., Cigada, A., and Scolari, P. Corros. Sci., 27, (10-11), 1987, 1205-1212.

6. SCRATA, Technical report No.50.

7. Bastien, P. Ontode 1961,12 Aug. 169 CEGB Translation No.420.

8. Tyson, W.; Canadian Metall. Quar., vol.18,No.1,1979.

9. Sunada, H.; Trans. ISIJ, vol. 28, 1988, (8),678-682.

10. Grant, F.R., and Russell, H.J.; J. Nuc. Mater. 155-157, (1988),760-765, North-Holland Amsterdan.

11. Iyer, K.J.L. Can. Metall. Quar., Vol. 28, No.2,1989, pp 153-158.

12. E. Snape. Corrosion. J.. 4, 253, 1969.

13. Charbonnier, et al. Rev. Metall., Cah. Inf. Tech., Jan. 1989,85,(1),91.

14. L. Coudreuse and J. Charles. Corrosion Sci., 27, (10-11), 1987, 1169-1181.

15. G.M. Pressouyre. Hydrogen Effects in Metals [Conf. Proc.]. The met. Soc. of AIME, Aug. 26-31, 1980, USA, 27-36.

16. R. Gibada and D.S. De Miglio. Hydrogen Effects in Metals. [Conf. Proc.]. The Metallurgical Society of AIME, Aug. 26-31, 1980, USA.

17. V. Pilous and K Lobl. Trans. ISIJ, Aug. 1987, 27,(8),673-676

18. L. Qiao, C. Hsiao, and W. Chu. Scr. Metall. May 1988, 22, (5), 627-630.

19. E. Snape. Corrosion 23, 154, 1967.

20. J. P. Hirth. Metall. Trans. A, 11A (1980), 861

21. H. Kimura and H. Matsui: Scr. Metall., 21(1987),319.

22. Zuliani, D.J., Hasegawa, M., Heard, R.A., Sosinsky, D.J., and McLean, A. Can. Met. Quart., 1981,20, 181-187.

23. Pocklington, D.N., Martin, E., and Betka, G., "Hydrogen in Steel" [Proc. Conf.], Bath, England, 14-16 Apr. 1982, The Institute of Metallurgists.

24. Okamoto, S., Veda, T., Marukawa, K., Yamasaki, I., and Hamana, T., "Proc. 7th International Conference on Vacuum Metallurgy", vol.2, Tokio Jpn., 26-30 Nov., 1982,
Iron and Steel Institute of Japan.

25. Riboud, P.V., and Gatellier, C., Ironmaking and Steel making, 1985, 12,(2),79-86.

26. Fruehan, R.J., "Ladle Metallurgy Principles and Practice". Iron and Steel Society-AIME, USA, 1985.

27. Haida, O., Nakanishi, K., and Emi, T., Scaninject II, part I, 2nd International Conference on Injection Metallurgy, Lulea, Sweden, June 12-13, 1980.

28. Harvey, D.J. "Hydrogen in Steel" [Proc. Conf.], Bath, England, 14-16 Apr. 1982, The Institute of Metallurgists.

29. Jaeger, H. et al. Investigation Regarding the control of Hydrogen and Aluminium content in ESR Ingots", Boehler Bros. and Co. Ltd.

30. Hills, AWD, private communication, Sheffield City Polytechnic (1988).

31. Borisov, V.M., et al. Steel USSR, May 1980, 10,(5), 287.

32. United States. "The Making, Shaping and Treating of Steel"; 9th Ed. Harold E. McGannon, USA, 1970.

33. Jackson, W.J. Monograph 4, Steelmaking for Steel Founders, "Gases in Steel". Steel Castings Research and Trade Association, Sheffield, U.K., 1975.

34. Gatellier, C., Gaye, H., Rev. Metall.,Cah. Inf. Tech., Jan. 1986,83,(1),25-42.

35. Vashukov, I.A., Steel USSR, Aug. 1983.13,(18), 346-349.

36. Carrier, B., Nadif, M., Gatellier, C., Rev. de Met.-CIT April 1988, 308-315.

37. Sommerville, I.D.; Scaninject IV part I 4th Internation al Conference on Injection Metallurgy, Lulea, Sweden, June 11-13, 1986.

38. Stermsek, R., and Lange, K.W.; Can. Met. Quart. Vol.20, 2,(1981), 189-197.

39. Schurmann, E., and Sittard, M., Steel Res.,1986,57,(11).

40. Apa, L., Metallurgy (Bucharest), Jan, 1985,37,(1), 20-24.

41. Schwerdfeger, K. and Schubert, H.G., Metall. Trans. B,vol. 9B, 1978, 143-44.

42. Sosinsky, D.J., Maeda, M. and McLean, A., Metall. Trans. B, vol.16B, 1985, 61-66.

43. Fhruehan, R.J. Electric Furnace Conference [Proc. Conf.], Kansas City, Mo., USA, 7-10 Dic. 1982, Iron and Steel Society/AIME.

44. Fhruehan, R.J., Electric Furnace Conference [Proc. Conf.], Canada, 4-7 Dic. 1984, Iron and Steel Socie ty/AIME.

45. Zuliani, D.J., Iwase, M., and McLean, A., Trans. ISS, 1982, vol.1, 61-67.

46. Iguchi, Y., and Fuwa, T., Trans. ISIJ, 1970, vol.10, 29-35.

47. Rein, R.H., and Chipman, J., TMS-AIME,1965, vol.233, 415-21.

48. Jeszensky, G., Kajita, T., Rawson, J.D.W., and Bryant, A.W. Metall. ABM, Jul. 1083,39,(308),345-49.

49. Mass, H., 7th Int. Conf. on Vacuum Metallurgy.

50. Sievensson, I., Solidification Technology in the Foundry and Cast House [Proc. Conf.], Coventry, England, 15-17, Sep. 1980, The Metals Society.

51. Latash, Yu. V., et al. Russ. Met., 1979,(3), 40-44.

52. Fruehan, R.J. Iron & Steelmaker, July, 1990.

53. Sobolev, V.V., and Nesterov, N.A., Steel USSR, Jan. 1986,16, (1), 25-27.

54. Yavoiskii, A.V., et al., Steel USSR, July 1981, 11, (7), 377-79.

55. Yavoiskii, A.V., Telkov, V.I., and Terziyan, S.P., Steel USSR, May 1981, 11,(5), 251-252.

56. Moriki, H., Akiyoshi, M., and Tsutomu, N., Sumitomo Search, Nov. 1979, (22),55-57.

57. Xuewu, Chen., Iron Steel (China), Dec. 1982, 17, (12), 34-41.

58. Teoh, L.L., 13th CMMI Congress. Vol.4, Metallurgy [Proc. Conf.], Singapore, 11-16 May 1986.

59. Fruehan, R.J., and Martonik, L.J., Metall. Trans.B, vol.12B, 1981, 379-84.

60. Riboud, P.V., and Gatellier, C., Iron Making and Steel Making, 1985, 12,(2), 79-86.

61. Susuki, K. et al, Iron & Steelmaker, July 1982, 33

62. Choudhury, A., Baver, K.H., Wagner, H., and Bruckmann; Steel Times Int. Oct. 1985.

63. Lefebure, G., Nicaise, P., and Andre, P., Secondary Steelmaking for Product Improvement. The Institute of Metals, London, Oct. 1984.

64. Binder, P., Rushe, J., Zahs, G., and Stolte G., Secondary Steelmaking for Product Improvement. The Institute of Metals, London, Oct. 1984.

65. Hills, A.W.D.; Chem. Eng. Sci., 23, (1968), 287.

66. Handbook of Chemistry and Physics. 68th Ed. 1987-1988.

67. Muller, M.B.; Scand. J. of Metall. 19, 1990, 64-71.

68. Anderson, L.C., and Vernon, J., J. Iron Steel Inst., 1970, 208, 329-335.

69. C.A. Natalie and J.W. Evans., Iron & Steelmaking 1979, 3

70. Slatter, D. de L., Ironmaking and Steelmaking, 1976,3.

71. Borras, A.L., and Albini, A.L., Siderurgia, Oct.-Nov.-Dec. 1977,4,(14), 97-135.

72. Chartterjee, A., et al., Trans. of the Indian Inst. of Metals, vol.36, No.2, Apr. 1983.

73. Gregory, J.A. et al., J. Iron Steel Inst., 1965, 203, 886.

74. Leonard, L.A., J. Iron Steel Inst., 1970,208,324.

75. Matsushima, M. et al., Trans. ISIJ, 1977, 17, 442.

76. Thomas, W.J., Comprehensive Chemical Kinetics, vol.23, Ed. C.H. Bamfor. 1985.

77. Szekely, J., Evans, J.W., and Sohn, H.Y., "Gas-Solid Reactions", Academic Press, N.Y. 1975.

78. Levenspiel, O., "Chemical Reaction Engineering", Second Ed., 1972, John Wiley & Sons, Inc.

79. Scott, D.S., and Dullien, F.A.L.; A.I.Ch.J. 8,113, 1962.

80. Wheeler, A., Catalisis, P.H. Emmet, Ed., vol.2, Chap.2, pp.105-66, Reinhold Publishng Corp., New York, 1955.

81. Mason, E.A., and Marrero, T.R.; Advances in Atomic and Molecular Physics, 6, 200, 1970.

82. Hoogschagen, J.; Ind. Eng. Chem. 47, 1955, 906.

83. Knudsen, M.; "The Kinetic Theory of Gases", 3rd Ed. Wiley, New York, 1950.

84. Mason, E.A., and Evans, R.B.,III.J.Chem. Educ. 46, 1969,358.

85. Evans, R.B.III, Watson, G.M., and Mason, E.A.; J. Chem. Phys., 1961, vol.35, pp.2076-83.

86. Bosanquet, C.H.; British TA Report BR-507, September 27, 1944.

87. Chapman, S., and Cowling, T.G., "The Mathematical Theory of Non-Uniform Gases", 3rd. Ed. Cambridge Univ. Press, 1970.

88. Hirschfelder, J.O., Curtiss, C.F., and Bird, R.B., "Molecular Theory of Gases and Liquids", Wiley, New York, 1954.

89. Sandler, S.I., and Mason, E.A., J. Chem. Phys. 48, 1968, 2873.

80. Olson, R.G., and McKewan, W.M., Trans. Metall. Soc. AIME 236(1966),1518.

91. Takahashi, R., Kani, A., Yagi, J., and Omori, Y., Bull. Res. Inst. Miner. Dressing Metall., Tohoku Univ., 31, (1975), 98.

92. Turkdogan, E.T., Olson, R.G., and Vinters, J.V.; Carbon, 8,(1970),545.

93. Wicke, E., and Kallenbach, R., Kolloid-Z., 2(1941),135.

94. Shigeno, Y., Kobayashi, S., Takeda, K., Goto, H., and Omori, Y.; Bull. Resh. Inst. Miner. Dressing Metall., Tohoku Univ., 39(1983), 25.

95. Shigeno, Y., Kobayashi, S., and Omori, Y., Trans. Iron Steel Inst. Jpn., 27(1987),169.

96. Shigeno, Y., Kobayashi, S., and Omori. Y., Trans. Iron and Steel Inst. Jpn., 28(1988),697.

97. Staia, M.H., Cambell, F.R., and Hills, A.W.D.; Ind. Eng. Chem. Res., 26, 3, (1987),438.

98. Evans, R.B., Watson, G.M., Mason, E.A.; J. Chem. Phys. 36, (1962),1894.

99. Ishida, M., and Wen, C.W.; AIChEJ, 14(1968),311.

100. Kunii, D., and Levenspiel, O.; "Fluidization Engineering", (1968), 481, J. Wiley, New York.

101. Satterfield, C.N., and Feakes, F. AIChEJ, 5(1959),115.

102. Hara, Y.; Trans. ISIJ, vol. 12(1972), 358.

103. Spitzer, R.H., Manning. F.S., and Philbrook, W.O.; Trans Met. Soc. AIME, 236 (1966). 1175.

104. Lahiri, A.K., and Seshadri, V.; JISI,206(1968),1118.

105. Wen, C.Y.; Ind. Eng. Chem., 60(1968),34.

106. Szekely, J., and Evans, J.W.; Chem. Eng. Sci.; 25(1970), 1091.

107. Szekely, J., Evans, J.W., Met. Trans. 2,(1971), 1691.

108. Sohn, H.Y., and Szekely, J.; Chem. Eng. Sci., 27,(1972),763

109. Bowen, J.H., and Cheng, C.K.; Chem. Eng. Sci.,24,(1969),1829.

110. Bird, R.B., W.E. Stewart, and E.N. Lightfoot, "Trans port Phenomena", John Wiley & Sons, New York, 1960.

111. Warner, N.A.; Trans. TMS-AIME, 1964, vol.230, pp. 163-78.

112. Wen, C.Y., and Wang, S.C.; Ind. Eng. Chem., 62, 30, (1970)

113. Hills, A.W.D., "Heterogeneous Kinetics at Elevated Temperatures." Ed. by G.R. Belton and W.L. Wor rell, Plenum Press, 1970, pp 449-501.

114. Ishida, M., and Wen, C.Y.; Chem. Eng. Sci., 26(1971),1031.

115. Ishida, M., Wen, C.Y., and Shirai, T., Chem. Eng. Sci., 26, (1971), 1043.

116. Kasama, S., Suzuki, S., and Sato, K., Trans. ISIJ, 26,1986.

117. Usui, T., Ohmi, M., and Yamamura, E.; ISIJ Intern., 30,(1990),5,347.

118. Staia, M.H., Ph. D. Thesis, Department of Metals and Materials Engineering, Sheffield City Polytechnic, England U.K., 1983.

119. Yagi, T., and Ono, Y., Trans. ISIJ, 8, 1968, 377-381.

120. Borgwardt, R.H., Roache, N.F., and Bruce K.R., Ind. Eng. Chem. Fundam. 1986, 25, 165-166.

121. Marsh, D.W., and Ulrichson, D.L., Chem. Eng. Sci., 40, (3), 1985, 423-433.

122. Barrer, R.M.B., and Fender,B.E.F.; J.Phiys. Chem. solids, 1961,21,12.

123. Fuller, E.N., Schettler, P.D., and Giddings, S.C., Inds. Eng. Chem. 58, 19, may 1966.

124. Geiger, G.H., and Poirier, D.R. "Transport Phenomena in Metallurgy". Addison-Wesley publishing Company, Massachusetts, 1972.

125. Kubaschwski, O., and Alcock, C.B. Metallurgical Thermochemistry. 5th Ed. Pergamon Press, Oxford, 1979.

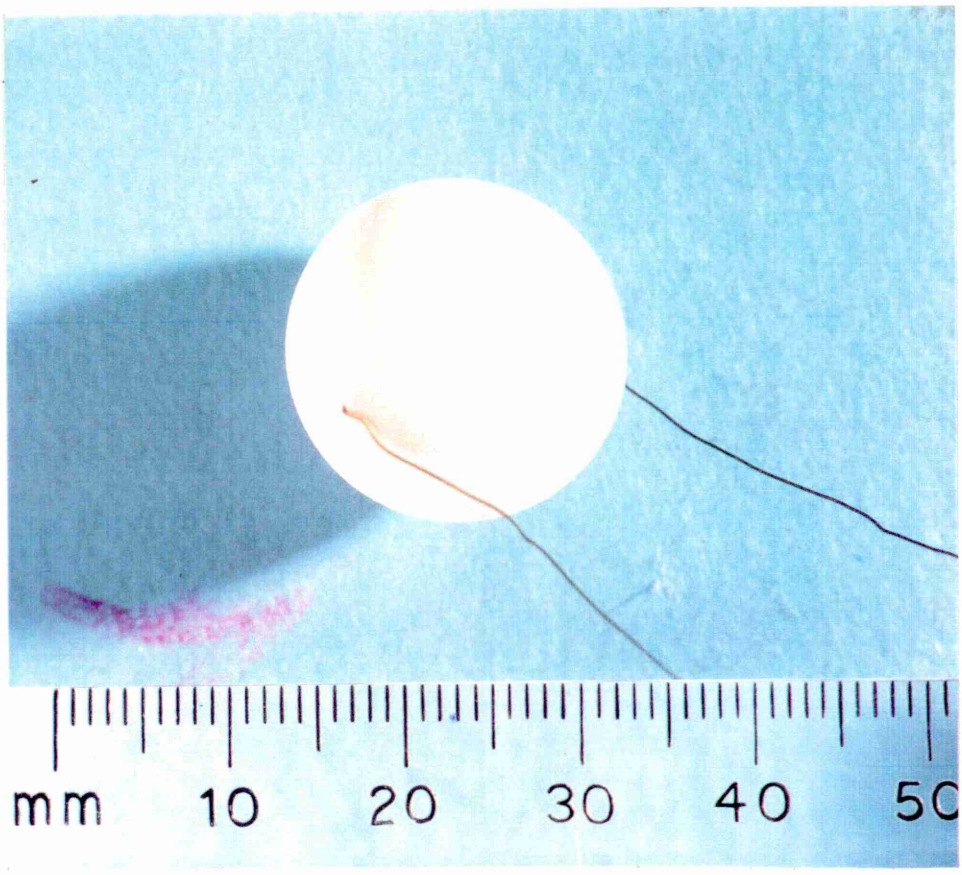

PLATE 1: LIME SPHERE AND THERMOCOUPLE LEADS.

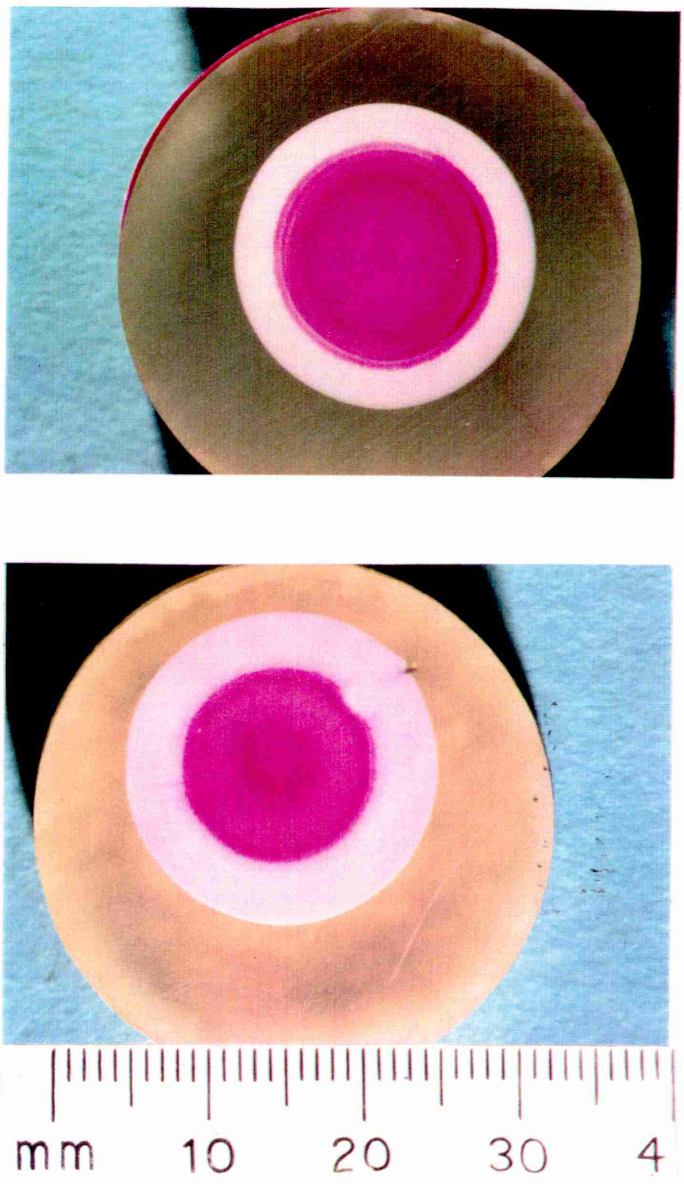

PLATE 2: PHOTOGRAPH SHOWS a) RECARBONISATION REACTION INTERFACE b) HYDRATION REACTION INTERFACE IN A RECARBONATED PELLET.

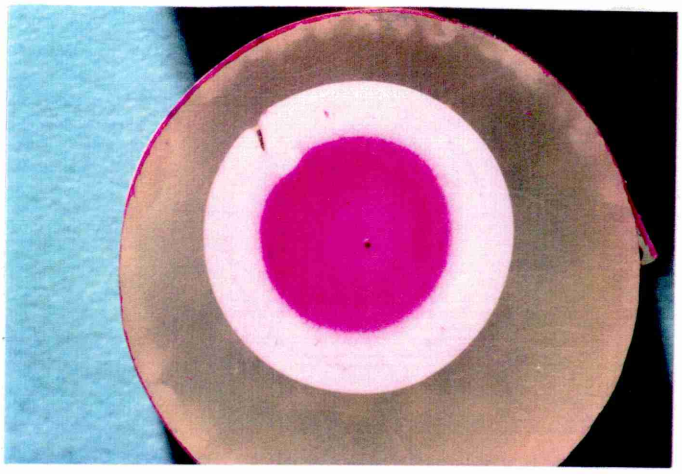

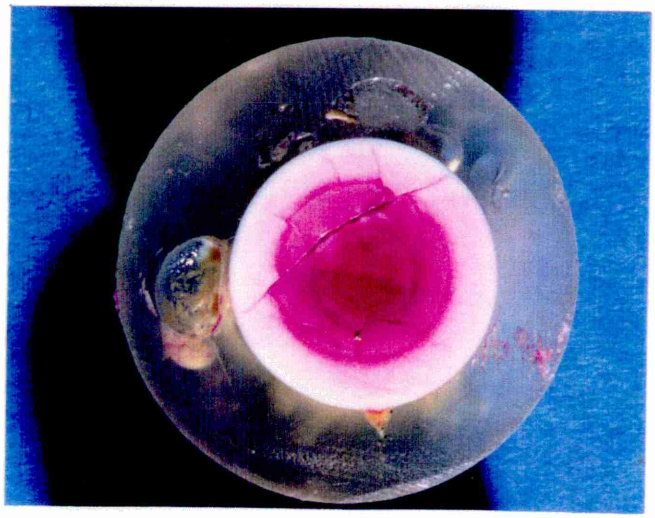

PLATE 3: PHOTOGRAPH SHOWS HYDRATION REACTION INTERFACE IN UNRECARBONATE PELLETS: a) PELLET WITHOUT CRACKS; b) CRACKED PELLET SHOWING A NON-SPHERICAL FRONT OF REACTION.

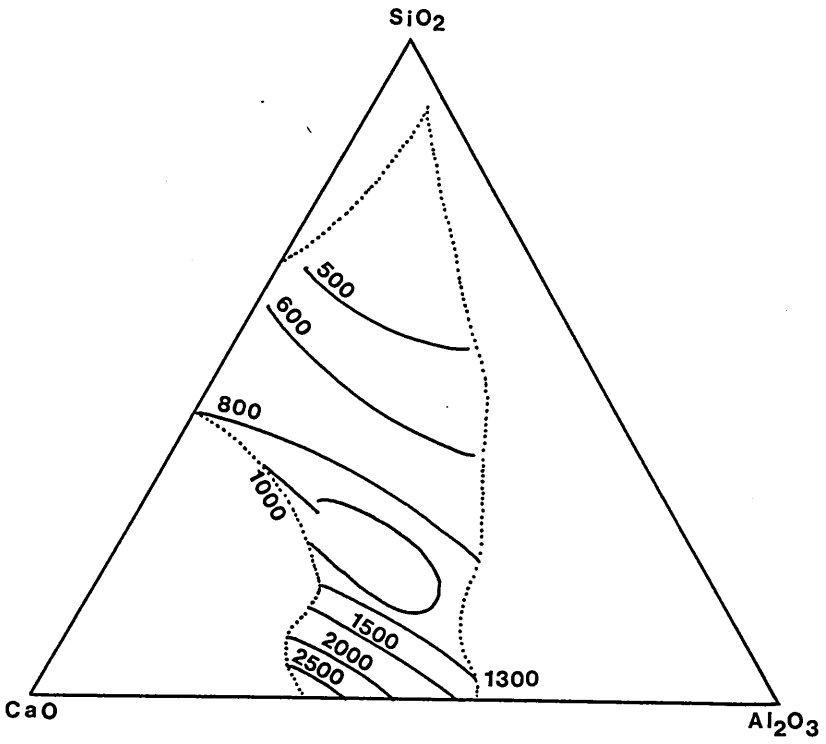

FIG.1: WATER CAPACITY OF $CaO-Al_2O_3-SiO_2$ SLAGS AT 1550 °C (Ref.25)

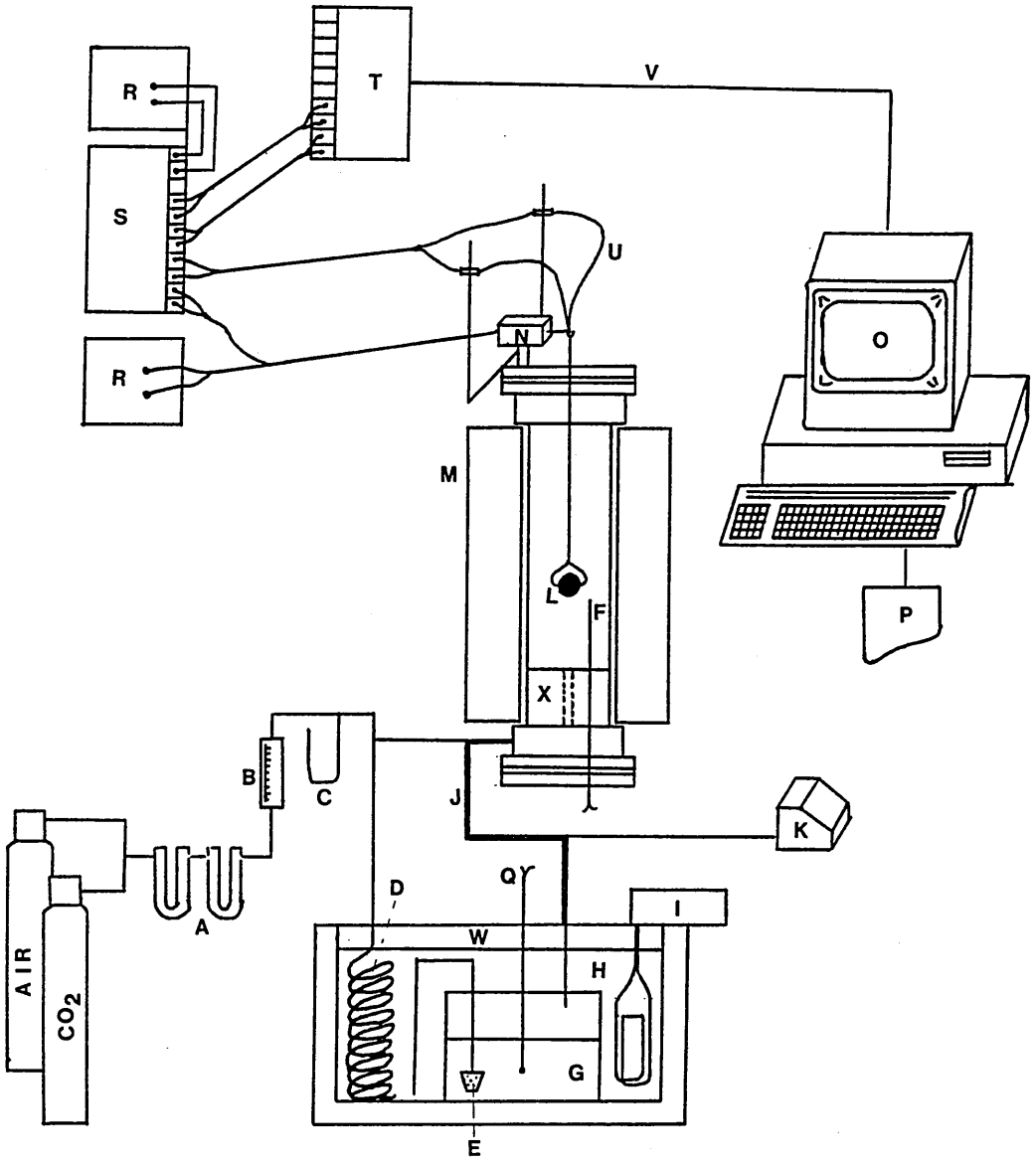

FIG.2: SCHEMATIC DIAGRAM OF APPARATUS FOR HYDRATION AND RECARBONISATION OF CALCIUM OXIDE.

A) Anhydrous Mg perclorate.
B) Rotameter.
C) Manometer.
D) Copper coil.
E) Porous ceramic.
F) Thermocouples.
G) Distilled water.
H) Water bath.
I) Thermostat
J) Heating tape
K) Dew point meter.
L) Sample.
M) Furnace.
N) Transducer.
O) Computer.
P) Printer.
Q) Digital thermocouple.
R) Regulator power supply.
S) Amplifier.
T) Conditioning card.
U) Thermocouple wires
V) Pin flat cable.
W) Plastic spheres layer.
X) Silica disc.

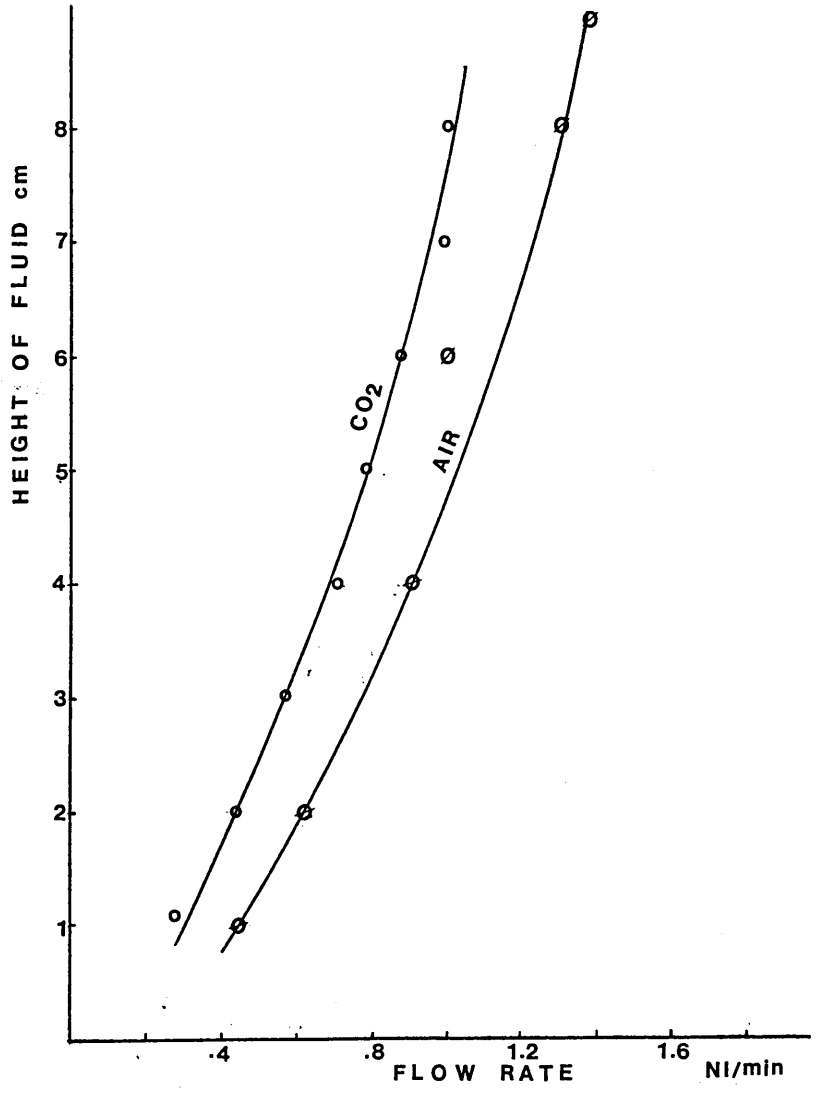

FIG.3: ORIFICE METER CALIBRATION.

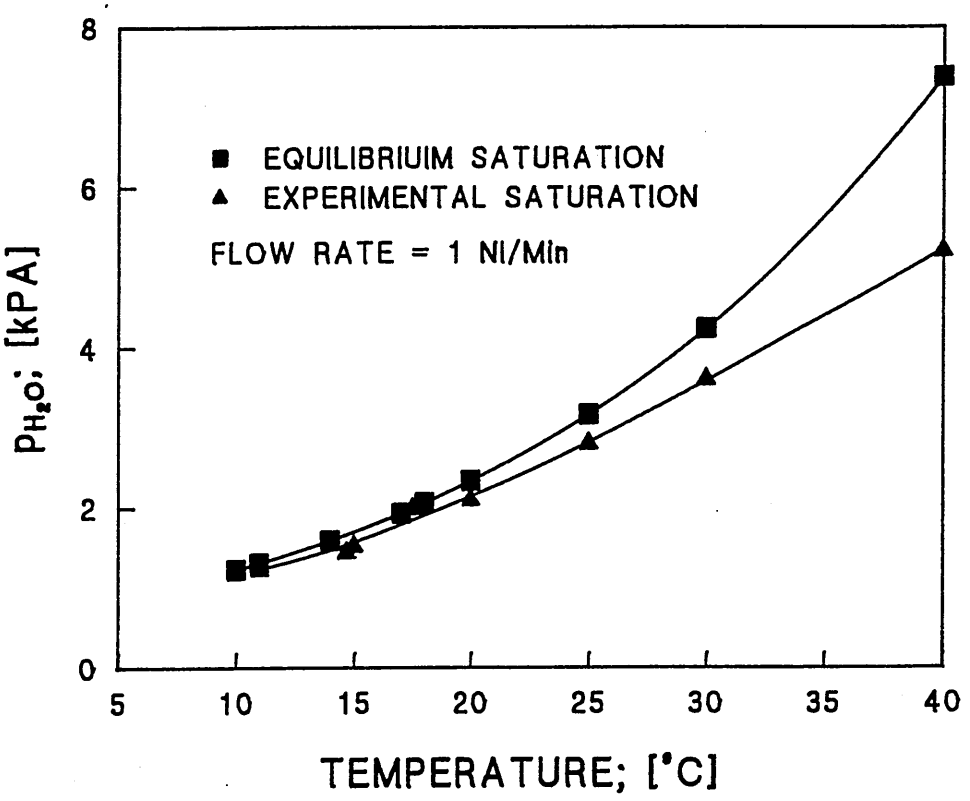

FIG.4: COMPARISON OF MEASURED p_{H_2O} FOR A RANGE OF BATH TEMPERATURES WITH VALUES REPORTED IN TABLES

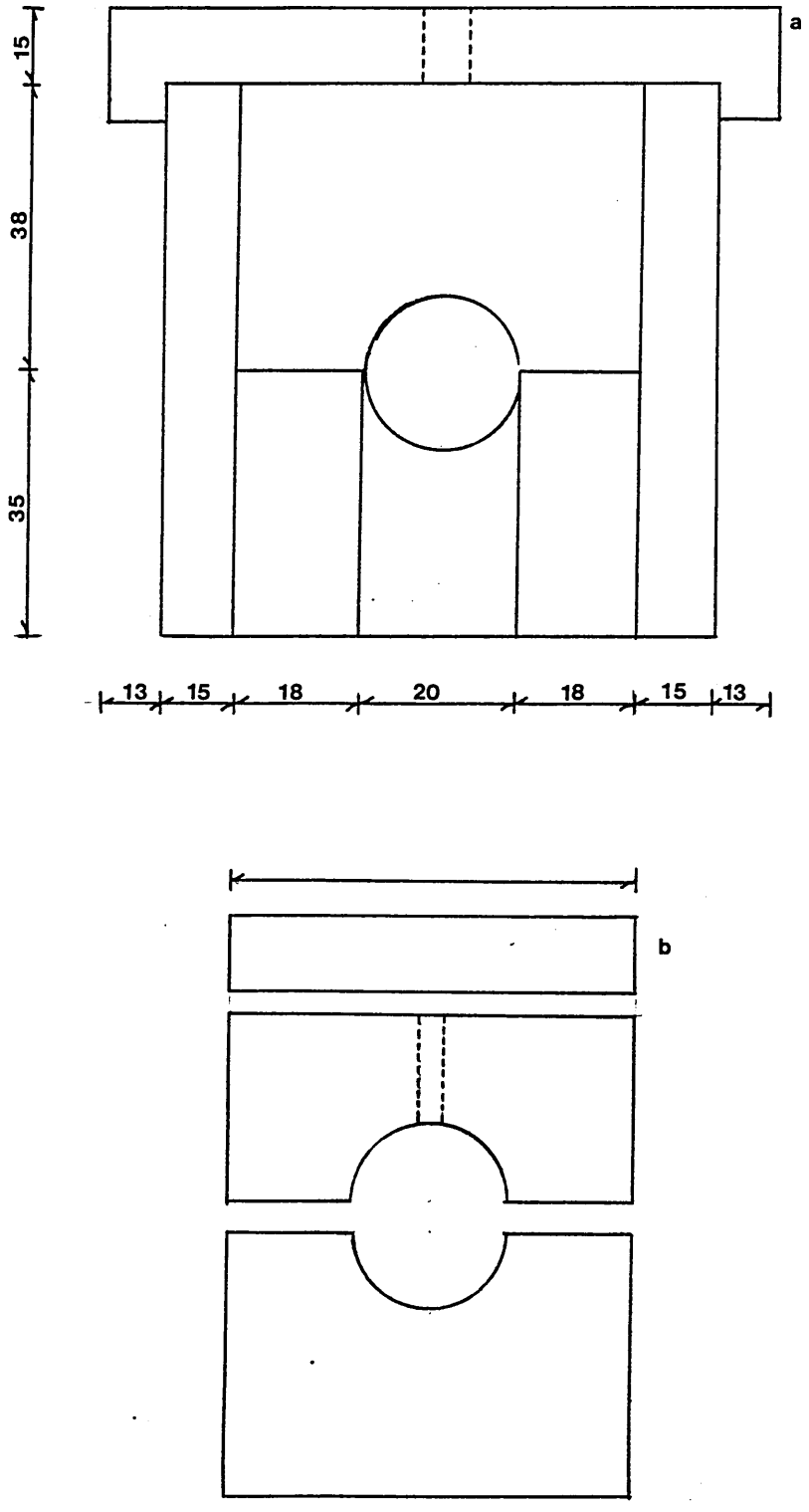

FIG.5: THE GEOMETRY AND DIMENSIONS OF a) THE STEEL DIE AND b) GELFLEX MOULDS. (all dimensions in mm)

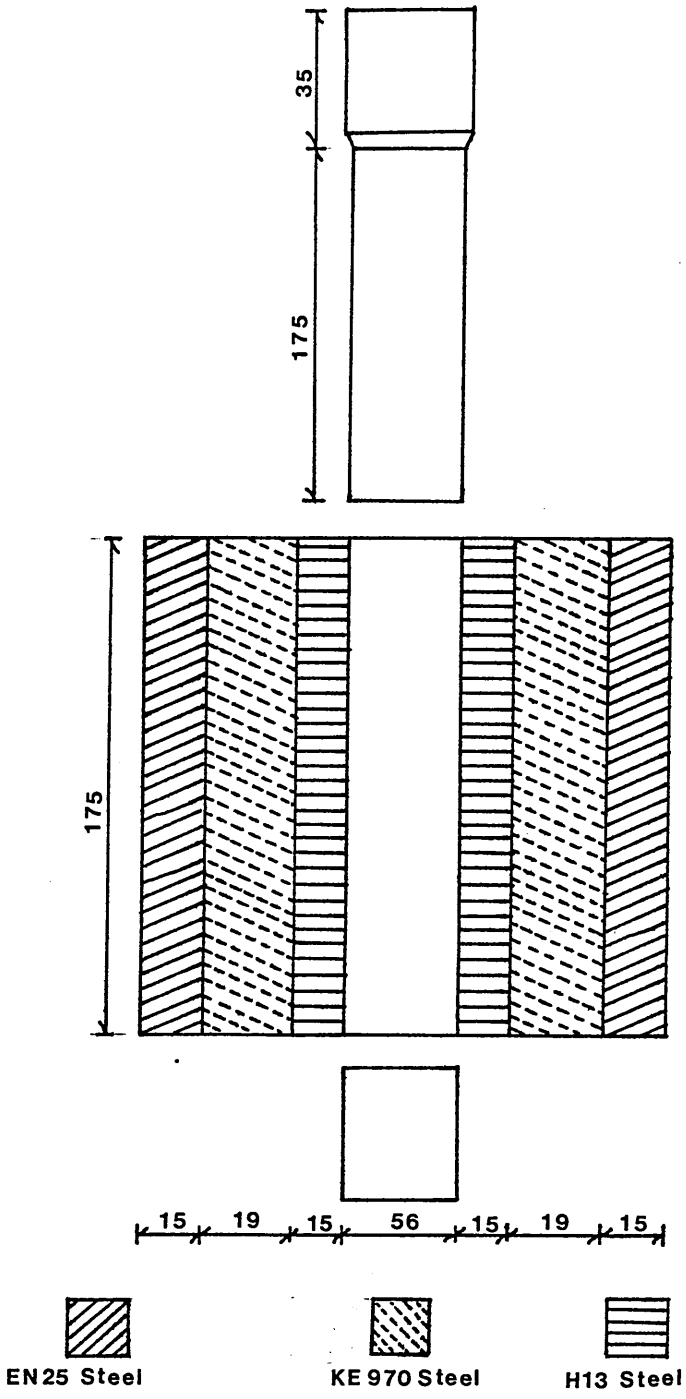

FIG.6. SECTIONAL VIEW OF THE POWDER COMPACTION DIE (all dimensions in mm).

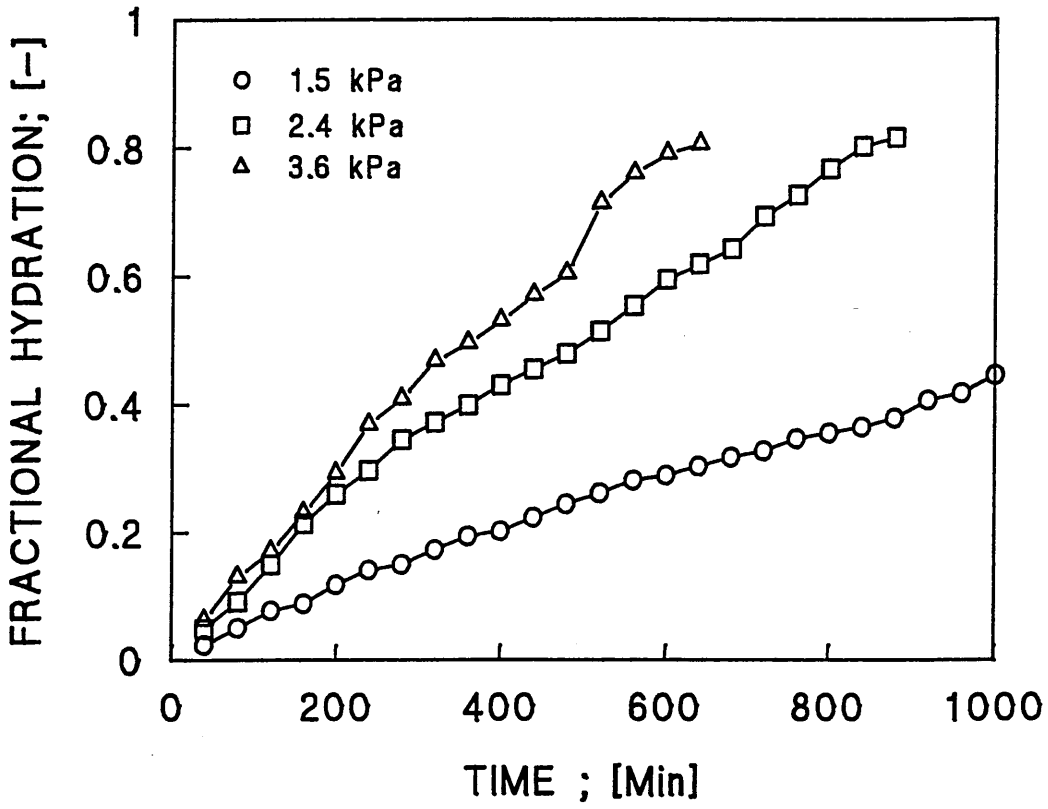

FIG.7: EFFECT OF p_{H_2O} ON HYDRATION RATE
SAMPLES CALCINED AT 850 °C

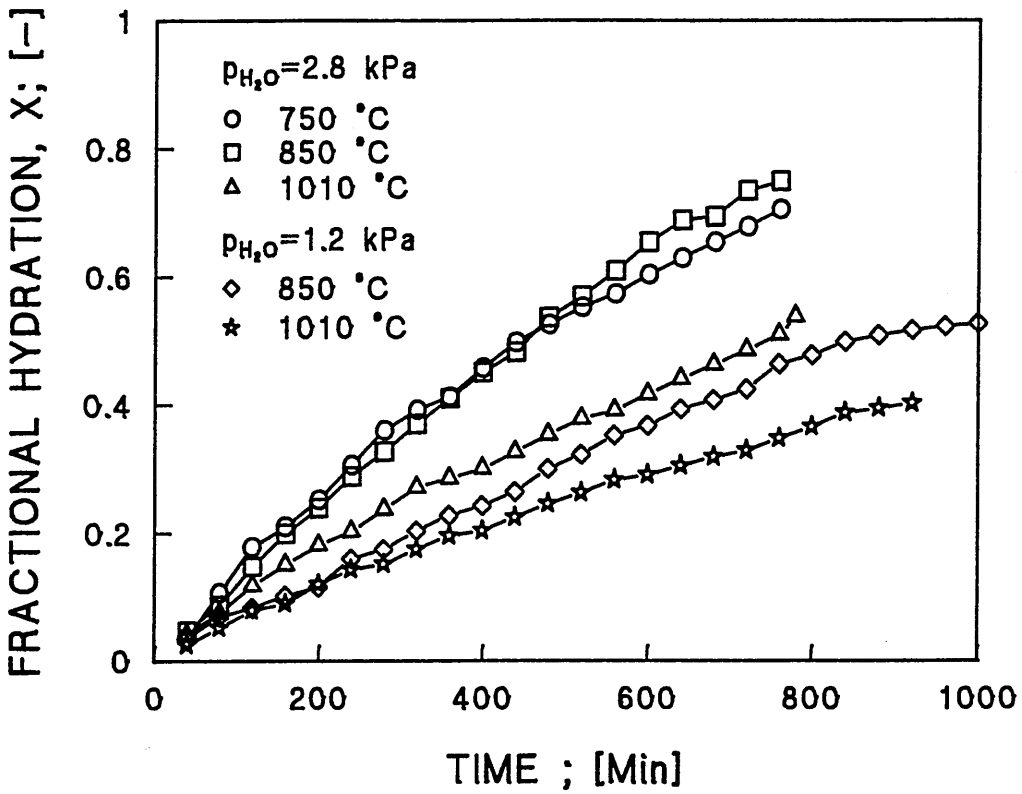

FIG.8: EFFECT OF THE CALCINATION TEMPERATURE ON HYDRATION RATE

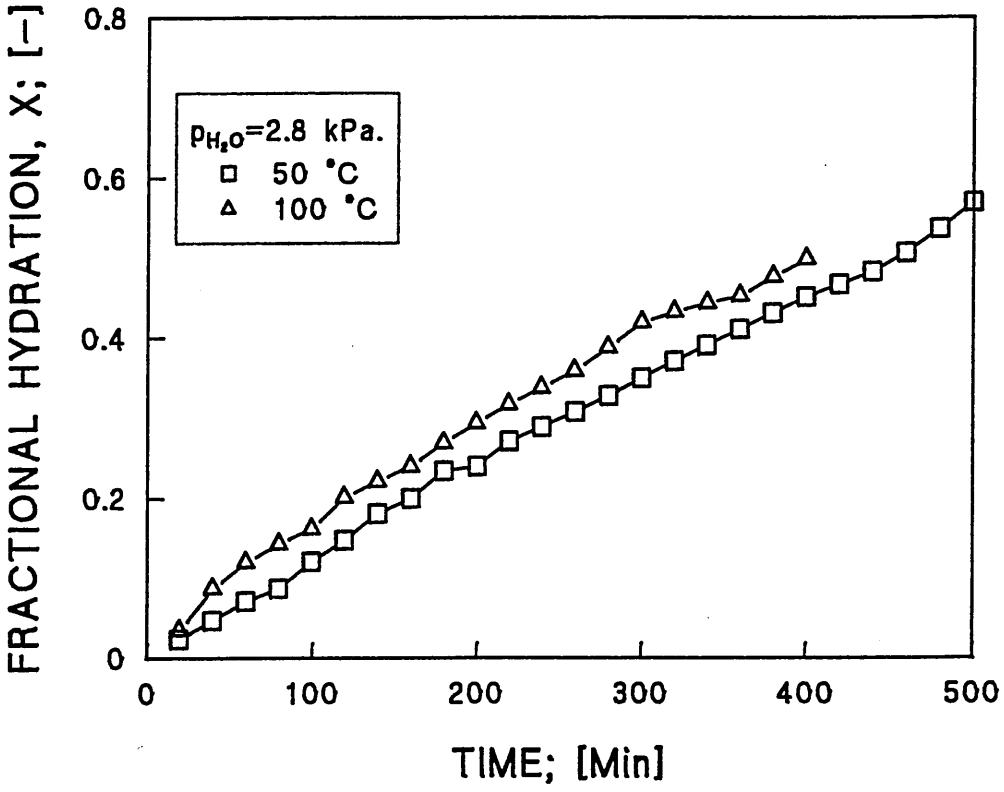

FIG.9: EFFECT OF THE TEMPERATURE ON HYDRATION RATE

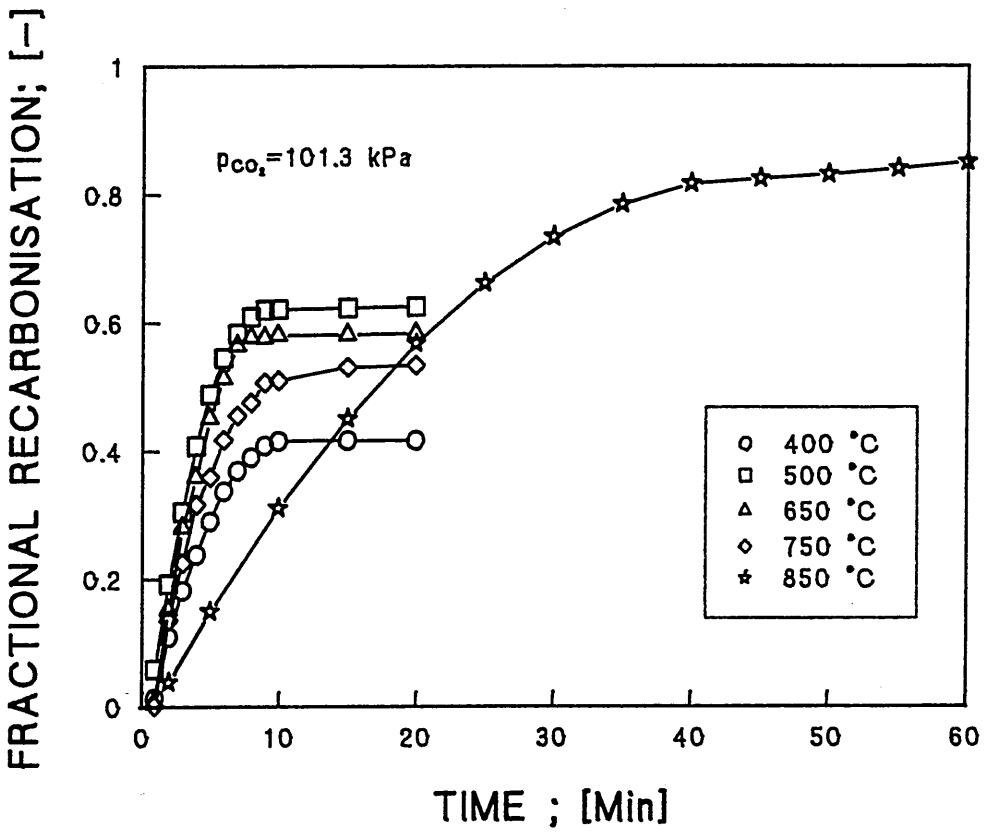

FIG.10: EFFECT OF THE TEMPERATURE ON RECARBONISATION RATE AND FRACTIONAL RECARBONISATION

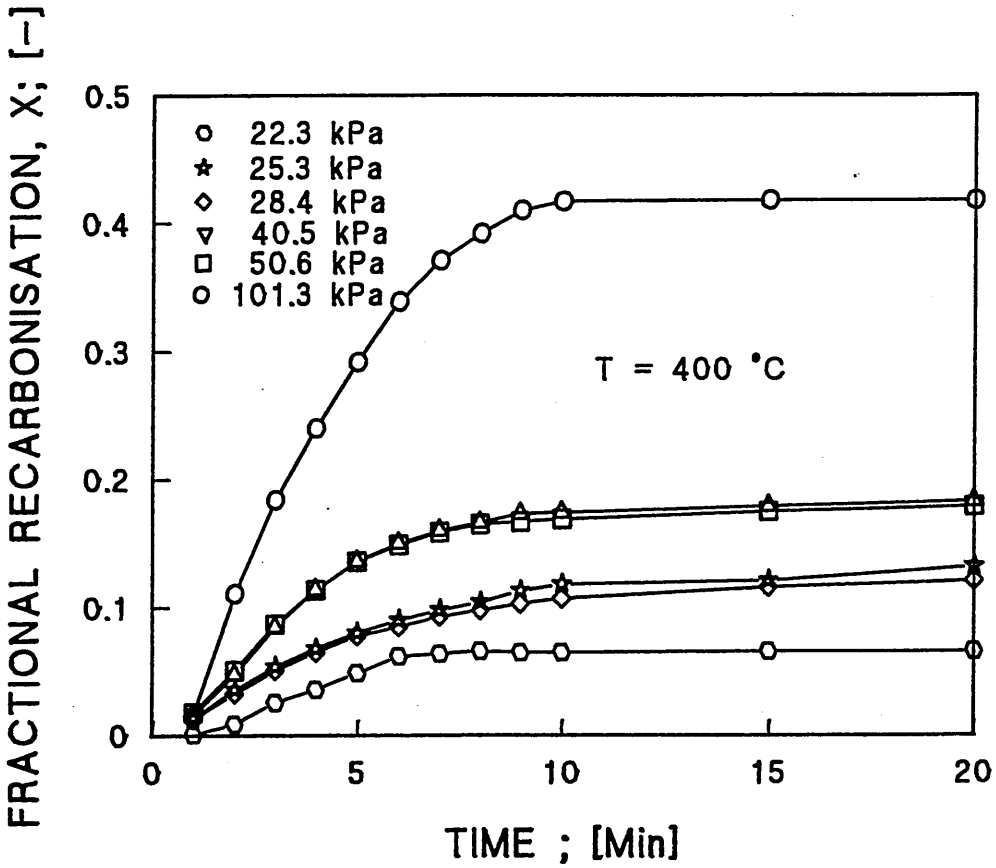

FIG.11: EFFECT OF p_{CO_2} ON RECARBONISATION RATE

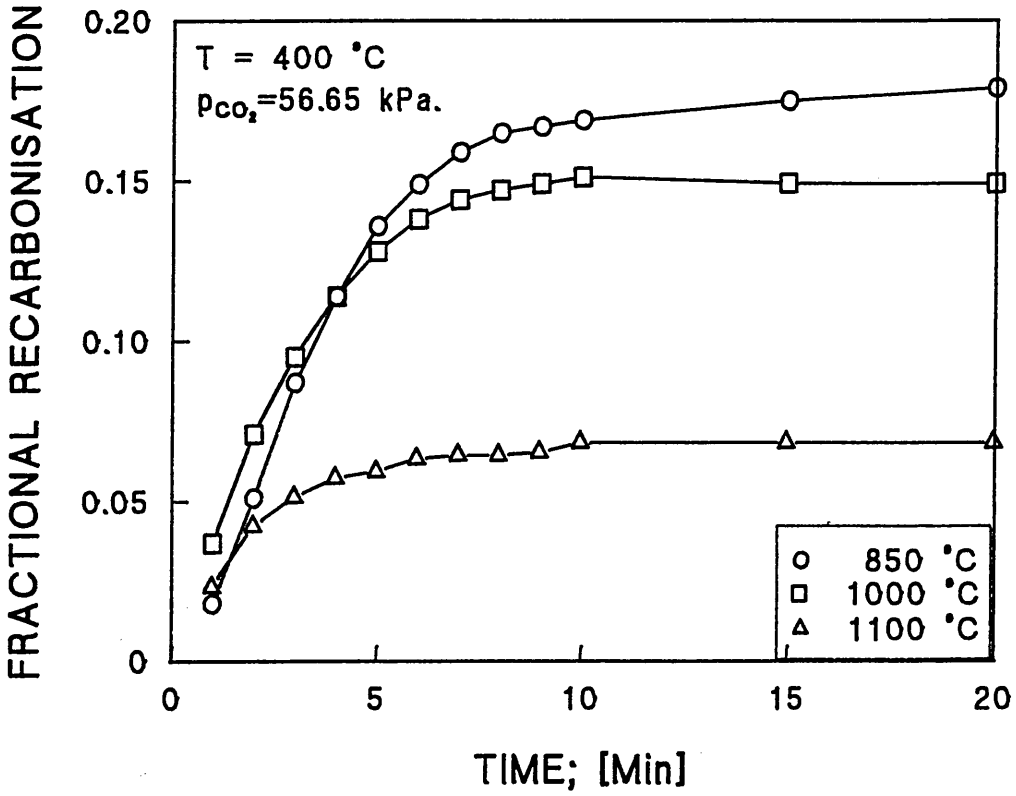

FIG.12: EFFECT OF CALCINATION TEMPERATURE ON RATE AND EXTENT OF RECARBONISATION

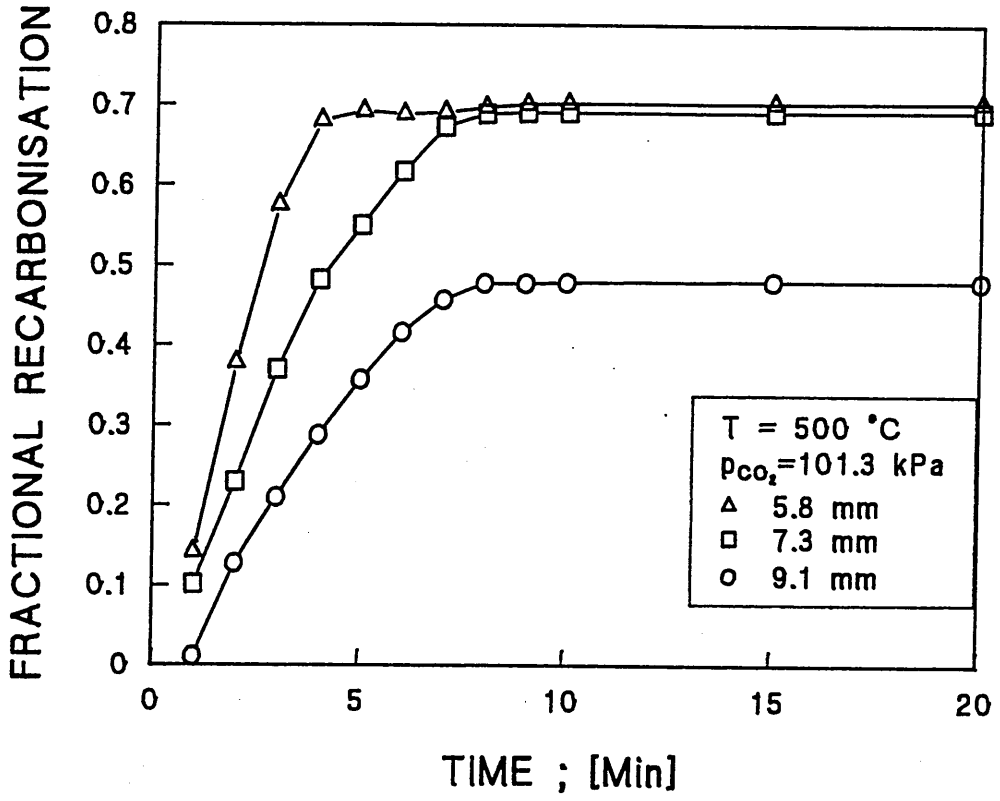

FIG.13: EFFECT OF SAMPLE SIZE ON RATE AND EXTENT OF RECARBONISATION

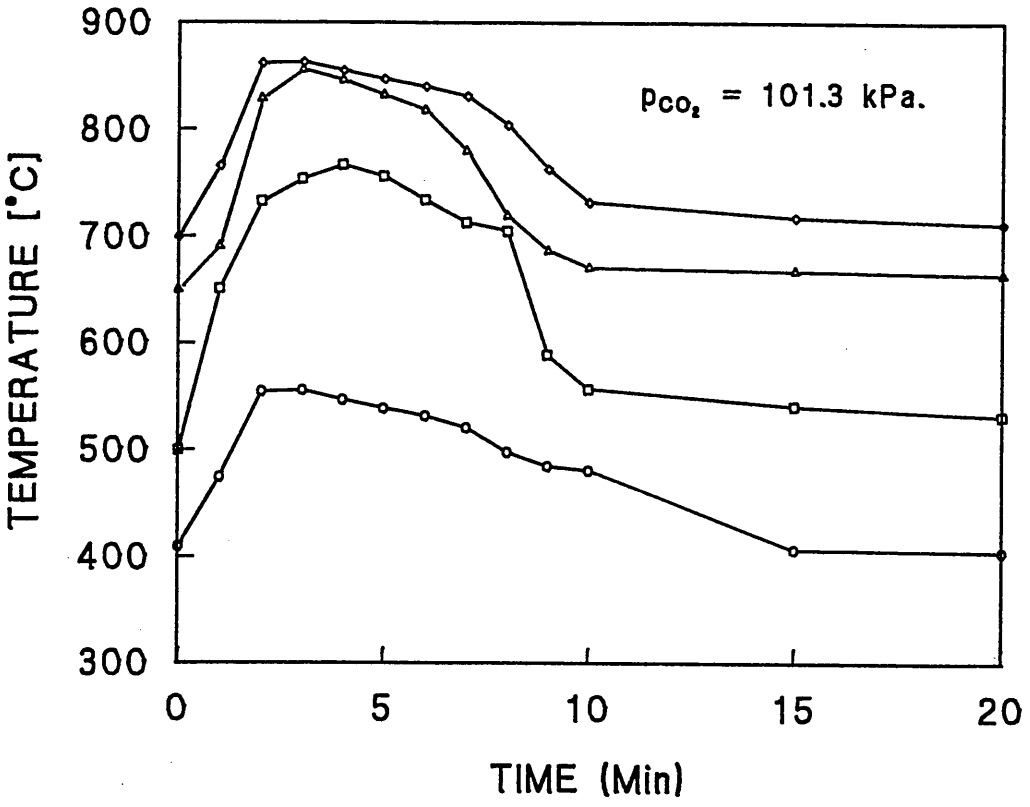

FIG.14: TEMPERATURE OF THE SAMPLE DURING RECARBONISATION REACTION

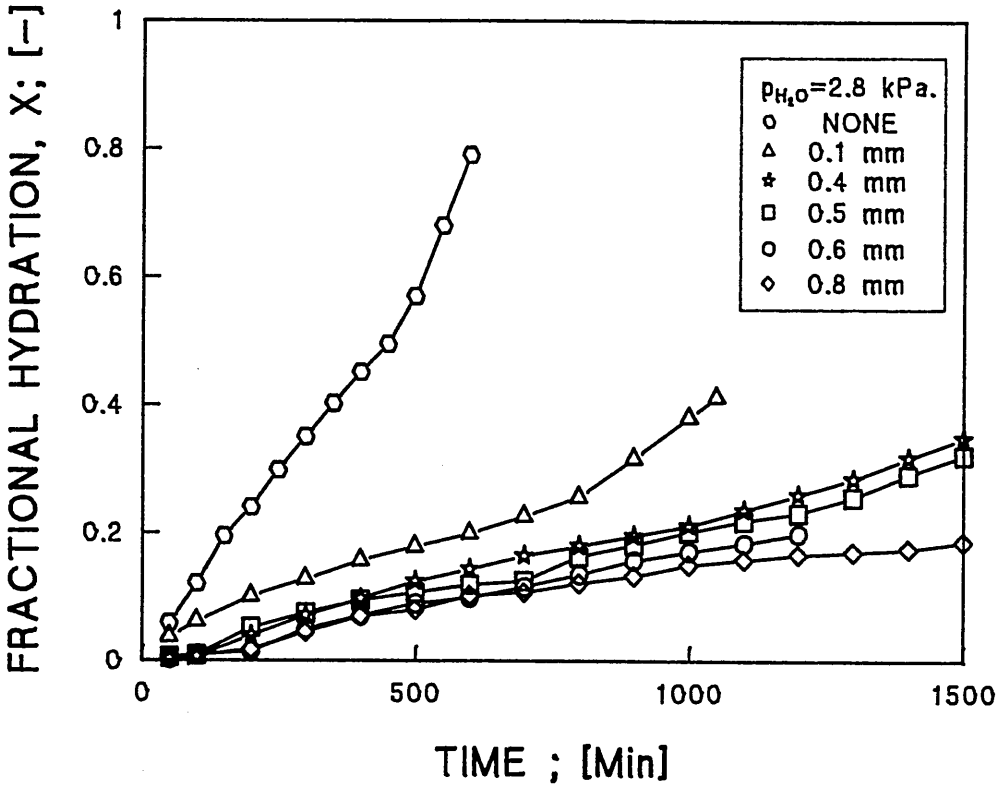

FIG.15: EFFECT OF THE LAYER THICKNESS ON HYDRATION RATE

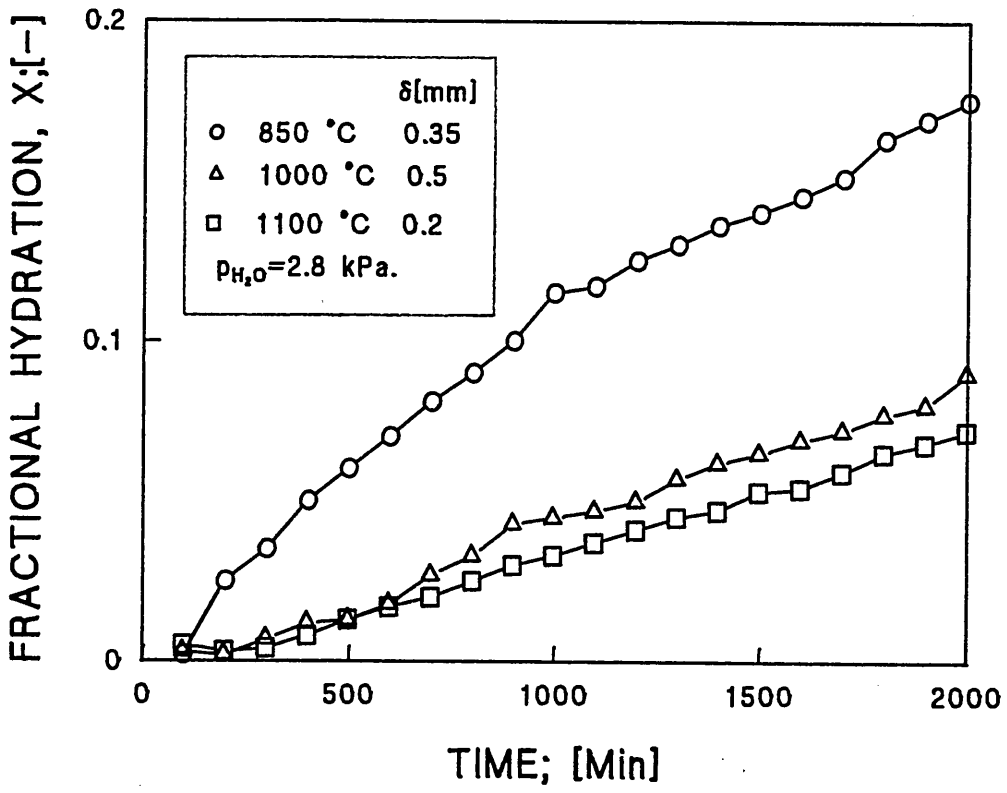

FIG.16: EFFECT OF THE CALCINATION TEMPERATURE ON HYDRATION RATE FOR RECARBONATED SAMPLES

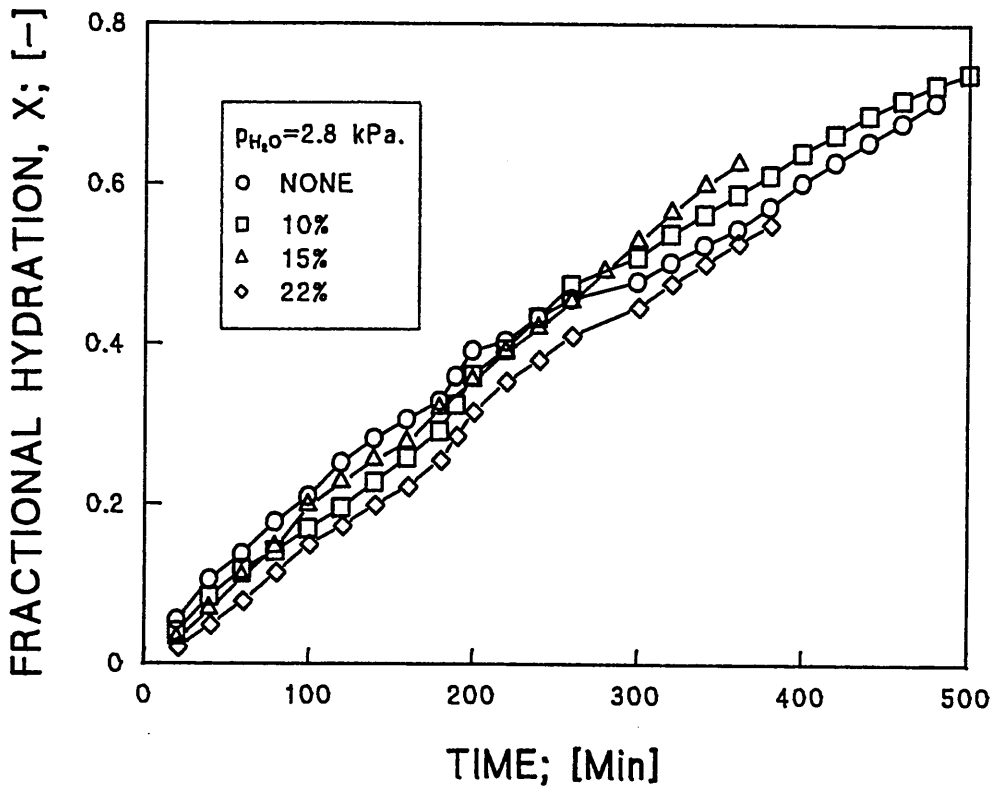

FIG.17: EFFECT OF CONCENTRATION OF ALUMINA ON HYDRATION RATE

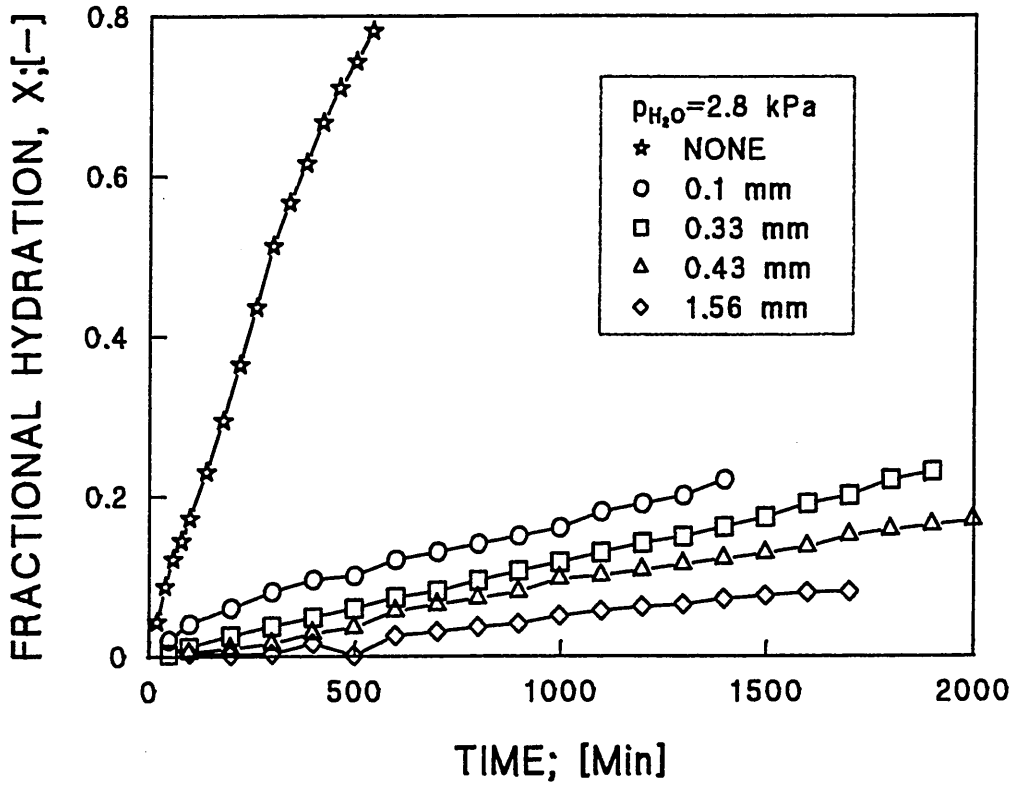

FIG.18: EFFECT OF THE RECARBONATED LAYER THICKNESS ON HYDRATION RATE; SAMPLES WITH 10% OF ALUMINA

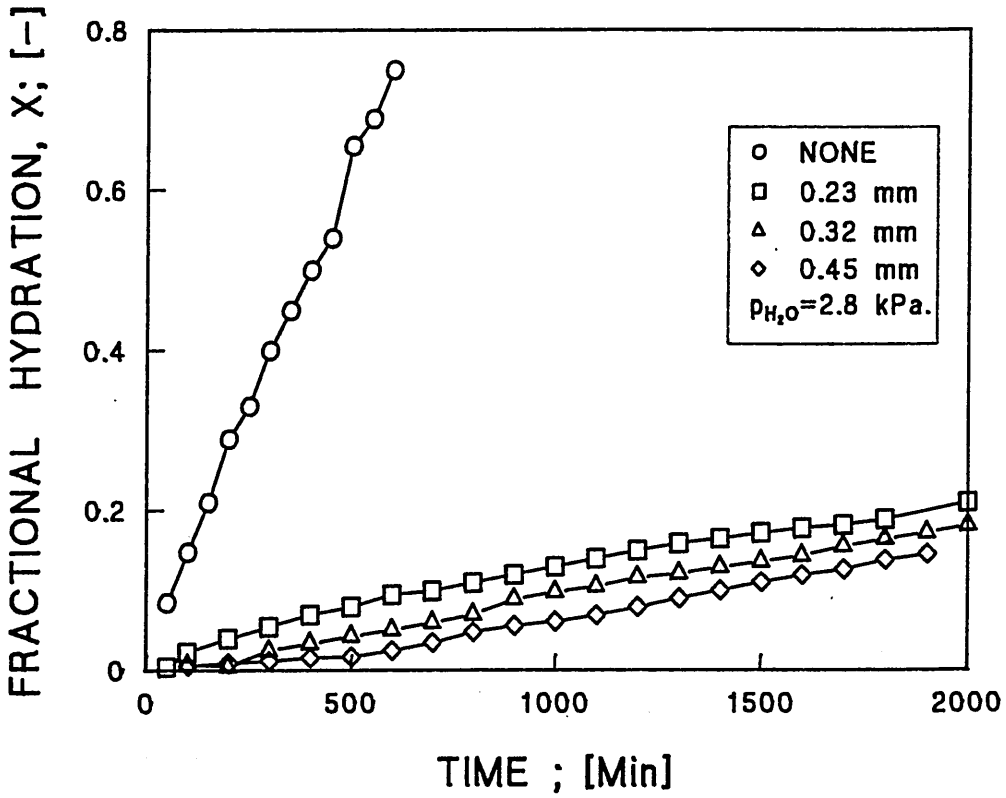

FIG.19: EFFECT OF THE RECARBONATED LAYER THICKNESS ON HYDRATION RATE; SAMPLES WITH 15% OF ALUMINA

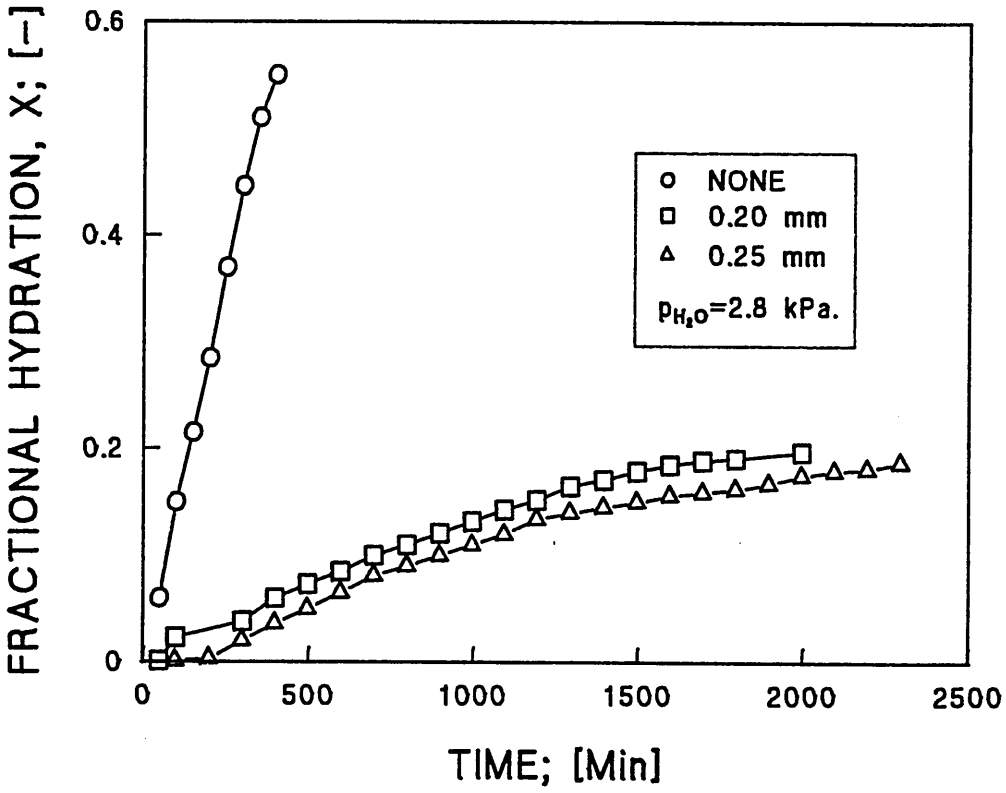

FIG.20: EFFECT OF RECARBONATED LAYER THICKNESS ON HYDRATION RATE; SAMPLES WITH 22% OF ALUMINA

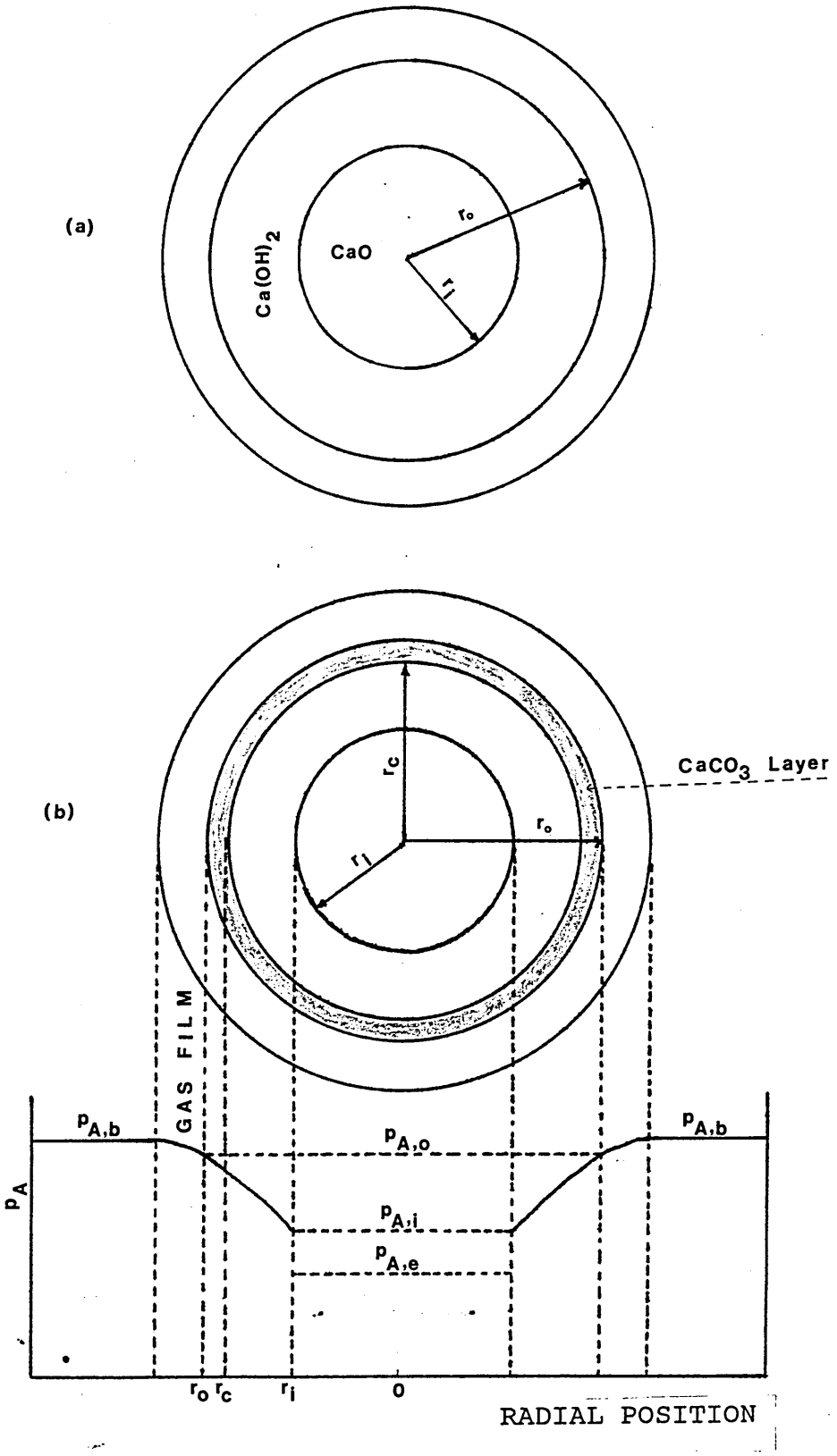

FIG.21: REPRESENTATION OF A REACTING PARTICLE UNDER MIXED CONTROL. a) NON-RECARBONATED PELLET; b) RECARBONATED PELLET.

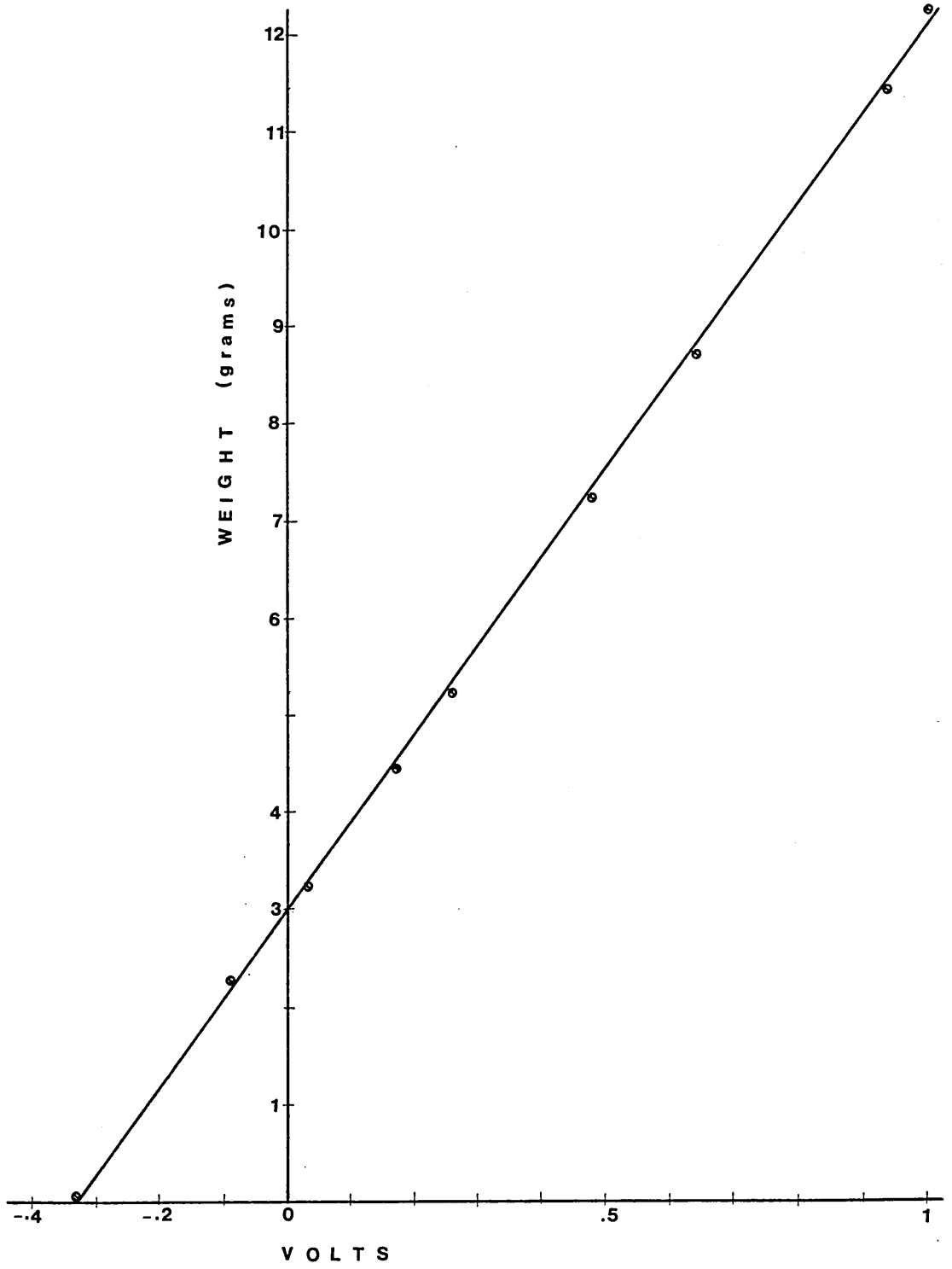

FIG.22: MICRO-FORCE TRANSDUCER CALIBRATION
WEIGHT vs VOLTS

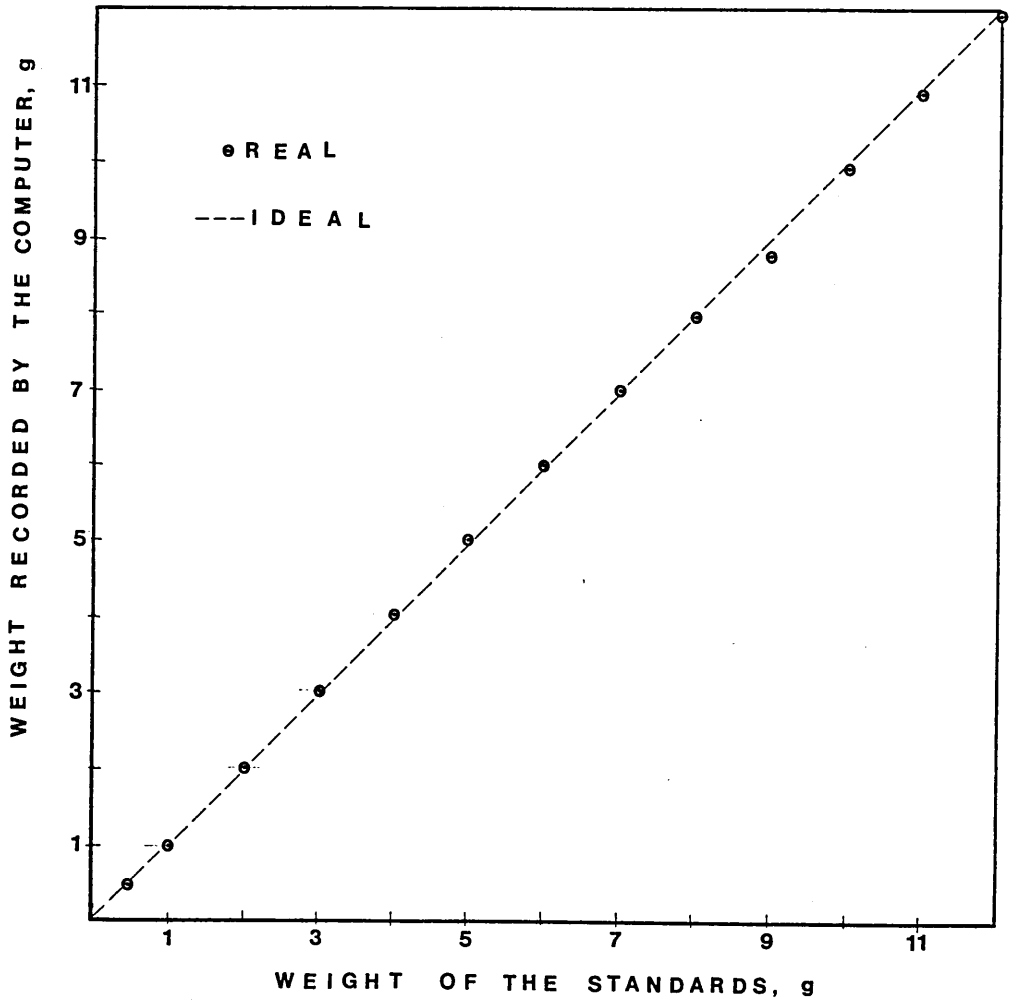

FIG.23: COMPARISON OF PREWEIGHED STANDARDS WITH THE WEIGHT DERIVED FROM EQ.(6.1).

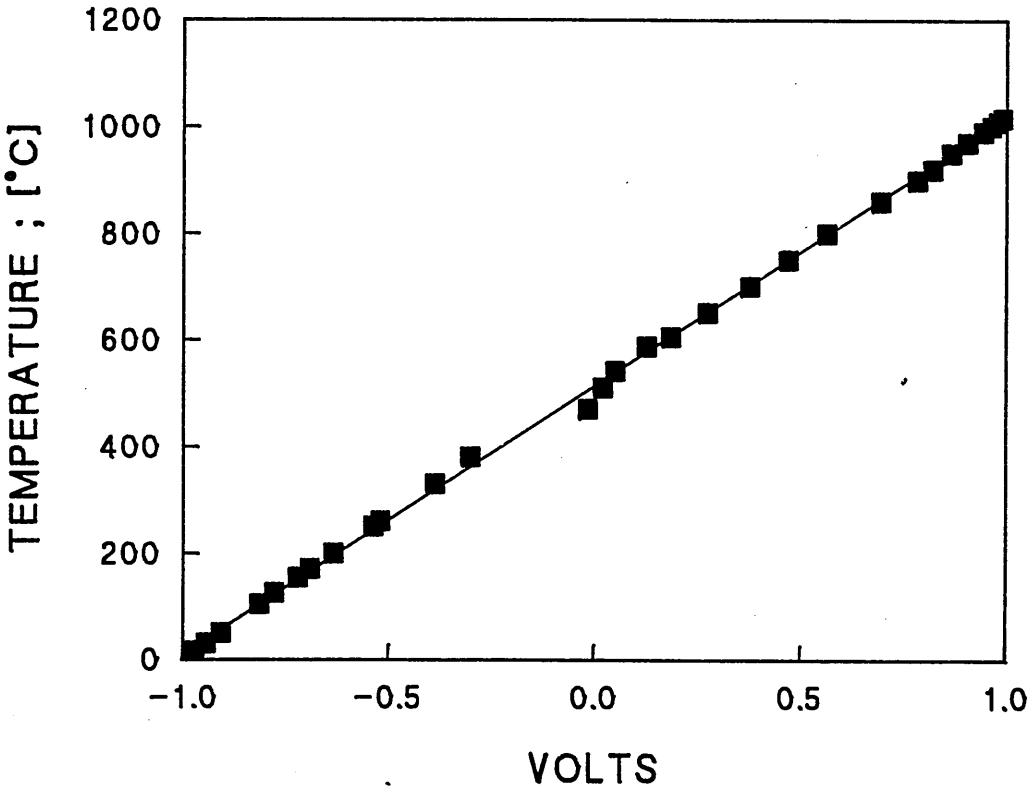

FIG.24: THERMOCOUPLE CALIBRATION

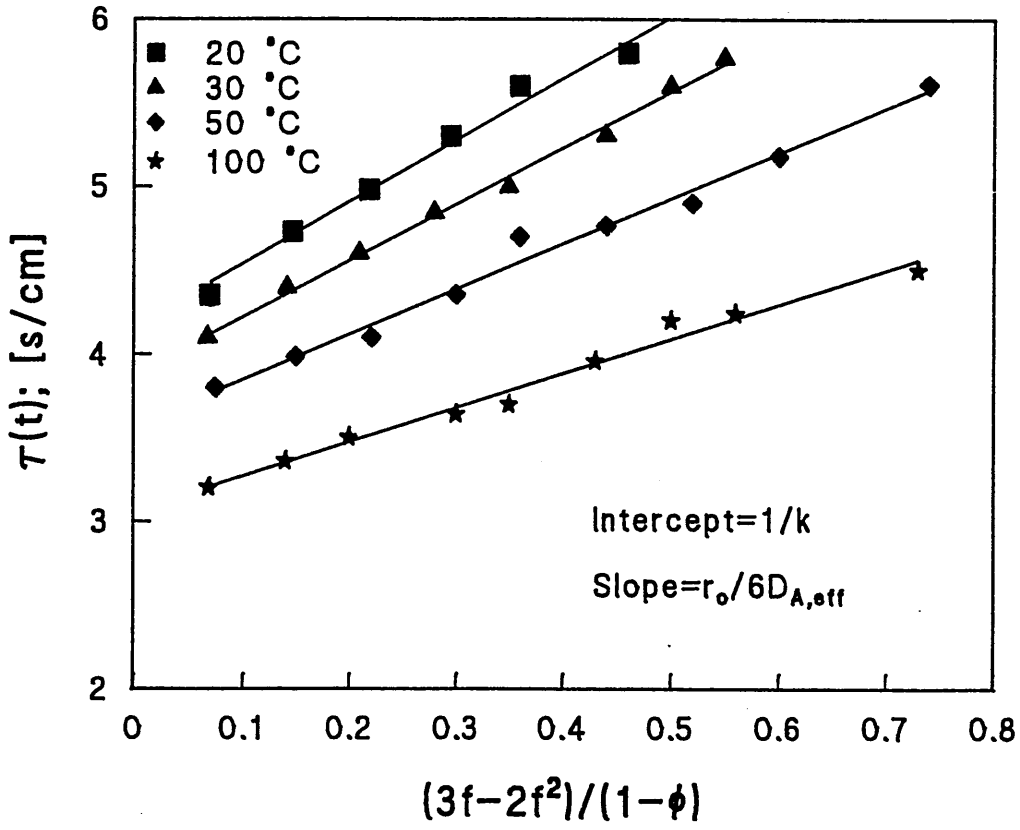

FIG.25: GRAPHICAL DETERMINATION OF k AND D_{eff}
(Samples calcined at 850 °C)

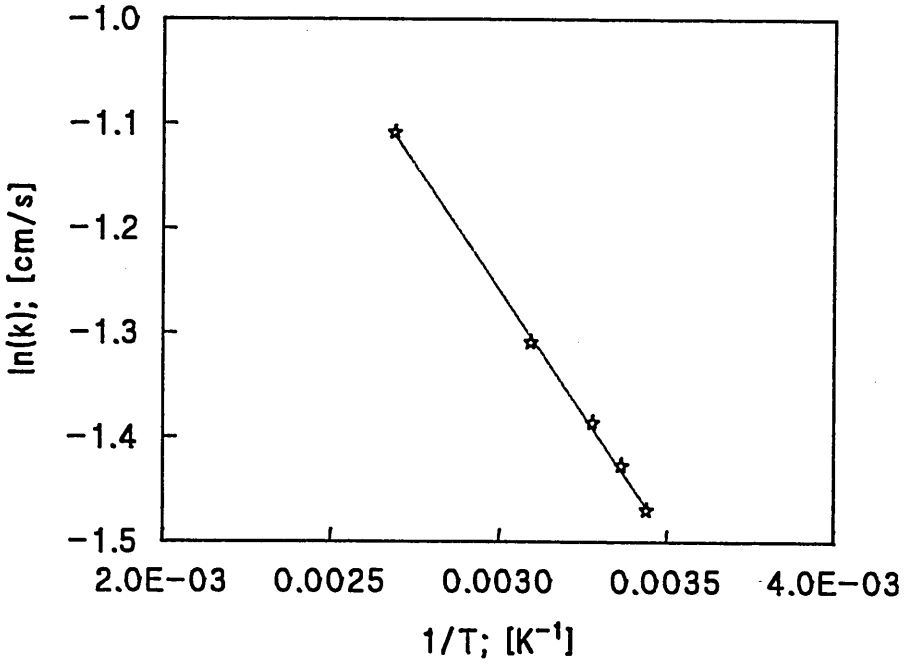

FIG.26: TEMPERATURE DEPENDENCE OF k

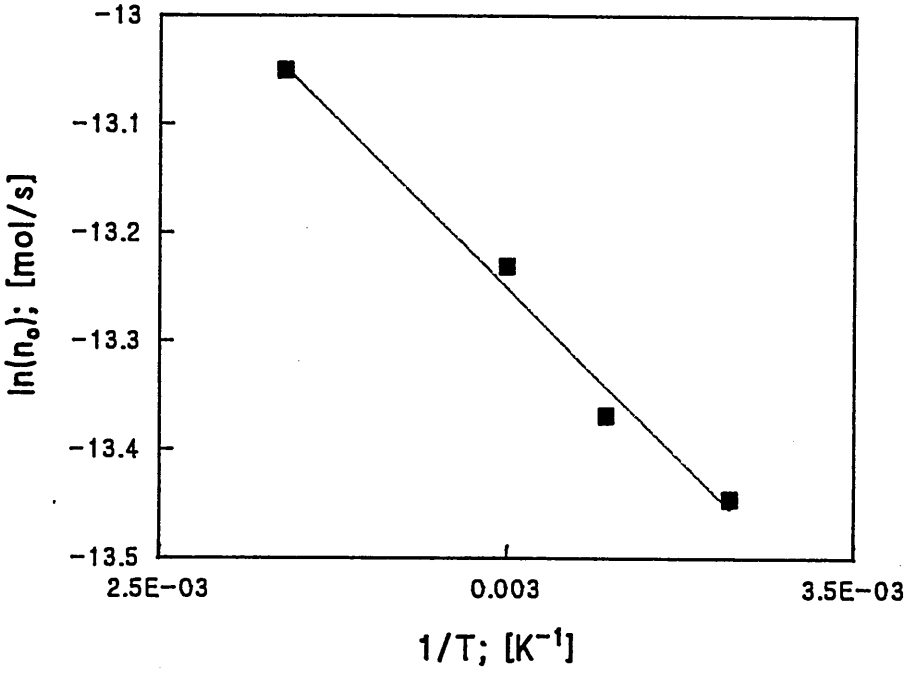

FIG.27: DETERMINATION OF THE ACTIVATION ENERGY FROM THE MEAN INITIAL RATES

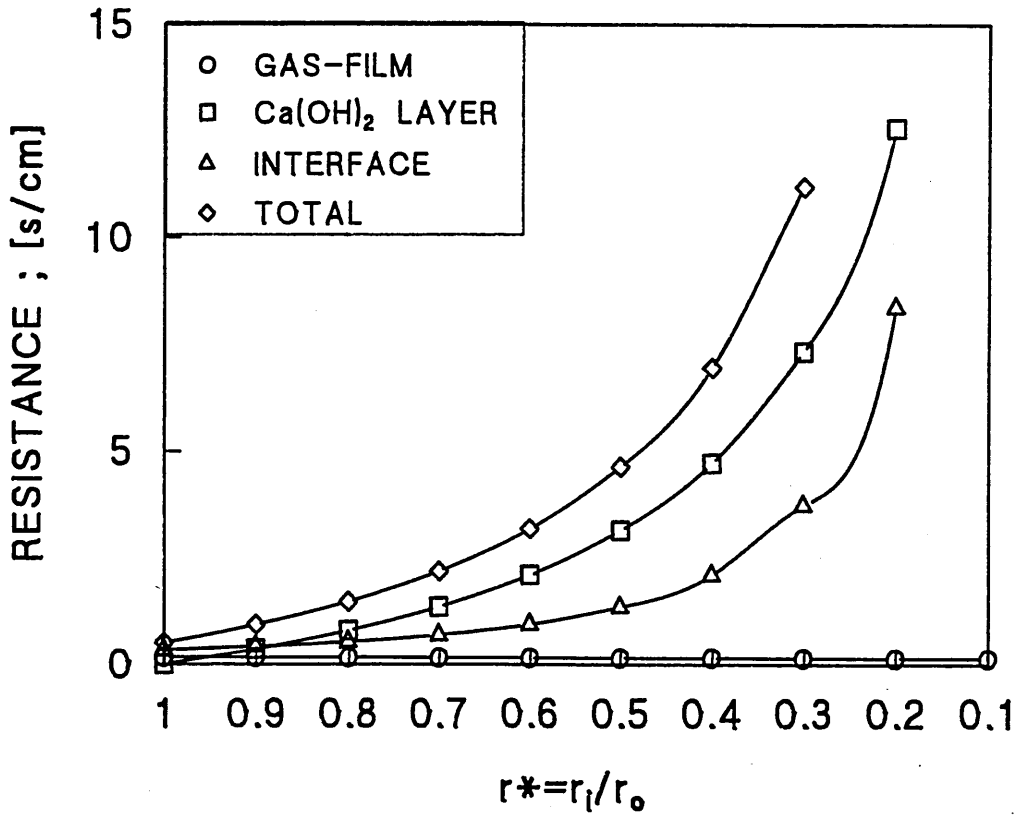

FIG.28: RESISTANCE TO GAS FLOW

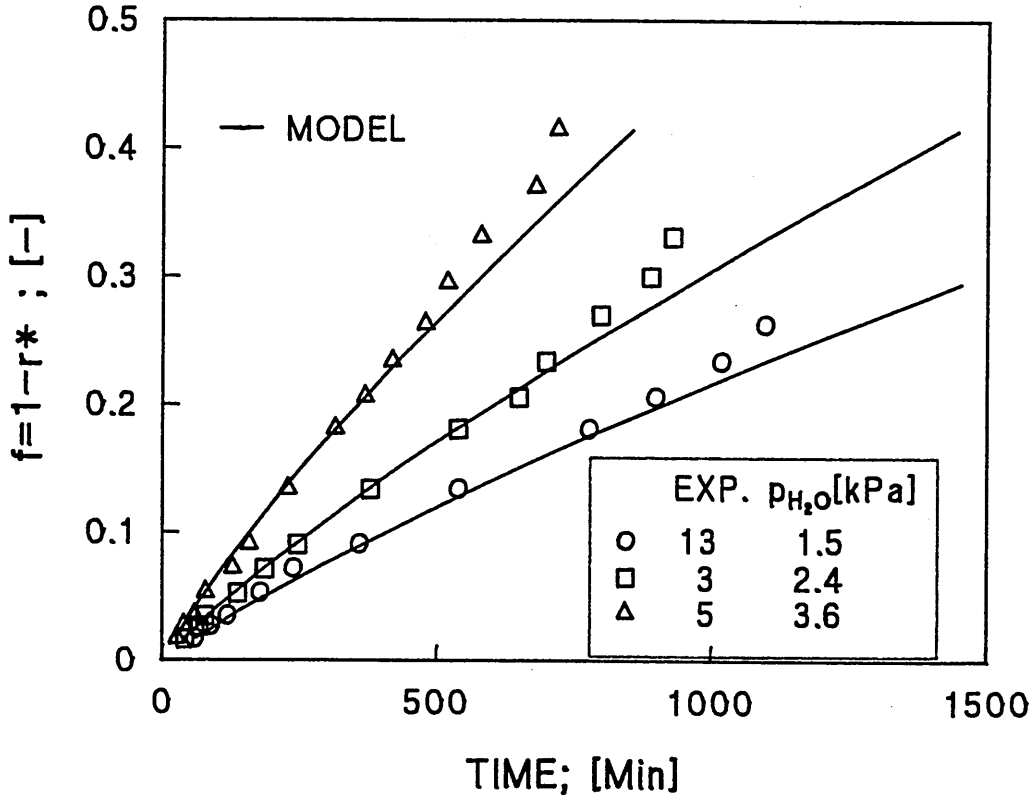

FIG.29: EFFECT OF p_{H_2O} ON HYDRATION RATE
Comparison Between Experiments and Theory

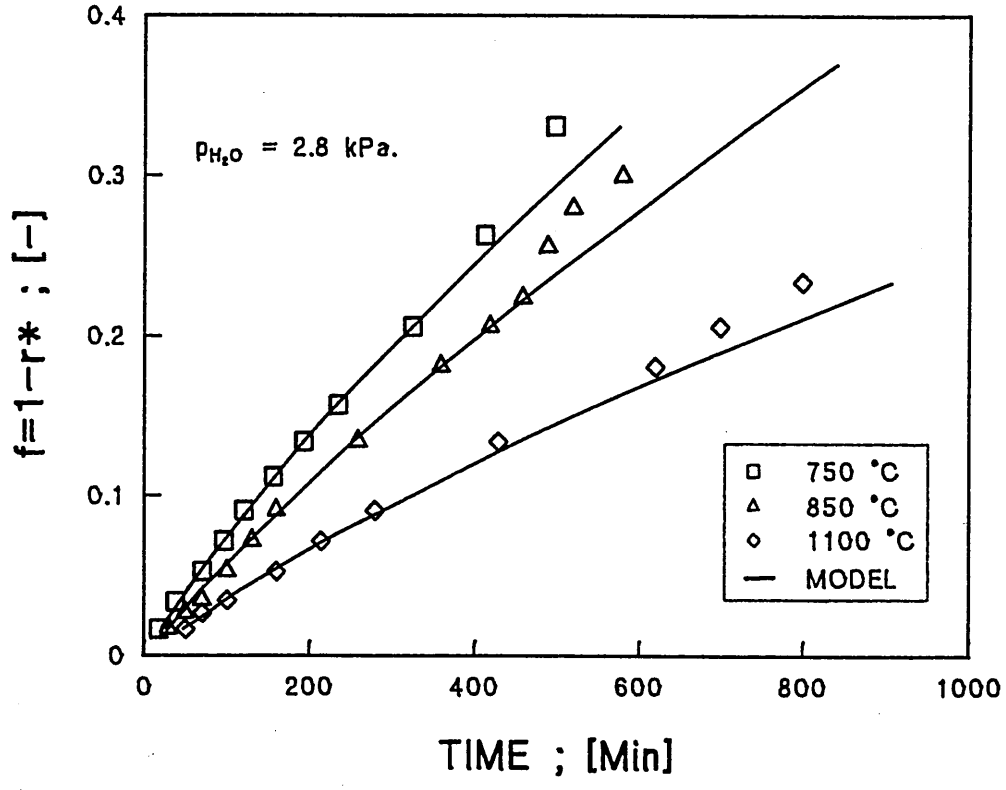

FIG.30: EFFECT OF THE CALCINATION TEMPERATURE ON HYDRATION RATE; EXPERIMENTS vs MODEL

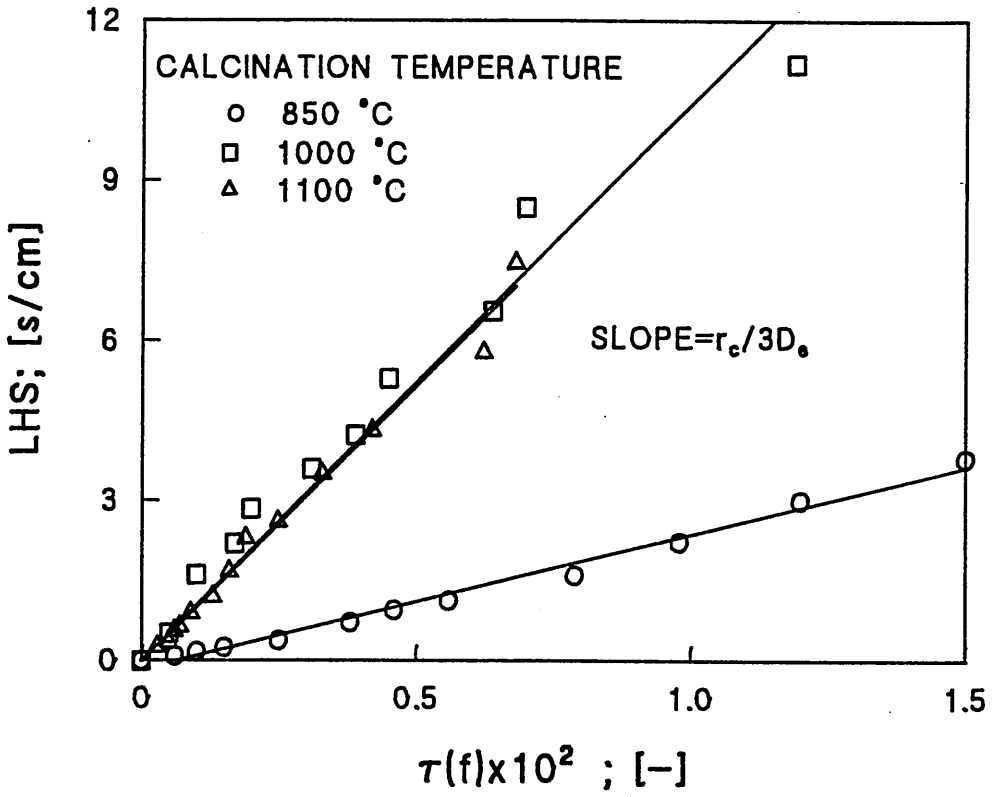

FIG.31: DETERMINATION OF EFFECTIVE DIFFUSIVITY FOR RECARBONATED SAMPLES

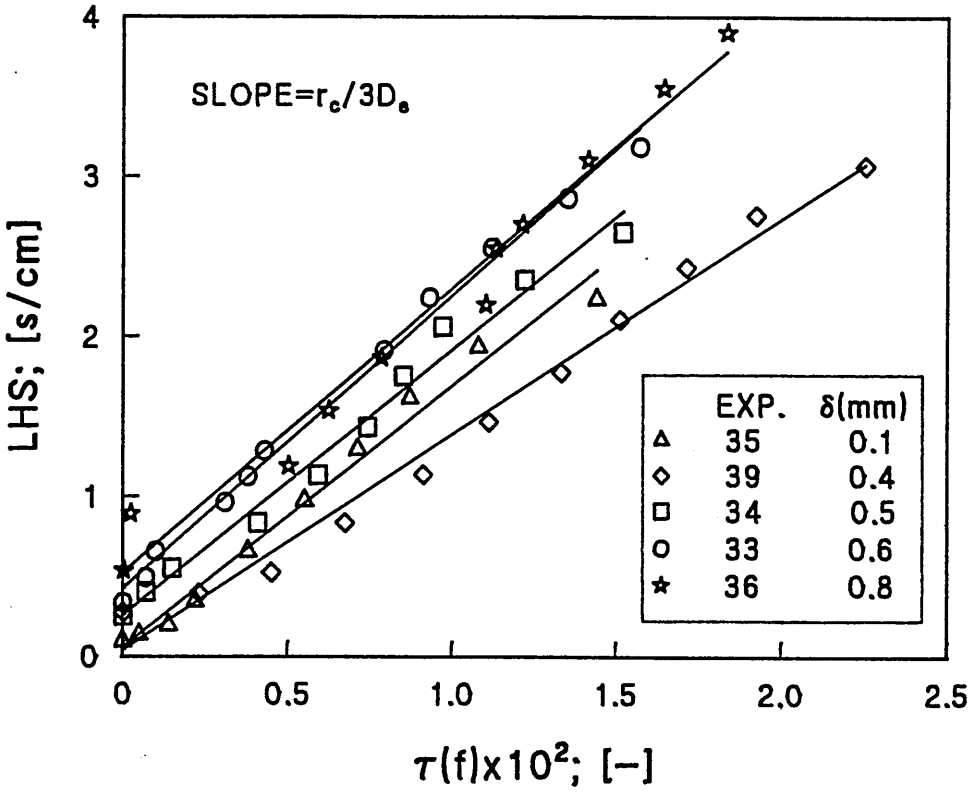

FIG.32: DETERMINATION OF EFFECTIVE DIFFUSIVITY FOR RECARBONATED SAMPLES

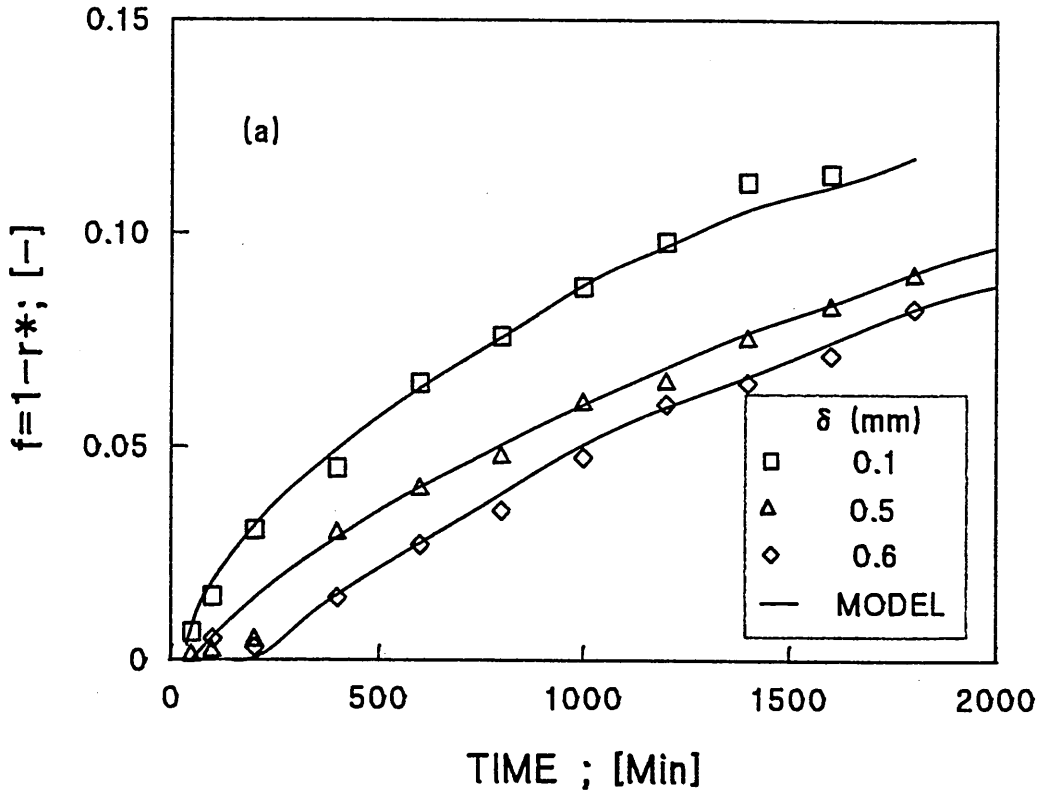

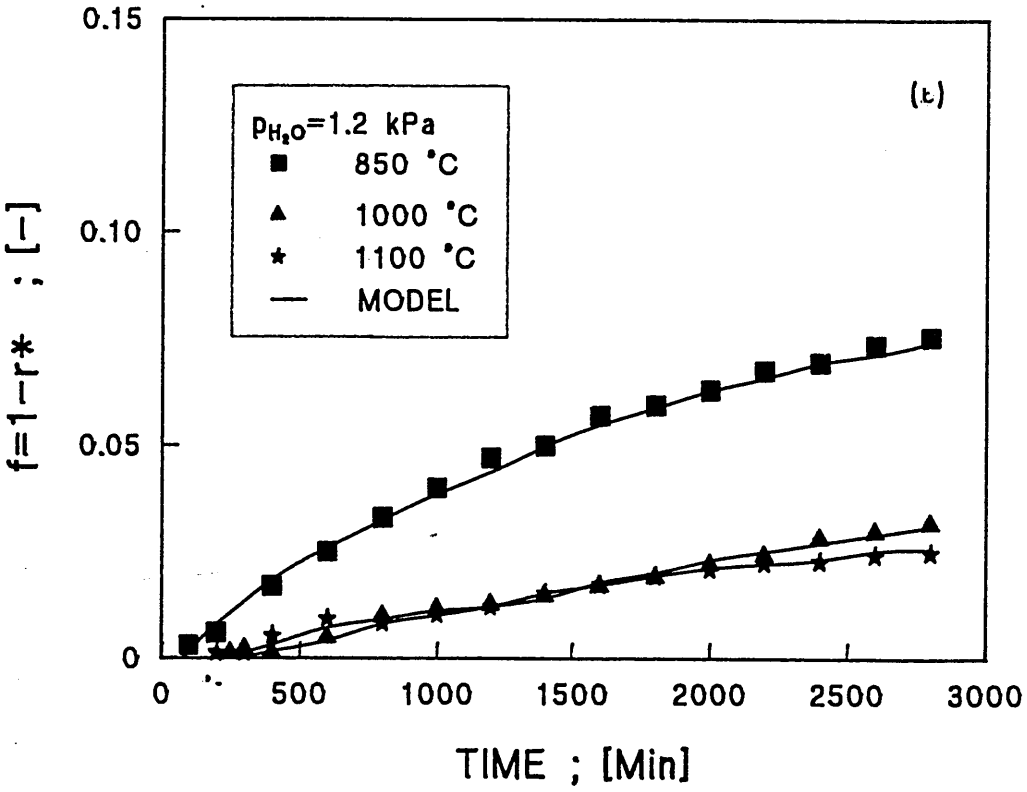

FIG.33: EFFECT OF RECARBONATED FILM ON HYDRATION RATE
(a) LAYER THICKNESS (b) CALCINATION TEMPERATURE

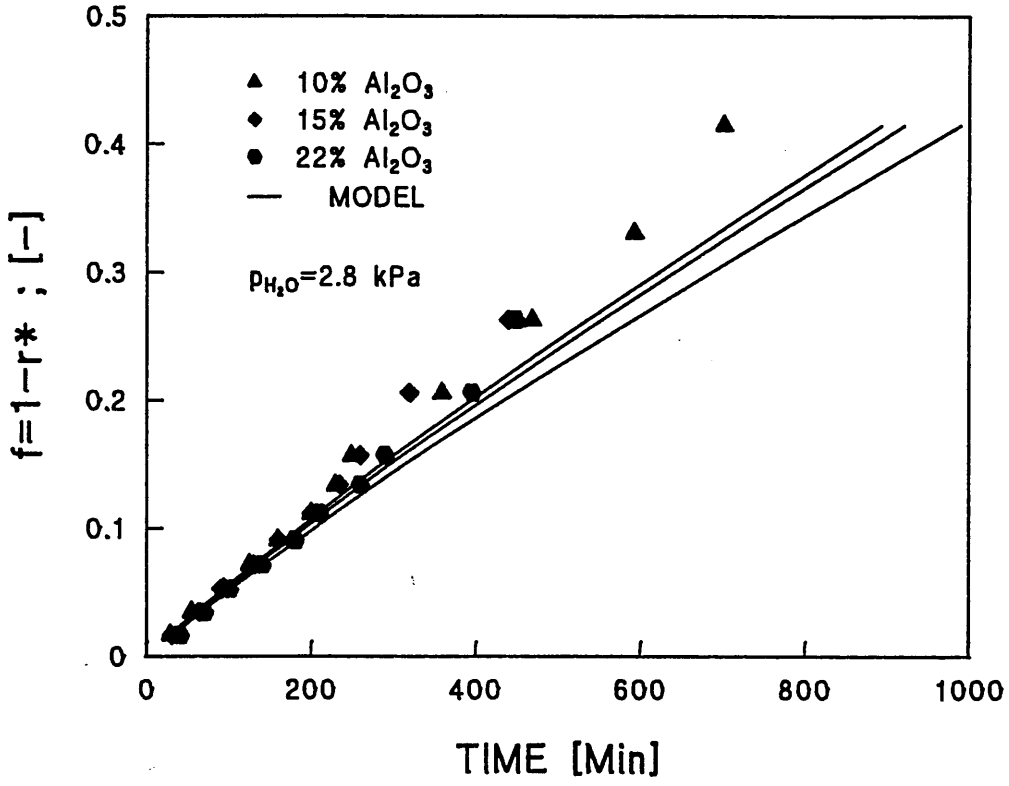

FIG.34: COMPARISON BETWEEN THEORY AND EXPERIMENTS FOR UNRECARBONATED SAMPLES WITH DIFFERENT ALUMINA CONTENT

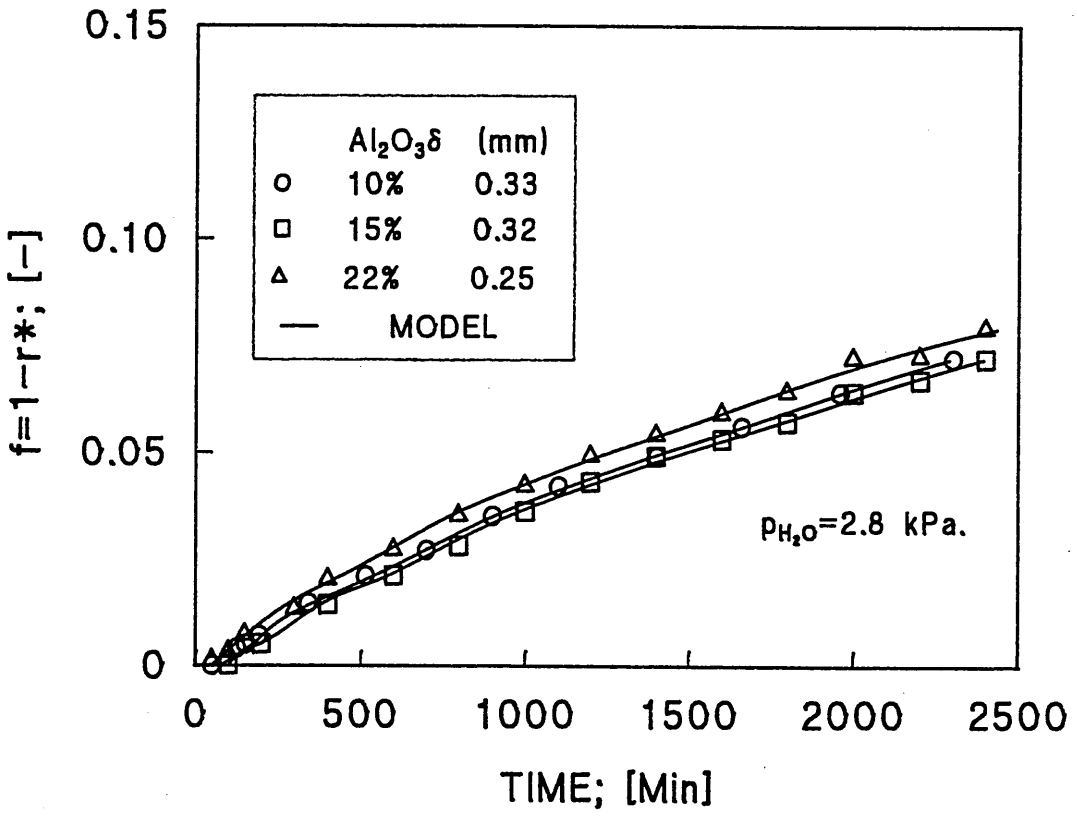

FIG.35: COMPARISON BETWEEN MODEL AND EXPERIMENTS FOR RECARBONATED SAMPLES.

TABLE I.
RUN No.1: HYDRATION.
PELLET WEIGHT = 3.6189 g
PELLET DIAMETER = 18.00 mm
PELLET POROSITY = 0.65
PARTIAL PRESSURE OF WATER VAPOUR = 2.8 KPa.
CALCINATION TEMPERATURE = 750 °C

TIME(min)	TEMP(°C)	WEIGHT(g)	X
0	52	3.6187	0.000
20	66	3.6618	0.036
40	68	3.7153	0.082
60	72	3.7434	0.107
80	69	3.7916	0.139
100	67	3.8373	0.179
120	66	3.8751	0.211
140	66	3.8909	0.232
160	65	3.9237	0.253
180	64	3.9481	0.283
200	64	3.9761	0.307
220	64	4.0027	0.330
240	65	4.0385	0.361
260	65	4.0561	0.375
280	65	4.0760	0.393
300	66	4.0899	0.405
320	67	4.1003	0.413
340	66	4.1248	0.435
260	67	4.1516	0.458
380	66	4.1770	0.480
400	65	4.1992	0.498
420	66	4.2050	0.504
440	67	4.2306	0.526
460	68	4.2541	0.546
480	67	4.2631	0.553
500	67	4.2865	0.574
540	66	4.3215	0.604
580	67	4.3517	0.630
620	66	4.3807	0.655
660	65	4.4087	0.679
700	64	4.4389	0.705

TABLE II.
RUN No.2: HYDRATION
PELLET WEIGHT = 3.3746 g
PELLET DIAMETER = 17.62 mm
PELLET POROSITY = 0.62
CALCINATION TEMPERATURE = 850 °C
PARTIAL PRESSURE OF WATER VAPOUR = 2.8 KPa.

TIME(min)	TEMP(°C)	WEIGHT(g)	X
0	50	3.3746	0.000
20	59	3.4245	0.047
40	59	3.4516	0.071
60	60	3.4689	0.087
80	60	3.5055	0.121
100	59	3.5351	0.148
120	60	3.5709	0.181
140	60	3.5915	0.200
160	59	3.6349	0.240
180	60	3.6685	0.271
200	60	3.6880	0.289
220	60	3.7083	0.308
240	61	3.7304	0.328
260	60	3.7542	0.350
280	61	3.7770	0.371
300	60	3.7987	0.391
320	61	3.8204	0.411
340	61	3.8421	0.431
360	61	3.8637	0.451
380	61	3.8812	0.467
400	62	3.8985	0.483
420	61	3.9245	0.507
440	62	3.9571	0.537
460	61	3.9928	0.570
480	61	4.0363	0.610
500	62	4.1122	0.655
520	61	4.0850	0.680
540	61	4.1122	0.689
560	60	4.1187	0.695
580	61	4.1446	0.735
600	60	4.1684	0.750

TABLE III.
RUN No.3: HYDRATION
PELLET WEIGHT = 3.9425 g.
PELLET DIAMETER = 18.14 mm.
PELLET POROSITY = 0.62
PARTIAL PRESSURE OF WATER VAPOUR = 2.4 KPa.
CALCINATION TEMPERATURE = 850 °C.

TIME(min)	TEMP(°C)f	WEIGHT(g)	X
0	50	3.9425	0.000
20	56	3.9881	0.036
40	56	4.0071	0.051
60	56	4.0286	0.068
80	57	4.0616	0.094
100	57	4.0958	0.121
120	56	4.1351	0.152
140	58	4.1756	0.184
160	58	4.2162	0.216
180	57	4.2529	0.245
200	57	4.2745	0.262
220	58	4.2846	0.270
240	57	4.3210	0.299
260	57	4.3613	0.330
280	58	4.3822	0.347
300	57	4.3894	0.353
320	57	4.4164	0.374
340	58	4.4253	0.381
360	58	4.4506	0.401
380	57	4.4734	0.419
400	58	4.4899	0.432
420	57	4.5102	0.448
440	58	4.5216	0.457
460	58	4.5292	0.463
480	57	4.5520	0.481
500	58	4.5786	0.502
540	58	4.5963	0.516
580	57	4.6471	0.556
620	58	4.6986	0.597
660	58	4.7300	0.621
700	57	4.7578	0.645
740	57	4.8244	0.696
780	57	4.8663	0.729
820	57	4.9271	0.777
860	56	4.9626	0.805
900	54	4.9803	0.819

TABLE IV.
RUN No.4: HYDRATION
PELLET WEIGHT = 3.6764 g
PELLET DIAMETER = 17.89 mm
PELLET POROSITY = 0.60
PARTIAL PRESSURE OF WATER VAPOUR = 2.8 KPa.
CALCINATION TEMPERATURE = 995 °C

TIME(min)	TEMP(°C)	WEIGHT(g)	X
0	47	3.6764	0.000
20	52	3.7143	0.032
40	53	3.7532	0.065
60	56	3.7886	0.095
80	55	3.8241	0.125
100	55	3.8643	0.159
120	55	3.8950	0.185
140	55	3.9257	0.211
160	55	3.9596	0.238
180	55	3.9656	0.245
200	56	3.9883	0.264
220	56	4.0996	0.290
240	57	4.0321	0.301
260	57	4.0498	0.316
280	58	4.0793	0.341
300	57	4.1113	0.368
320	58	4.1408	0.393
340	58	4.1728	0.420
360	58	4.2011	0.444
380	56	4.2176	0.451
400	57	4.2294	0.468
420	58	4.2536	0.481
440	61	4.2589	0.493
460	60	4.2873	0.517
400	60	4.3157	0.541
480	59	4.3148	0.532
500	59	4.3286	0.552
540	59	4.3535	0.573
580	59	4.4007	0.613
620	58	4.4646	0.667
660	59	4.4847	0.684
700	59	4.5184	0.712
740	58	4.5674	0.754
780	58	4.5969	0.779
820	57	4.6335	0.810

TABLE V.
RUN No.5: HYDRATION
PELLET WEIGHT = 3.9217 g
PELLET DIAMETER = 18.19 mm
PELLET POROSITY = 0.62
PARTIAL PRESSURE OF WATER VAPOUR = 3.6 KPa
CALCINATION TEMPERATURE = 850 °C

TIME(min)	TEMP(°C)	WEIGHT(g)	X
0	50	3.9082	0.000
20	58	3.9771	0.044
40	58	3.9919	0.065
60	59	4.0326	0.088
80	59	4.0893	0.133
100	60	4.1015	0.152
120	60	4.1397	0.173
140	62	4.1939	0.216
160	61	4.2035	0.233
180	63	4.2444	0.257
200	62	4.2935	0.295
220	62	4.3403	0.332
240	62	4.3893	0.371
260	63	4.4052	0.393
280	63	4.4240	0.411
300	63	4.4666	0.443
320	63	4.5141	0.470
340	62	4.5161	0.481
360	63	4.5494	0.498
380	63	4.5809	0.523
400	63	4.5816	0.533
420	63	4.6162	0.551
440	64	4.6439	0.573
460	64	4.6553	0.582
480	64	4.6748	0.607
500	63	4.7069	0.623
520	63	4.8253	0.717
540	63	4.8462	0.743
560	64	4.8600	0.763
580	63	4.8827	0.772
600	64	4.8994	0.794
620	63	4.9179	0.809

TABLE VI.
RUN No.6: HYDRATION
PELLET WEIGHT = 3.7004 g
PELLET DIAMETER = 17.88 mm
PELLET POROSITY = 0.62
CALCINATION TEMPERATURE = 850 °C
PARTIAL PRESSURE OF WATER VAPOUR = 3.2 KPa

TIME(min)	TEMP(°C)	WEIGHT(g)	X
0	54	3.6998	0.000
20	66	3.7503	0.043
40	67	3.8015	0.085
60	66	3.8317	0.115
80	66	3.8823	0.154
100	67	3.9275	0.191
120	66	3.9412	0.203
140	67	3.9656	0.223
160	66	4.0040	0.255
180	65	4.0417	0.287
200	64	4.0774	0.317
220	63	4.0816	0.321
240	62	4.0937	0.348
260	62	4.1456	0.376
280	63	4.1613	0.388
300	62	4.1797	0.406
320	64	4.2118	0.430
340	64	4.2434	0.456
360	64	4.2576	0.469
380	65	4.2743	0.482
400	65	4.3034	0.507
420	65	4.3089	0.512
440	66	4.3391	0.537
460	65	4.3867	0.577
480	64	4.3932	0.583
500	64	4.4223	0.607
540	62	4.4580	0.637
580	62	4.4937	0.667
620	63	4.5282	0.696
660	63	4.5615	0.724
700	62	4.5984	0.755
740	62	4.6364	0.787
780	62	4.6697	0.815

TABLE VII.
RUN No.7: HYDRATION
PELLET WEIGHT = 4.3788 g
PELLET DIAMETER = 18.72 mm
PELLET POROSITY = 0.62
CALCINATION TEMPERATURE = 850 °C
PARTIAL PRESSURE OF WATER VAPOUR = 2.4 KPa

TIME(min)	TEMP(°C)	WEIGHT(G)	X
0	52	4.3787	0.000
20	61	4.4182	0.028
40	64	4.4576	0.056
60	65	4.4872	0.077
80	67	4.5226	0.102
100	66	4.5617	0.130
120	65	4.5966	0.154
140	64	4.5979	0.156
160	63	4.6645	0.203
180	63	4.6954	0.225
200	62	4.7038	0.231
220	63	4.7278	0.248
240	63	4.7594	0.270
260	62	4.7897	0.292
280	63	4.8052	0.303
300	63	4.8362	0.325
320	63	4.8533	0.339
340	62	4.8833	0.360
360	62	4.8925	0.367
380	61	4.9206	0.385
400	61	4.9503	0.406
420	61	4.9797	0.427
440	62	4.9555	0.412
460	62	5.0097	0.447
480	62	5.0348	0.466
500	62	5.0599	0.484
520	62	5.0409	0.473
540	63	5.0867	0.503
560	62	5.1205	0.527
580	62	5.1011	0.516
600	61	5.1571	0.553
640	61	5.1908	0.577
680	61	5.2232	0.600
720	61	5.2542	0.622
760	62	5.2795	0.640
800	61	5.3062	0.659
840	62	5.3302	0.676
880	62	5.3527	0.692
920	61	5.3710	0.705

TABLE VIII.
RUN No.8: HYDRATION
PELLET WEIGHT = 4.3188 g
PELLET DIAMETER = 17.59 mm
PELLET POROSITY = 0.54
CALCINATION TEMPERATURE = 1010 °C
PARTIAL PRESSURE OF WATER VAPOUR = 2.3 KPa

TIME(min)	TEMP(^{o}C)f	WEIGHT(g)	X
0	54	4.3187	0.000
20	54	4.3479	0.021
40	53	4.3771	0.042
60	54	4.4062	0.063
80	53	4.4229	0.075
100	54	4.4576	0.100
120	54	4.4826	0.118
140	55	4.5075	0.136
160	54	4.5284	0.151
180	55	4.5506	0.167
200	54	4.5714	0.182
220	55	4.5839	0.189
240	54	4.6041	0.203
260	55	4.6295	0.222
280	55	4.6519	0.238
300	54	4.6803	0.258
320	54	4.6975	0.272
340	55	4.7758	0.286
360	54	4.7352	0.301
380	55	4.7533	0.313
400	54	4.7727	0.327
420	54	4.7908	0.340
440	55	4.8102	0.354
460	54	4.8268	0.366
480	55	4.8449	0.379
500	55	4.8629	0.392
520	54	4.8810	0.405
540	54	4.8976	0.417
560	55	4.9143	0.429
580	54	4.9309	0.441
600	54	4.9463	0.452
620	55	4.9616	0.463
640	54	4.9796	0.476
660	55	4.9935	0.486
680	54	5.0100	0.498
700	55	5.0267	0.510
720	54	5.0462	0.524
740	53	5.0656	0.538

TABLE IX.
RUN No.9: HYDRATION
PELLET WEIGHT = 3.4950 g
PELLET DIAMETER = 17.65 mm
PELLET POROSITY = 0.62
CALCINATION TEMPERATURE = 850 °C
PARTIAL PRESSURE OF WATER VAPOUR = 2.0 KPa

TIME(min)	TEMP(°C)	WEIGHT(g)	X
0	28	3.4941	0.000
20	37	3.5328	0.035
40	37	3.5502	0.051
60	37	3.5718	0.069
80	38	3.6060	0.100
100	38	3.1325	0.118
120	37	3.6420	0.132
140	37	3.6701	0.157
160	37	3.6839	0.169
180	37	3.7036	0.187
200	38	3.7377	0.217
220	38	3.7490	0.227
240	38	3.7673	0.243
260	37	3.7771	0.252
280	38	3.8032	0.275
300	38	3.8152	0.285
320	37	3.8220	0.292
340	38	3.8387	0.306
360	37	3.8445	0.312
380	38	3.8623	0.327
400	38	3.8870	0.349
420	37	3.8883	0.351
440	37	3.9106	0.370
460	37	3.9342	0.391
480	37	3.9467	0.403
500	37	3.9566	0.411
520	38	3.9780	0.430
540	37	3.9993	0.449
560	37	4.0040	0.454
580	37	4.0195	0.467
600	38	4.0398	0.485
640	37	4.0600	0.503
680	36	4.0791	0.520
720	36	4.1004	0.539
760	37	4.1229	0.557
800	36	4.1375	0.572
840	36	4.1656	0.597
880	36	4.1869	0.616
920	36	4.2118	0.639
960	36	4.2218	0.648

TABLE X.
RUN No.10: HYDRATION
PELLET WEIGHT = 3.5918 g
PELLET DIAMETER = 17.63 mm
PELLET POROSITY = 0.62
PARTIAL PRESSURE OF WATER VAPOUR = 2.0 KPa
CALCINATION TEMPERATURE = 850 °C

TIME(min)	TEMP(°C)	WEIGHT(g)	X
0	24	3.5918	0.000
20	33	3.6284	0.032
40	33	3.6535	0.053
60	34	3.6843	0.080
80	34	3.6975	0.092
100	34	3.7149	0.106
120	33	3.7429	0.131
140	33	3.7756	0.159
160	33	3.8043	0.184
180	33	3.8123	0.191
200	33	3.8279	0.204
220	33	3.8773	0.230
240	33	3.8700	0.241
260	34	3.8850	0.254
280	33	3.8934	0.261
300	34	3.9195	0.284
320	34	3.9347	0.320
340	33	3.9458	0.306
360	34	3.9724	0.329
380	33	3.9967	0.351
400	33	4.0242	0.374
420	33	4.0034	0.420
440	33	4.0528	0.399
460	32	4.0639	0.409
480	32	4.0847	0.428
500	32	4.1090	0.448
520	32	4.1113	0.450
540	32	4.1228	0.460
560	32	4.1829	0.471
580	32	4.1494	0.483
600	32	4.1558	0.488
620	32	4.1667	0.498
640	32	4.1863	0.515
660	33	4.2089	0.534
680	32	4.2175	0.542
700	32	4.2302	0.556
720	33	4.2475	0.568
740	32	4.2637	0.582
760	31	4.2822	0.598
780	32	4.3006	0.614

TABLE XI.
RUN No.11: HYDRATION
PELLET WEIGHT = 3.6081 g
PELLET DIAMETER = 17.81 mm
PELLET POROSITY = 0.63
CALCINATION TEMPERATURE = 850 °C
PARTIAL PRESSURE OF WATER VAPOUR = 2.8 KPa

TIME(min)	TEMP(°C)	WEIGHT(g)	X
0	34	3.6082	0.000
20	41	3.6498	0.036
40	42	3.6985	0.078
60	43	3.7298	0.105
80	43	3.7669	0.137
100	43	3.8041	0.169
120	43	3.8169	0.180
140	44	3.8578	0.214
160	44	3.8933	0.246
180	43	3.8938	0.252
200	43	3.9311	0.284
220	43	3.9635	0.312
240	43	4.0082	0.345
260	44	4.0337	0.367
280	44	4.0429	0.373
300	44	4.0638	0.393
320	43	4.0928	0.418
340	43	4.1126	0.428
360	43	4.1228	0.443
380	43	4.1508	0.468
400	42	4.1634	0.471
420	42	4.1798	0.493
440	43	4.2053	0.515
460	43	4.2389	0.544
480	42	4.2567	0.558
500	42	4.2737	0.574
540	43	4.3074	0.603
580	42	4.2876	0.583
620	43	4.3375	0.629
660	42	4.3677	0.655
700	43	4.3920	0.676

TABLE XII.
RUN No.12: HYDRATION
PELLET WEIGHT = 4.0538 g
PELLET DIAMETER = 18.41 mm
PELLET POROSITY = 0.62
CALCINATION TEMPERATURE = 850 °C
PARTIAL PRESSURE OF WATER VAPOUR = 3.6 KPa

TIME(min)	TEMP(°C)	WEIGHT(g)	X
0	32	4.0538	0.000
20	43	4.1144	0.046
40	42	4.1556	0.078
60	42	4.2062	0.117
80	42	4.2518	0.152
100	42	4.2973	0.186
120	42	4.3391	0.219
140	42	4.3834	0.253
160	42	4.4171	0.278
180	42	4.4746	0.309
200	42	4.4947	0.338
220	42	4.5090	0.350
240	42	4.5293	0.365
260	42	4.5645	0.392
280	41	4.5997	0.419
300	43	4.6336	0.445
320	42	4.6675	0.471
340	42	4.7013	0.497
360	42	4.7168	0.510
380	43	4.7339	0.522
400	42	4.7639	0.545
420	42	4.7701	0.551
440	42	4.7913	0.566
460	42	4.7987	0.573
480	42	4.8252	0.592
500	41	4.8468	0.610
540	41	4.8616	0.620
580	41	4.9033	0.652
600	42	4.9411	0.681
640	41	4.9750	0.707

TABLE XIII.
RUN No.13: HYDRATION
PELLET WEIGHT = 3.9762 g
PELLET DIAMETER = 18.32 mm
PELLET POROSITY = 0.62
CALCINATION TEMPERATURE = 850 °C
PARTIAL PRESSURE OF WATER VAPOUR = 1.5 KPa

TIME(min)	TEMP(°C)	WEIGHT(g)	X
0	47	3.9762	0.000
20	54	4.0094	0.026
40	54	4.0209	0.035
60	53	4.0388	0.049
80	53	4.0677	0.072
100	53	4.0988	0.096
120	53	4.1053	0.101
140	53	4.1296	0.120
160	54	4.1615	0.145
180	54	4.1703	0.152
200	54	4.1926	0.169
210	55	4.2213	0.193
220	54	4.2548	0.218
240	54	4.2331	0.201
260	55	4.2424	0.224
280	55	4.2586	0.221
300	54	4.2714	0.231
320	54	4.3021	0.255
340	54	4.2842	0.241
360	53	4.3277	0.275
380	53	4.3098	0.261
400	53	4.3583	0.299
440	53	4.3875	0.322
480	53	4.4094	0.339
520	53	4.4311	0.356
560	53	4.4529	0.373
600	53	4.4733	0.389
640	53	4.4976	0.408
680	54	4.5207	0.426
720	55	4.5436	0.444
740	54	4.5692	0.464
800	54	4.5909	0.481
840	54	4.6139	0.499
880	54	4.6305	0.512
920	53	4.6561	0.532
960	53	4.6829	0.553
1000	53	4.7110	0.575
1040	53	4.7353	0.594
1080	53	4.7583	0.612
1120	53	4.7787	0.628

TABLE XIV.
RUN No.14: HYDRATION
PELLET WEIGHT = 3.9047 g
PELLET DIAMETER = 18.39 mm
PELLET POROSITY =0.63
CALCINATION TEMPERATURE = 850 °C
PARTIAL PRESSURE OF WATER VAPOUR = 1.2 KPa

TIME(min)	TEMP(°C)	WEIGHT(g)	X
0	20	3.9046	0.000
20	24	3.9272	0.018
40	25	3.9486	0.035
60	24	3.9712	0.053
80	25	3.9912	0.069
100	25	3.9987	0.075
120	25	4.0088	0.083
140	24	4.0289	0.099
160	24	4.0326	0.102
180	24	4.0377	0.106
200	24	4.0503	0.116
220	24	4.0628	0.126
240	24	4.1037	0.160
260	24	4.1167	0.169
280	25	4.1243	0.175
300	24	4.1419	0.189
320	24	4.1607	0.204
340	25	4.1783	0.218
360	25	4.1908	0.228
380	24	4.1946	0.231
400	24	4.2096	0.243
420	25	4.2235	0.254
440	24	4.2373	0.265
460	24	4.2674	0.289
480	24	4.2825	0.301
500	24	4.2975	0.313
520	24	4.2911	0.308
540	25	4.3101	0.323
560	25	4.3251	0.335
580	24	4.3477	0.353
600	23	4.3665	0.368
620	22	4.3552	0.359
640	24	4.3841	0.382
660	24	4.3992	0.394
680	24	4.4067	0.400
700	23	4.4192	0.410
740	23	4.4381	0.425
780	23	4.4858	0.463
820	23	4.5046	0.478
860	23	4.5308	0.499
900	23	4.5530	0.517
940	23	4.5610	0.523
980	23	4.5660	0.527

TABLE XV.
RUN No.15: HYDRATION
PELLET WEIGHT = 3.8268 g
PELLET DIAMETER = 17.14 mm
PELLET POROSITY = 0.56
CALCINATION TEMPERATURE = 1010 °C
PARTIAL PRESSURE OF WATER VAPOUR = 1.2 KPa

TIME(min)	TEMP(°C)	WEIGHT(g)	X
0	20	3.8268	0.000
20	22	3.8427	0.014
40	22	3.8575	0.025
60	22	3.8735	0.038
80	22	3.8907	0.052
100	22	3.9092	0.067
120	22	3.9239	0.079
140	22	3.9264	0.081
160	22	3.9375	0.090
180	22	3.9510	0.101
200	22	3.9744	0.120
220	22	3.9879	0.131
240	22	4.0017	0.143
260	22	4.0100	0.149
280	22	4.0139	0.152
300	22	4.0285	0.164
320	22	4.0420	0.175
340	22	4.0568	0.187
360	22	4.0620	0.196
380	22	4.0666	0.195
400	22	4.0777	0.204
420	22	4.0889	0.213
440	22	4.1035	0.225
460	22	4.1146	0.234
480	22	4.1293	0.246
500	22	4.1392	0.254
520	22	4.1503	0.263
540	22	4.1613	0.272
560	22	4.1749	0.283
580	22	4.1822	0.289
600	22	4.1847	0.291
620	22	4.1970	0.301
640	23	4.2019	0.305
660	22	4.2068	0.309
660	22	4.2192	0.319
700	22	4.2265	0.325
720	22	4.2315	0.329
740	22	4.2425	0.338
760	22	4.2548	0.348
780	22	4.2659	0.357
800	21	4.2770	0.366
820	22	4.2905	0.377
840	22	4.3041	0.388
860	22	4.3126	0.395
880	22	4.225	0.403

TABLE XVI.
RUN No.16: HYDRATION
PELLET WEIGHT = 4.0429 g
PELLET DIAMETER = 18.50 mm
PELLET POROSITY = 0.63
PARTIAL PRESSURE OF WATER VAPOUR = 2.8 kPa.
CALCINATION TEMPERATURE 850 °C

TIME(min)	TEMP(°C)	WEIGHT(g)	X
0	100	4.0428	0.000
20	105	4.0751	0.025
40	106	4.1295	0.067
60	109	4.1631	0.093
80	110	4.2114	0.130
100	110	4.2355	0.148
120	108	4.3125	0.208
140	107	4.3297	0.221
160	105	4.3744	0.255
180	104	4.4091	0.282
200	103	4.4243	0.294
220	101	4.4546	0.317
240	102	4.4691	0.328
260	102	4.4992	0.351
280	103	4.5376	0.381
300	104	4.5778	0.412
320	103	4.5879	0.419
340	100	4.5956	0.425
360	101	4.6207	0.445
380	101	4.5998	0.429
400	101	4.6113	0.437
420	100	4.6326	0.454
440	101	4.6426	0.462
460	100	4.6661	0.482
480	100	4.7172	0.502
500	100	4.7432	0.539
520	101	4.7705	0.560
540	101	4.7955	0.579
560	100	4.8186	0.597
580	101	4.8381	0.612
600	101	4.8536	0.624

TABLE XVII.
RUN No.17: RECARBONISATION
PELLET WEIGHT = 3.0228 g
PELLET DIAMETER = 17.38 mm
POROSITY OF CALCIUM OXIDE = 0.65
POROSITY OF CALCIUM CARBONATE LAYER = 0.28
CALCINATION TEMPERATURE = 750 °C
PARTIAL PRESSURE OF CO_2 = 101.3 kPa.

TIME(Min)	TEMP(°C)	WEIGHT(g)	X
0	651	3.0255	0.000
1	691	3.0448	0.008
2	829	3.3890	0.154
3	856	3.6914	0.282
4	846	3.8785	0.361
5	832	4.0965	0.453
6	818	4.2430	0.515
7	780	4.3653	0.566
8	719	4.3951	0.579
9	687	4.3860	0.578
10	671	4.4028	0.582
15	668	4.4074	0.583
20	665	4.4121	0.585

TABLE XVIII.
RUN No.18: RECARBONISATION
PELLET WEIGHT = 3.0228 g
PELLET DIAMETER = 17.20 mm
CALCINATION TEMPERATURE = 850 °C
POROSITY OF CALCIUM OXIDE = 0.63
POROSITY OF CALCIUM CARBONATE LAYER = 0.23
PARTIAL PRESSURE OF CO_2 = 101.3 kPa.

TIME(Min)	TEMP(°C)	WEIGHT(g)	X
0	696	3.0261	0.000
1	766	3.0558	0.004
2	862	3.3733	0.137
3	863	3.5885	0.227
4	855	3.8064	0.318
5	847	3.9107	0.361
6	840	4.0502	0.419
7	831	4.1403	0.457
8	804	4.1887	0.477
9	763	4.2614	0.508
10	732	4.2705	0.511
11	718	4.2984	0.523
12	712	4.3016	0.524
13	704	4.3048	0.526
14	704	4.3113	0.529
15	703	4.3187	0.532
16	703	4.3273	0.535

TABLE XVII.
RUN No.17: RECARBONISATION
PELLET WEIGHT = 3.0228 g
PELLET DIAMETER = 17.38 mm
POROSITY OF CALCIUM OXIDE = 0.65
POROSITY OF CALCIUM CARBONATE LAYER = 0.28
CALCINATION TEMPERATURE = 750 °C
PARTIAL PRESSURE OF CO_2 = 101.3 kPa.

TIME(Min)	TEMP(°C)	WEIGHT(g)	X
0	651	3.0255	0.000
1	691	3.0448	0.008
2	829	3.3890	0.154
3	856	3.6914	0.282
4	846	3.8785	0.361
5	832	4.0965	0.453
6	818	4.2430	0.515
7	780	4.3653	0.566
8	719	4.3951	0.579
9	687	4.3860	0.578
10	671	4.4028	0.582
15	668	4.4074	0.583
20	665	4.4121	0.585

TABLE XVIII.
RUN No.18: RECARBONISATION
PELLET WEIGHT = 3.0228 g
PELLET DIAMETER = 17.20 mm
CALCINATION TEMPERATURE = 850 °C
POROSITY OF CALCIUM OXIDE = 0.63
POROSITY OF CALCIUM CARBONATE LAYER = 0.23
PARTIAL PRESSURE OF CO_2 = 101.3 kPa.

TIME(Min)	TEMP(°C)	WEIGHT(g)	X
0	696	3.0261	0.000
1	766	3.0558	0.004
2	862	3.3733	0.137
3	863	3.5885	0.227
4	855	3.8064	0.318
5	847	3.9107	0.361
6	840	4.0502	0.419
7	831	4.1403	0.457
8	804	4.1887	0.477
9	763	4.2614	0.508
10	732	4.2705	0.511
11	718	4.2984	0.523
12	712	4.3016	0.524
13	704	4.3048	0.526
14	704	4.3113	0.529
15	703	4.3187	0.532
16	703	4.3273	0.535

TABLE XXV.
RUN No.19: RECARBONISATION
PELLET WEIGHT = 2.5317 g
PELLET DIAMETER = 16.33 mm
CALCINATION TEMPERATURE = 850 °C
POROSITY OF CALCIUM OXIDE = 0.63
POROSITY OF CALCIUM LAYER = 0.23
PARTIAL PRESSURE OF CO_2 = 101.3 kPa.

TIME(Min)	TEMP(°C)	WEIGHT(g)	X
0	853	2.5323	0.000
5	897	2.8318	0.151
10	894	3.1512	0.312
15	892	3.4283	0.451
20	890	3.6625	0.569
25	886	3.8517	0.664
30	879	3.9942	0.736
35	870	4.0966	0.787
40	860	4.1606	0.819
45	852	4.1766	0.827
50	852	4.1893	0.834
60	851	4.2081	0.843
70	851	4.2273	0.853
80	851	4.2396	0.859
90	852	4.2549	0.867
100	851	4.2651	0.872
110	851	4.2690	0.874
120	850	4.2774	0.878
130	850	4.2874	0.879
140	850	4.2942	0.887
150	851	4.3033	0.891

TABLE XX.
RUN No.20: RECARBONISATION
PELLET WEIGHT = 4.0178 g
PELLET DIAMETER = 18.48 mm
CALCINATION TEMPERATURE = 850 °C
POROSITY OF CALCIUM OXIDE = 0.63
POROSITY OF CALCIUM CARBONATE LAYER = 0.23
PARTIAL PRESSURE OF CO_2 = 101.3 kPa

TIME(min)	TEMP(°C)	WEIGHT(g)	X
0	410	4.0178	0.000
1	475	4.3682	0.015
2	555	4.3182	0.111
3	556	4.5986	0.184
4	547	4.7754	0.240
5	539	4.9395	0.292
6	532	5.0879	0.339
7	521	5.1889	0.371
8	598	5.2553	0.392
9	485	5.3120	0.410
10	481	5.3349	0.417
20	407	5.3393	0.418
30	405	5.3431	0.420
40	409	5.3441	0.421
50	410	5.3463	0.422
60	408	5.3481	0.423

TABLE XXI.
RUN No.21: RECARBONISATION
PELLET WEIGHT = 4.1013 g
PELLET DIAMETER = 18.20 mm
CALCIUM OXIDE POROSITY = 0.60
CALCIUM CARBONATE LAYER POROSITY = 0.20
RECALCINED AT 800 °C
PARTIAL PRESSURE OF CO_2 = 101.3 kPa.

TIME(min)	TEMP(°C)	WEIGHT(g)	X
0	501	4.1255	0.000
1	520	4.1621	0.011
2	712	4.5418	0.128
3	723	4.8086	0.210
4	731	5.0587	0.288
5	740	5.2852	0.357
6	746	5.4736	0.416
7	746	5.6072	0.457
8	658	5.6756	0.478
9	580	5.6763	0.478
10	551	5.6795	0.479
11	535	5.6804	0.479
12	526	5.6818	0.480
13	522	5.6775	0.478
14	519	5.6826	0.480
15	517	5.6831	0.480
16	515	5.6818	0.480
17	515	5.6822	0.480
18	514	5.6833	0.480
19	514	5.6843	0.481
20	514	5.6841	0.480
21	513	5.6844	0.481
22	513	5.6882	0.482
23	513	5.6879	0.482
24	513	5.6869	0.481
25	513	5.6864	0.481
50	513	5.7007	0.486
100	514	5.7206	0.492
140	513	5.7344	0.496

TABLE XXVIII.
RUN No.22: RECARBONISATION
PELLET WEIGHT = 3.3110 g
PELLET DIAMETER = 17.21 mm
POROSITY OF CALCIUM OXIDE = 0.62
POROSITY OF CALCIUM CARBONATE = 0.22
PARTIAL PRESSURE OF CO_2 = 101.3 kPa.
CALCINATION TEMPERATURE = 850 °C

FIRST RECARBONISATION

TIME(min)	TEMP(°C)	WEIGHT(g)	X
0	503	3.3104	0.000
1	651	3.4703	0.061
2	733	3.8148	0.194
3	754	4.1091	0.307
4	767	4.3765	0.410
5	756	4.5862	0.490
6	734	4.7335	0.547
7	713	4.8330	0.585
8	705	4.8996	0.611
9	589	4.9291	0.622
10	557	4.9306	0.623
11	541	4.9347	0.624
12	532	4.9325	0.623
13	528	4.9364	0.625
14	525	4.9383	0.626
15	524	4.9379	0.625
16	523	4.9374	0.625
17	522	4.9384	0.626
SECOND RECARBONISATION			
0	500	3.3110	0.000
1	613	3.4617	0.058
2	710	3.7566	0.171
3	717	3.9819	0.258
4	713	4.1753	0.336
5	689	4.3217	0.389
6	668	4.4247	0.428
7	656	4.4971	0.456
8	633	4.5754	0.484
9	564	4.5581	0.480
10	541	4.5619	0.481
11	532	4.5639	0.482
12	526	4.5650	0.482
13	523	4.5651	0.482
14	522	4.5701	0.483
15	520	4.5695	0.483
20	520	4.5713	0.485
30	520	4.5774	0.487
35	521	4.5797	0.488

TABLE XXVI (Continued)

40	521	4.5782	0.487
50	522	4.5797	0.488

3TH RECARBURISATION

0	496	3.3126	0.000
1	550	3.3770	0.023
2	704	3.6506	0.128
3	704	3.8513	0.205
4	694	4.0205	0.269
5	675	4.1274	0.310
6	612	4.1815	0.331
7	559	4.1852	0.333
8	537	4.1910	0.335
9	526	4.1905	0.335
10	521	4.1926	0.335
11	519	4.1914	0.335
12	518	4.1906	0.335
13	517	4.1962	0.337
14	517	4.1935	0.336
15	517	4.1975	0.337

TABLE XXIII.
RUN No.23: RECARBONISATION
PELLET WEIGHT = 2.7826 g
PELLET DIAMETER = 16.38 mm
POROSITY OF CALCIUM OXIDE = 0.63
POROSITY OF CALCIUM CARBONATE LAYER = 0.23
CALCINATION TEMPERATURE = 850 °C
PARTIAL PRESSURE OF CO_2 = 22.286 kPa.

TIME(min)	TEMP(°C)f	WEIGHT(g)	X
0	450	2.7825	0.000
1	452	2.7856	0.001
2	454	2.8028	0.009
3	454	2.8399	0.026
4	453	2.8613	0.036
5	454	2.8889	0.049
6	454	2.9177	0.062
7	454	2.9233	0.064
8	454	2.9264	0.066
9	454	2.9239	0.065
10	454	2.9251	0.065

TABLE XXIV.
RUN No.24: RECARBONISATION
PELLET WEIGHT = 3.4549 g
PELLET DIAMETER = 17.60 mm
POROSITY OF CALCIUM OXIDE = 0.63
POROSITY OF CALCIUM CARBONATE LAYER = 0.23
CALCINATION TEMPERATURE = 850 °C
PARTIAL PRESSURE OF CO_2 = 28.364 kPa.

TIME(min)	TEMP(°C)	WEIGHT(g)	X
0	400	3.4549	0.000
1	425	3.4906	0.013
2	456	3.5457	0.033
3	462	3.5927	0.051
4	460	3.6304	0.065
5	454	3.6654	0.078
6	446	3.6853	0.085
7	439	3.7062	0.093
8	432	3.7225	0.098
9	426	3.7362	0.103
10	421	3.7472	0.107
15	408	3.7714	0.116
20	407	3.7866	0.121
30	407	3.8139	0.131
40	406	3.8441	0.142
50	406	3.8675	0.151
100	406	3.9612	0.185
150	405	4.0359	0.213
200	405	4.0957	0.234
218	405	4.1141	0.241

TABLE XXV.
RUN No.25: RECARBONISATION
PELLET WEIGHT = 3.6758 g
PELLET DIAMETER = 17.98 mm
POROSITY OF CALCIUM OXIDE = 0.63
POROSITY OF CALCIUM CARBONATE LAYER = 0.23
CALCINATION TEMPERATURE = 850 °C
PARTIAL PRESSURE OF CO_2 = 50.65 kPa.

TIME(min)	TEMP(°C)f	WEIGHT(g)	X
0	401	3.6758	0.000
1	401	3.7278	0.018
2	402	3.8231	0.051
3	405	3.9270	0.087
4	408	4.0050	0.114
5	408	4.0686	0.136
6	407	4.1061	0.149
7	406	4.1350	0.159
8	405	4.1523	0.165
9	405	4.1581	0.167
10	404	4.1638	0.169
15	403	4.1812	0.175
20	403	4.1927	0.179
25	403	4.2101	0.185
30	403	4.2245	0.190
35	403	4.2332	0.193
40	402	4.2447	0.197
43	403	4.2534	0.200

TABLE XXVI.
RUN No.26: RECARBONISATION
PELLET WEIGHT = 2.0443 g
PELLET DIAMETER = 14.55 mm
POROSITY OF CALCIUM OXIDE = 0.62
POROSITY OF CALCIUM LAYER = 0.21
CALCINATION TEMPERATURE = 850 °C
PARTIAL PRESSURE OF CO_2 = 101.3 kPa.

TIME(min)	TEMP(°C)f	WEIGHT(g)	X
0	500	2.0443	0.000
1	501	2.2089	0.102
2	501	2.4138	0.230
3	503	2.6387	0.370
4	502	2.8329	0.482
5	503	2.9278	0.550
6	502	3.0529	0.617
7	503	3.1448	0.673
8	503	3.1716	0.689
9	502	3.1737	0.691
10	502	3.1744	0.691
11	503	3.1743	0.691

TABLE XXVII.
RUN No.27: RECARBONISATION
PELLET WEIGHT =0.9778 g
PELLET DIAMETER = 11.55 mm
POROSITY OF CALCIUM CARBONATE = 0.63
POROSITY OF CALCIUM CARBONATE LAYER = 0.23
CALCINATION TEMPERATURE = 850 °C
PARTIAL PRESSURE OF CO_2 = 101.3 kpa.

TIME(min)	TEMP(°C)f	WEIGHT(g)	X
0	510	0.9774	0.000
1	510	1.0832	0.142
2	512	1.2637	0.378
3	514	1.4141	0.575
4	512	1.4942	0.680
5	510	1.5030	0.692
6	510	1.5003	0.688
7	510	1.5023	0.691
8	511	1.5071	0.697
9	510	1.5101	0.701
10	509	1.5110	0.702
11	510	1.5109	0.702

TABLE XXVIII.
RUN No.28: RECARBONISATION
PELLET WEIGHT = 4.0771 g
PELLET DIAMETER = 18.60 mm
POROSITY OF CALCIUM OXIDE = 0.63
POROSITY OF CALCIUM CARBONATE LAYER = 0.23
CALCINATION TEMPERATURE = 850 °C
PARTIAL PRESSURE OF CO_2 = 30.39 kPa.

TIME(min)	TEMP(°C)	WEIGHT(g)	X
0	311	4.0770	0.000
1	342	4.1080	0.012
2	355	4.1410	0.022
3	340	4.1473	0.024
4	330	4.1497	0.025
5	324	4.1519	0.025
10	317	4.1570	0.027
15	317	4.1625	0.029
20	317	4.1733	0.031
30	314	4.1735	0.031
40	313	4.1734	0.031

TABLE XXIX.
RUN No.29: RECARBONISATION
PELLET WEIGHT = 3.2686 g
PELLET DIAMETER = 17.15 mm
POROSITY OF CALCIUM OXIDE = 0.627
POROSITY OF CALCIUM CARBONATE LAYER = 0.22
CALCINATION TEMPERATURE = 850 °C
PARTIAL PRESSURE OF CO_2 = 41.5 kPa.

TIME(min)	TEMP(°C)	WEIGHT(g)	X
0	406	3.2705	0.000
1	409	3.3086	0.016
2	413	3.3902	0.048
3	416	3.4845	0.085
4	416	3.5590	0.114
5	415	3.6154	0.136
6	414	3.6535	0.150
7	414	3.6787	0.160
8	412	3.6959	0.166
9	412	3.7109	0.173
10	412	3.7134	0.174
15	409	3.7264	0.179
20	408	3.7364	0.183
25	408	3.7434	0.185
30	408	3.7516	0.189
35	407	3.7639	0.193
40	407	3.7634	0.193
45	406	3.7741	0.197
50	405	3.7790	0.199

TABLE XXX.
RUN No.30: RECARBONISATION
PELLET WEIGHT = 3.7612 g
PELLET DIAMETER = 17.13 mm
POROSITY OF CALCIUM OXIDE = 0.63
POROSITY OF CALCIUM CARBONATE LAYER = 0.23
CALCINATION TEMPERATURE = 850 °C
PARTIAL PRESSURE OF CO_2 = 25.325 kpa.

TIME(min)	TEMP(°C)	WEIGHT(g)	X
0	400	3.7613	0.000
1	424	3.8001	0.013
2	465	3.8662	0.036
3	467	3.9203	0.054
4	464	3.9615	0.068
5	458	3.9965	0.080
6	452	4.0250	0.090
7	446	4.4903	0.098
8	442	4.0690	0.104
9	438	4.0937	0.113
10	435	4.1110	0.118
11	432	4.1197	0.121
12	428	4.1337	0.126
13	424	4.1431	0.129
14	422	4.1501	0.132
15	420	4.1506	0.132
16	419	4.1615	0.135
17	418	4.1720	0.139
18	417	4.1735	0.140
19	416	4.1770	0.141
20	415	4.1884	0.145
21	414	4.1900	0.145

TABLE XXXI.
RUN No.31:RECARBONISATION
PELLET WEIGHT = 4.0495 g
PELLET DIAMETER = 17.3 mm
CALCINATION TEMPERATURE = 1010 °C
POROSITY OF CALCIUM OXIDE = 0.59
POROSITY OF CALCIUM CARBONATE LAYER = 0.14
PARTIAL PRESSURE OF CO_2 = 50.65 kPa.

TIME(min)	TEMP(°C)	WEIGHT(g)	X
0	400	4.0496	0.000
1	484	4.1639	0.037
2	520	4.2737	0.071
3	520	4.3497	0.095
4	507	4.4096	0.114
5	490	4.4533	0.128
6	471	4.4863	0.138
7	454	4.5042	0.144
8	438	4.5156	0.147
9	427	4.5223	0.149
10	421	4.5265	0.151
11	417	4.5224	0.149

TABLE XXXII.
RUN No.32: RECARBONISATION
PELLET WEIGHT = 3.8785 g
PELLET DIAMETER =16.46 mm
POROSITY OF CALCIUM OXIDE = 0.50
POROSITY OF CALCIUM CARBONATE LAYER = 0.03
CALCINATION TEMPERATURE = 1100 °C
PARTIAL PRESSURE OF CO_2 = 50.65 kPa.

TIME(min)	TEMP(°C)	WEIGHT(g)	X
0	400	3.8785	0.000
1	432	3.9482	0.023
2	476	4.0062	0.042
3	462	4.0317	0.051
4	437	4.0506	0.057
5	425	4.0583	0.059
6	417	4.0678	0.063
7	409	4.0694	0.064
8	406	4.0748	0.064
9	404	4.0820	0.065
10	402	4.0854	0.068
15	401	4.0858	0.068

TABLE XXXIII.
RUN No.33: HYDRATION
PELLET WEIGHT = 4.3761 g
PELLET DIAMETER = 18.05 mm
CALCINATION TEMPERATURE = 850 °C
δ = 0.6 mm
PARTIAL PRESSURE OF WATER VAPOUR = 2.8 KPa.

TIME(Min)	TEMP(°C)	WEIGHT(g)	X
0	50	4.3762	0.000
10	50	4.3776	0.001
20	50	4.3797	0.002
30	50	4.3801	0.003
40	51	4.3810	0.004
50	52	4.3803	0.003
100	52	4.3901	0.010
150	53	4.3832	0.015
200	53	4.3973	0.033
250	54	4.4226	0.042
300	53	4.4452	0.050
350	53	4.4465	0.059
400	53	4.4591	0.071
450	52	4.4629	0.082
500	53	4.4761	0.090
550	52	4.5028	0.095
600	53	4.5157	0.099
650	52	4.5298	0.109
700	52	4.5397	0.116
750	52	4.5538	0.126
800	52	4.5665	0.135
850	53	4.5820	0.146
900	53	4.5975	0.157
950	53	4.6073	0.164
1000	52	4.6172	0.171
1050	53	4.6243	0.176
1100	52	4.6355	0.184
1150	52	4.6426	0.189
1200	52	4.6567	0.199

TABLE XXXIV.
RUN No.34: HYDRATION
PELLET WEIGHT = 3.2847 g
PELLET DIAMETER = 18.10 mm
PELLET DENSITY = 0.021796 mol/cm^3
FRAC. RECARBONATED = 0.13
δ = 0.5 mm
CALCINATION TEMPERATURE = 850 °C.
PARTIAL PRESSURE OF WATER VAPOUR = 2.8 KPa.

TIME(min)	TEMP(°C)	WEIGHT(g)	X
0	60	3.2846	0.000
10	60	3.2876	0.001
20	60	3.2842	0.000
30	61	3.2865	0.002
40	61	3.2864	0.002
50	61	3.2911	0.006
100	61	3.3001	0.012
150	62	3.3044	0.025
200	61	3.3374	0.052
250	62	3.3395	0.062
300	62	3.3500	0.075
350	61	3.3544	0.085
400	62	3.3589	0.095
450	62	3.3637	0.101
500	61	3.3912	0.107
550	61	3.3975	0.113
600	62	3.4039	0.119
650	63	3.4102	0.125
700	63	3.4166	0.130
750	63	3.4218	0.149
800	63	3.4419	0.163
850	63	3.4566	0.175
900	63	3.4694	0.181
950	63	3.4757	0.192
1000	63	3.4873	0.202
1050	64	3.4989	0.209
1150	63	3.5052	0.219
1200	63	3.5242	0.226
1250	63	3.5295	0.231
1300	62	3.5453	0.246
1350	62	3.5560	0.256
1400	62	3.5719	0.271
1450	62	3.5931	0.291
1500	62	3.6091	0.306
1550	62	3.6249	0.321

TABLE XXXV.
RUN No.35: HYDRATION
PELLET WEIGHT = 2.6630 g
PELLET DIAMETER = 16.38 mm
CALCINATION TEMPERATURE = 850 °C
δ = 0.1 mm
FRAC. OF RECARBONISATION = 0.070
PARTIAL PRESSURE OF WATER VAPOUR = 2.8 KPa.

TIME(min)	TEMP(°C)	WEIGHT(g)	X
0	53	2.6630	0.000
10	52	2.6635	0.000
20	53	2.6646	0.002
30	52	2.6698	0.008
40	54	2.6766	0.016
50	53	2.6947	0.037
100	55	2.7161	0.062
150	55	2.7349	0.084
200	55	2.7494	0.101
250	55	2.7623	0.116
300	55	2.7726	0.128
350	55	2.7871	0.145
400	54	2.7974	0.157
450	54	2.8059	0.167
500	54	2.8162	0.179
550	54	2.8239	0.188
600	55	2.8333	0.199
650	55	2.8436	0.211
700	54	2.8564	0.226
750	55	2.8736	0.246
800	55	2.8821	0.256
850	54	2.9078	0.286
900	55	2.9335	0.316
950	54	2.9583	0.345
1000	55	2.9882	0.380
1050	55	3.0156	0.412

TABLE XXXVI.
RUN No.36: HYDRATION
MASS OF CALCIUM OXIDE = 2.8039 g
PELLET DIAMETER = 17.60 mm
FRAC. RECARBONISED = 0.24
δ = 0.80 mm
PARTIAL PRESSURE OF WATER VAPOUR = 2.8 KPa
CALCINATION TEMPERATURE = 850 °C

TIME(min)	TEMP(°C)	WEIGHT(g)	X
0	50	2.8039	0.000
10	51	2.8041	0.000
20	50	2.8046	0.001
30	51	2.8049	0.001
40	51	2.8057	0.002
50	51	2.8065	0.005
100	52	2.8046	0.008
150	51	2.8264	0.025
200	50	2.8354	0.035
250	50	2.8489	0.050
300	50	2.8570	0.059
350	51	2.8673	0.061
400	51	2.8769	0.070
450	50	2.8800	0.075
500	51	2.8885	0.080
550	51	2.8902	0.101
600	51	2.8958	0.102
650	51	2.8976	0.104
700	52	2.9003	0.107
750	52	2.9030	0.110
800	52	2.9129	0.121
850	52	2.9165	0.125
900	51	2.9228	0.132
950	51	2.9309	0.141
1000	51	2.9390	0.150
1050	51	2.9426	0.154
1100	51	2.9462	0.158
1150	52	2.9499	0.162
1200	52	2.9535	0.166
1250	52	2.9553	0.168
1300	52	2.9571	0.170
1350	52	2.9589	0.172
1400	52	2.9616	0.175
1450	52	2.9715	0.179
1500	52	2.9769	0.186
1550	52	2.9832	0.192
1600	52	2.9860	0.199
1650	51	2.9914	0.203

TABLE XXXVII.
RUN No.37: HYDRATION
PELLET WEIGHT = 3.4886 g
PELLET DIAMETER = 18.27 mm
δ = 0.35 mm
CALCINATION TEMPERATURE = 850 °C
FRACTIONAL OF RECARBONISATION = 0.10
PARTIAL PRESSURE OF WATER VAPOUR = 1.2 KPa.

TIME(min)	TEMP(°C)	WEIGHT(g)	X
0	20	3.4886	0.000
20	21	3.4888	0.000
40	21	3.4908	0.002
60	21	3.4931	0.004
80	22	3.4987	0.009
100	22	3.5166	0.025
200	22	3.5278	0.035
300	22	3.5446	0.050
400	23	3.5592	0.063
500	25	3.5670	0.070
600	25	3.5793	0.081
700	24	3.5895	0.090
800	24	3.6007	0.100
900	24	3.6175	0.115
1000	24	3.6197	0.117
1100	23	3.6287	0.125
1200	24	3.6343	0.130
1300	24	3.6411	0.136
1400	24	3.6455	0.140
1500	24	3.6511	0.145
1600	24	3.6579	0.151
1700	24	3.6713	0.163
1800	24	3.6781	0.169
1900	25	3.6848	0.181
2000	24	3.6915	0.186
2100	24	3.6971	0.191
2200	24	3.7027	0.194
2300	24	3.7061	0.199
2400	24	3.7117	0.204
2500	24	3.7173	0.206
2600	24	3.7195	0.209
2700	25	3.7229	0.213

TABLE XXXVIII.
RUN No.38: HYDRATION
PELLET WEIGHT = 3.9202 g
PELLET DIAMETER = 18.59 mm
δ = 0.097 mm
FRACTIONAL OF RECARBONISATION = 0.03
CALCINATION TEMPERATURE = 850 °C
PARTIAL PRESSURE OF WATER VAPOUR = 2.8 kPa.

TIME(min)	TEMP(°C)	WEIGHT(g)	X
0	32	3.9203	0.000
50	35	3.9635	0.003
100	37	4.0072	0.030
150	36	4.0312	0.070
200	37	4.0539	0.100
250	37	4.0728	0.121
300	37	4.0892	0.134
350	37	4.1081	0.149
400	37	4.1257	0.163
450	36	4.1358	0.171
500	36	4.1499	0.182
550	36	4.1635	0.193
600	36	4.1774	0.204
650	37	4.1849	0.211
700	37	4.2038	0.225
750	38	4.2328	0.248
800	38	4.2441	0.257
850	39	4.2845	0.289
900	39	4.3147	0.313
950	40	4.4601	0.349
1000	40	4.4054	0.385
1050	41	4.4306	0.405
1100	40	4.4710	0.437
1150	41	4.4962	0.457
1200	42	4.5579	0.506
1250	43	4.5856	0.528
1300	43	4.6105	0.548
1350	44	4.6261	0.561
1400	43	4.6352	0.566
1450	44	4.6644	0.589
1500	44	4.6858	0.606
1550	44	4.7081	0.624
1600	44	4.7358	0.646

TABLE XXXIX.
RUN No.39: HYDRATION
PELLET WEIGHT = 3.2319 g
PELLET DIAMETER = 18.13 mm
FRAC. RECARBONISED = 0.14
δ = 0.47 mm
CALCINATION TEMPERATURE = 850 °C
PARTIAL PRESSURE OF WATER VAPOUR = 2.8 KPa.

TIME(min)	TEMP(°C)	WEIGHT(g)	X
0	35	3.2320	0.000
50	36	3.2339	0.002
100	37	3.2328	0.001
150	37	3.2371	0.005
200	37	3.2724	0.039
250	37	3.2901	0.056
300	37	3.3057	0.071
350	37	3.3223	0.087
400	37	3.3327	0.097
450	37	3.3482	0.112
500	36	3.3607	0.124
550	36	3.3690	0.132
600	36	3.3821	0.143
650	36	3.3908	0.153
700	36	3.4023	0.164
750	37	3.4137	0.175
800	37	3.4178	0.179
850	36	3.4262	0.187
900	37	3.4345	0.195
950	37	3.4469	0.207
1000	37	3.4511	0.211
1050	37	3.4636	0.223
1100	37	3.4760	0.235
1150	36	3.4895	0.248
1200	36	3.5009	0.259
1250	37	3.5113	0.269
1300	37	3.5269	0.284
1350	38	3.5446	0.302
1400	39	3.5612	0.317
1450	40	3.5778	0.333
1500	40	3.5934	0.348
1550	39	3.6079	0.362
1600	39	3.6225	0.376
1650	38	3.6360	0.389
1700	38	3.6505	0.403
1750	38	3.6640	0.416
1800	37	3.6786	0.430

TABLE XL.
RUN No.40: HYDRATION
PELLET WEIGHT = 3.4421 g
PELLET DIAMETER = 17.88 mm
FRAC. RECARBONISED = 0.15
δ = 0.47 mm
PARTIAL PRESSURE OF WATER VAPOUR = 1.2 KPa.
CALCINATION TEMPERATURE = 1000 °C

TIME(Min)	TEMP(°C)	WEIGHT(g)	X
0	30	3.4423	0.000
100	30	3.4437	0.001
200	30	3.4456	0.003
300	30	3.4456	0.003
400	31	3.4478	0.004
500	30	3.4467	0.008
600	32	3.4511	0.012
700	30	3.4555	0.016
800	31	3.4601	0.019
900	32	3.4633	0.024
1000	33	3.4668	0.028
1100	31	3.4732	0.032
1200	31	3.4777	0.035
1300	30	3.4854	0.039
1400	32	3.4876	0.041
1500	31	3.4909	0.044
1600	32	3.4943	0.047
1700	33	3.4976	0.050
1800	32	3.5009	0.053
1900	33	3.5020	0.054
2000	33	3.5053	0.057
2100	32	3.5086	0.060
2200	32	3.5120	0.063
2300	32	3.5164	0.067
2400	32	3.5197	0.070
2500	32	3.5230	0.073
2600	32	3.5263	0.076
2700	32	3.5308	0.080
2800	32	3.5330	0.082
2900	32	3.5363	0.085
3000	32	3.5401	0.088

TABLE XLI.
RUN No.41: HYDRATION
PELLET WEIGHT = 3.6186 g
PELLET DIAMETER = 16.46 mm
δ = 0.20 mm
CALCINATION TEMPERATURE = 1100 °C
FRACTIONAL OF RECARBONISATION = 0.068
PARTIAL PRESSURE OF WATER VAPOUR = 1.2 kPa.

TIME(min)	TEMP(°C)	WEIGHT(g)	X
0	25	3.6186	0.000
100	25	3.6202	0.002
200	25	3.6189	0.001
300	25	3.6236	0.004
400	25	3.6282	0.008
500	25	3.6329	0.012
600	25	3.6375	0.016
700	25	3.6410	0.019
800	25	3.6445	0.022
900	25	3.6492	0.026
1000	25	3.6526	0.029
1100	25	3.6561	0.032
1200	25	3.6596	0.035
1300	25	3.6631	0.038
1400	25	3.6666	0.041
1500	25	3.6689	0.043
1600	25	3.6736	0.047
1700	25	3.6771	0.050
1800	25	3.6796	0.052
1900	25	3.6829	0.055
2000	25	3.6852	0.057
2100	25	3.6875	0.059
2200	25	3.6899	0.061
2300	25	3.6922	0.063
2400	25	3.6934	0.064
2500	25	3.6957	0.066
2600	25	3.6981	0.068
2700	25	3.7003	0.070
2800	25	3.7023	0.072
2900	25	3.7050	0.074
3000	25	3.7078	0.078

TABLE XLII.
RUN No.42: HYDRATION
MASS OF CaO =3.3085 g
PELLET DIAMETER =17.56 mm
CALCINATION TEMPERATURE = 850 °C
FRACTION OF INERT MATERIAL = 10%
PARTIAL PRESSURE OF WATER VAPOUR = 2.8 kPa.

TIME(min)	TEMP(°C)	WEIGHT(g)	X
0	30	3.3085	0.000
20	35	3.3530	0.042
40	37	3.4002	0.086
60	37	3.4362	0.120
80	37	3.4601	0.143
100	36	3.4898	0.171
120	37	3.5176	0.197
140	37	3.5518	0.229
160	37	3.5855	0.260
180	37	3.6200	0.293
200	37	3.6552	0.326
220	37	3.6951	0.363
240	37	3.7290	0.395
260	37	3.7713	0.435
280	38	3.8146	0.476
300	38	3.8515	0.511
320	38	3.8831	0.540
340	37	3.9093	0.565
360	37	3.9355	0.590
380	37	3.9616	0.614
400	37	3.9915	0.642
420	38	4.0157	0.665
440	37	4.0410	0.689
460	37	4.0618	0.708
480	37	4.0817	0.727
500	37	4.0962	0.741
520	36	4.1169	0.760
540	36	4.1379	0.780
560	36	4.1597	0.800

TABLE XLIII.
RUN No.43: HYDRATION
PELLET DIAMETER = 17.85 mm
MASS OF CaO = 2.8625 g
FRACTION OF INERT MATERIAL = 10%
FRACTIONAL OF RECARBONISATION = 0.08
δ = 0.10 mm
PARTIAL PRESSURE OF WATER VAPOUR = 2.8 kPa.

TIME(min)	TEMP(°C)	WEIGHT(g)	X
0	40	2.8625	0.000
50	41	2.9058	0.020
100	41	2.9500	0.040
200	42	3.9348	0.060
300	43	3.0760	0.080
400	43	3.0874	0.095
500	42	3.1324	0.100
600	42	3.1549	0.120
700	42	3.1774	0.131
800	42	3.1999	0.140
900	42	3.2224	0.152
1000	43	3.2673	0.160
1100	42	3.2898	0.118
1200	42	3.3075	0.119
1300	42	3.3123	0.200
1400	43	3.3573	0.220

TABLE XLIV.
RUN No.44:HYDRATION
PELLET DIAMETER = 18.04 mm
MASS OF CaO = 3.2994 g
FRACTIONAL RECARBONATED = 0.11
δ = 0.33 mm
FRACTION OF INERT MATERIAL = 10%
PARTIAL PRESSURE OF WATER VAPOUR = 2.8 kPa.

TIME(min)	TEMP(°C)	WEIGHT(g)	X
0	37	3.2994	0.000
50	37	3.3015	0.002
100	37	3.3047	0.011
200	37	3.3259	0.025
300	36	3.3385	0.037
400	37	3.3503	0.048
500	37	3.3620	0.059
600	36	3.3768	0.073
700	36	3.3853	0.081
800	37	3.3991	0.094
900	38	3.4118	0.106
1000	38	3.4235	0.117
1100	38	3.4362	0.129
1200	38	3.4489	0.141
1300	38	3.4617	0.153
1400	37	3.4754	0.166
1500	36	3.4988	0.188
1600	36	3.7920	0.192
1700	35	3.8179	0.201
1800	36	3.8438	0.210
1900	35	3.8697	0.220
2000	36	3.8956	0.230

TABLE XLV.
RUN No.45: HYDRATION
PELLET DIAMETER = 18.38 mm
MASS OF CaO = 3.2010 g
FRACTIONAL RECARBONATED = 0.13
δ = 0.43 mm
FRACTION OF INERT MATERIAL = 10%
PARTIAL PRESSURE OF WATER VAPOUR = 2.8 kPa.

TIME(min)	TEMP(°C)	WEIGHT(g)	X
0	43	3.2010	0.000
100	42	3.2051	0.004
200	42	3.2103	0.009
300	43	3.2387	0.015
400	43	3.2700	0.028
500	43	3.2893	0.035
600	44	3.3316	0.056
700	44	3.3698	0.064
800	44	3.3811	0.072
900	44	3.4073	0.080
1000	43	3.4427	0.096
1100	42	3.4509	0.100
1200	42	3.4670	0.107
1300	42	3.4835	0.114
1400	42	3.5096	0.121
1500	42	3.5220	0.128
1600	42	3.5432	0.136
1700	42	3.5773	0.150
1800	42	3.5949	0.157
1900	42	3.6100	0.163
2000	42	3.6250	0.169
2100	42	3.46351	0.173

TABLE XLVI.
RUN No.46: HYDRATION
PELLET DIAMETER = 18.15 mm
MASS OF CaO = 2.3772 g
FRACTIONAL RECARBONATED = 0.33
δ = 1.56 mm
FRACTION OF INERT MATERIAL = 10%
PARTIAL PRESSURE OF WATER VAPOUR = 2.8 kPa.

TIME(min)	TEMP(°C)	WEIGHT(g)	X
0	41	2.3772	0.000
100	41	2.3795	0.003
200	43	2.3781	0.001
300	43	2.3787	0.002
400	43	2.3833	0.008
500	44	2.3847	0.010
600	44	2.4052	0.015
700	43	2.4146	0.020
800	42	2.4239	0.025
900	42	2.4332	0.030
1000	42	2.4444	0.036
1100	41	2.4519	0.040
1200	42	2.4706	0.050
1300	43	2.4818	0.056
1400	43	2.4911	0.061
1500	43	2.4917	0.064
1600	43	2.5123	0.071
1700	43	2.5159	0.075
1800	42	2.5199	0.079
1900	43	2.5217	0.081

TABLE XLVII.
RUN No.47: HYDRATION
PELLET DIAMETER =17.57 mm
MASS OF CaO = 3.2632 g
FRACTION OF INERT MATERIAL = 15%
PARTIAL PRESSURE OF WATER VAPOUR = 2.8 kPa.

TIME(min)	TEMP(°C)	WEIGHT(g)	X
0	50	3.2632	0.000
10	51	3.2789	0.015
20	54	3.2978	0.033
30	54	3.3177	0.052
40	55	3.3365	0.070
50	54	3.3586	0.091
60	55	3.3796	0.111
70	54	3.3996	0.130
80	54	3.4183	0.148
90	53	3.4572	0.185
100	53	3.4730	0.200
110	53	3.4877	0.214
120	53	3.5034	0.229
130	53	3.5190	0.244
140	53	3.5328	0.257
150	53	3.5339	0.260
160	53	3.5558	0.279
170	53	3.5779	0.300
180	53	3.5999	0.321
190	54	3.6188	0.339
200	54	3.6366	0.356
210	54	3.6554	0.374
220	54	3.6744	0.392
230	54	3.6827	0.400
240	53	3.7058	0.422
250	52	3.7205	0.436
260	53	3.7404	0.455
270	53	3.7614	0.475
280	53	3.7803	0.493
290	53	3.8013	0.513
300	52	3.8202	0.531
310	53	3.8369	0.547
320	53	3.8579	0.567
330	53	3.8768	0.585
340	54	3.8936	0.601
350	53	3.9114	0.618
360	52	3.9219	0.628
370	52	3.9397	0.645

TABLE XLVIII.
RUN No.48: HYDRATION
PELLET DIAMETER = 17.52 mm
MASS OF CaO = 2.8293 g
FRACTIONAL RECARBONATED = 0.077
δ = 0.23 mm
FRACTION OF INERT MATERIAL = 15%
PARTIAL PRESSURE OF WATER VAPOUR = 2.8 kPa.

TIME(min)	TEMP(°C)	WEIGHT(g)	X
0	47	2.8293	0.000
50	48	2.8338	0.005
100	47	2.8411	0.023
200	48	2.9182	0.040
300	47	2.9516	0.055
400	47	2.9849	0.070
500	48	3.0071	0.080
600	48	3.0293	0.095
700	48	3.0516	0.100
800	47	3.0738	0.110
900	48	3.0961	0.120
1000	47	3.1183	0.130
1100	48	3.1405	0.140
1200	47	3.1628	0.151
1300	48	3.1728	0.153
1400	48	3.1961	0.160
1500	48	3.2117	0.172
1600	48	3.2251	0.178
1700	48	3.2339	0.189
1800	48	3.2964	0.210

TABLE XLIX.
RUN No.49: HYDRATION
PELLET DIAMETER = 18.19 mm
MASS OF CaO = 3.3234 g
FRACTIONAL OF RECARBONISATION = 0.102
δ = 0.316 mm
FRACTION OF INERT MATERIAL = 15%
PARTIAL PRESSURE OF WATER VAPOUR = 2.8 kPa.

TIME(min)	TEMP(°C)	WEIGHT(g)	X
0	50	3.3234	0.000
100	53	3.3309	0.007
200	53	3.3197	0.003
200	52	3.3287	0.005
400	52	3.3501	0.025
500	52	3.3597	0.034
600	52	3.3693	0.043
700	52	3.3779	0.051
800	52	3.3875	0.060
900	52	3.5584	0.070
1000	52	3.4057	0.089
1100	52	3.4153	0.098
1200	52	3.4249	0.105
1300	52	3.4334	0.116
1400	52	3.4420	0.121
1500	52	3.4516	0.129
1600	52	3.4612	0.136
1700	52	3.4697	0.155
1800	52	3.4804	0.164
1900	52	3.4890	0.172
2000	52	3.4986	0.181
2100	52	3.5071	0.190
2200	52	3.5167	0.197
2300	52	3.5264	0.207
2400	52	3.5338	0.197
2500	52	3.5445	0.207

TABLE L.
RUN No.50: HYDRATION
PELLET DIAMETER = 18.24 mm
MASS OF CaO= 3.0302 g
FRACTIONAL OF RECARBONISATION = 0.142
δ = 0.45 mm
FRACTION OF INERT MATERIAL = 15%
PARTIAL PRESSURE OF WATER VAPOUR = 2.8 kPa.

TIME(min)	TEMP(°C)	WEIGHT(g)	X
0	40	3.0302	0.000
50	40	3.0331	0.003
100	42	3.0360	0.006
150	42	3.0370	0.007
200	42	3.0390	0.009
300	42	3.0419	0.012
400	42	3.0458	0.016
500	43	3.0468	0.025
600	43	3.0526	0.035
700	43	3.0565	0.048
900	43	3.0623	0.056
1000	43	3.0653	0.061
1100	43	3.0701	0.069
1200	43	3.0721	0.078
1300	43	3.0731	0.090
1400	43	3.0750	0.100
1500	43	3.0840	0.110
1600	43	3.0818	0.119
1700	43	3.0847	0.126
1800	43	3.0877	0.131
1900	43	3.0916	0.136
2000	44	3.0945	0.145
2100	44	3.0974	0.150
2200	44	3.1013	0.151
2300	44	3.1042	0.152
2400	44	3.1062	0.153
2500	44	3.1101	0.154
2600	44	3.1140	0.156
2700	44	3.1169	0.157
2800	44	3.1208	0.159
2900	44	3.1227	0.161
3000	44	3.1257	0.162
3100	44	3.1305	0.164
3200	43	3.1325	0.165
3300	43	3.1403	0.166

TABLE LI.
RUN No.51: HYDRATION
PELLET DIAMETER = 18.98 mm
MASS OF CaO = 3.9195 g
FRACTIONAL OF INERT MATERIAL = 22%
PARTIAL PRESSURE OF WATER VAPOUR = 2.8 kPa.

TIME(min)	TEMP(°C)	WEIGHT(g)	X
0	50	3.9195	0.000
10	51	3.9233	0.003
20	53	3.9460	0.021
30	53	3.9636	0.035
40	54	3.9812	0.049
50	54	3.9951	0.060
60	54	4.0190	0.079
70	53	4.0417	0.097
80	53	4.0645	0.115
90	53	4.0858	0.132
100	53	4.1085	0.150
110	53	4.1211	0.160
120	53	4.1374	0.173
130	53	4.1151	0.187
140	53	4.1702	0.199
150	53	4.1903	0.215
160	54	4.1992	0.222
170	54	4.2231	0.241
180	54	4.2407	0.255
190	54	4.2609	0.271
200	54	4.2785	0.285
210	54	4.2962	0.299
220	54	4.3163	0.315
230	54	4.3441	0.337
240	54	4.3642	0.353
250	54	4.3856	0.370
260	54	4.3982	0.380
270	54	4.4159	0.394
280	53	4.4360	0.410
290	53	4.4587	0.428
300	53	4.4814	0.446
310	54	4.4952	0.457
320	53	4.5192	0.476
330	53	4.5305	0.485
340	54	4.5507	0.501
350	54	4.5620	0.510
360	53	4.5834	0.527
370	54	4.5985	0.539
380	54	4.6124	0.550

TABLE LII.
RUN No.52: HYDRATION
PELLET DIAMETER = 18.51 mm
MASS OF CaO = 3.3868 g
FRACTIONAL OF RECARBONISATION = 0.08
δ = 0.25 mm
FRACTION OF INERT MATERIAL = 22%
PARTIAL PRESSURE OF WATER VAPOUR = 2.8 kPa.

TIME(min)	TEMP(°C)	WEIGHT(g)	X
0	58	3.3868	0.000
100	57	3.3879	0.001
200	57	3.3901	0.003
300	56	3.3921	0.005
400	56	3.4404	0.020
500	57	3.4818	0.037
600	57	3.4862	0.050
700	56	3.5201	0.065
800	56	3.5271	0.081
900	56	3.5314	0.090
1000	56	3.5369	0.100
1100	56	3.5380	0.113
1200	56	3.5423	0.121
1300	56	3.5695	0.135
1400	56	3.7757	0.142
1500	56	3.7754	0.145
1600	56	3.7986	0.150
1700	56	3.8052	0.156
1800	57	3.8106	0.159
1900	56	3.8393	0.162
2000	56	3.8437	0.167
2100	56	3.8480	0.169
2200	56	3.8567	0.175
2300	56	3.8633	0.179
2400	56	3.8798	0.181
2500	56	3.8809	0.184
2600	56	3.8885	0.187
2700	56	3.8929	0.192

TABLE LIII.
RUN No.53:HYDRATION
PELLET DIAMETER = 18.51 mm
MASS OF CaO = 3.4129 g
FRACTIONAL OF RECARBONISATION = 0.063
δ = 0.20 mm
FRACTION OF INERT MATERIAL = 22%
PARTIAL PRESSURE OF WATER VAPOUR = 2.8 kPa.

TIME(min)	TEMP(°C)	WEIGHT (g)	X
0	47	3.4133	0.000
50	47	3.4206	0.007
100	47	3.4508	0.014
200	46	3.4750	0.017
300	47	3.5125	0.023
400	48	3.5742	0.038
500	47	3.6091	0.068
600	47	3.6413	0.073
700	47	3.6815	0.085
800	47	3.7083	0.100
900	47	3.7351	0.110
1000	47	3.7619	0.121
1100	48	3.7888	0.132
1200	48	3.8209	0.142
1300	49	3.8558	0.152
1400	48	3.8719	0.165
1500	47	3.8934	0.171
1600	47	3.9094	0.179
1700	47	3.9202	0.185
1800	47	3.9255	0.189
1900	46	3.9416	0.191
2000	47	3.9738	0.197
2100	48	3.9819	0.209
2200	47	3.9899	0.212
2300	47	3.5636	0.215

TABLE LIV: Comparison of measured Effective Diffusivity, $D_{A,eff}$, With Those Calculated From Pore Structure Considerations.

RUN No.	r_o [cm]	ϵ $Ca(OH)_2$	TEMP ^oC	p_{H_2O} kPa	$D_{A,k}$ cm^2/s	$D_{eff}(c)$* cm^2/s	$D_{eff}(g)$+ cm^2/s
1	0.90	0.65	50	2.8	0.377	0.095	0.081
2	0.88	0.63	50	2.8	0.372	0.092	0.077
3	0.91	0.62	50	2.4	0.368	0.089	0.077
4	0.90	0.60	45	2.8	0.361	0.084	0.071
5	0.91	0.62	50	3.6	0.368	0.088	0.072
6	0.90	0.62	55	3.2	0.371	0.091	0.074
7	0.94	0.61	50	2.4	0.366	0.089	0.073
8	0.88	0.54	55	2.3	0.343	0.079	0.054
9	0.88	0.62	28	2.1	0.355	0.080	0.066
10	0.88	0.60	24	2.1	0.349	0.075	0.063
11	0.90	0.63	35	2.8	0.364	0.083	0.073
12	0.92	0.62	32	3.6	0.358	0.081	0.067
13	0.92	0.62	45	1.5	0.365	0.088	0.072
14	0.92	0.63	20	1.2	0.355	0.077	0.067
15	0.86	0.56	20	1.2	0.328	0.068	0.052
16	0.92	0.63	100	2.8	0.400	0.117	0.093

* c=calculated; + g=graphically.

TABLE LV: Effective diffusivity for $CaCO_3$ layer.

EXP. No.	CALCINAT. TEMP.[°C]	δ[mm]	INOCULATION TIME [MIN]	POROSITY	D_e [$cm^2.S^{-1}$]
33	850	0.6	90	0.22	$6.7x10^{-7}$
34	850	0.5	90	0.22	$4.6x10^{-7}$
35	850	0.1	40	0.22	$4.2x10^{-8}$
36	850	0.8	190	0.22	$5.6x10^{-7}$
37	850	0.35	90	0.22	$2.3x10^{-7}$
38	850	0.1	40	0.22	$4.2x10^{-8}$
39	850	0.47	90	0.22	$4.1x10^{-7}$
40	1000	0.47	375	0.0	$9.8x10^{-8}$
41	1100	0.20	325	0.0	$2.1x10^{-8}$

APPENDICES

APPENDIX A. DETERMINATION OF COIL LENGTH

EXPERIMENTAL DATA:

Internal diameter of the pipe = 0.25 mm.

Maximum flow rate of air = 5 Nl/min.

PHYSICAL PROPERTY VALUES (Ref.66)

$\mu_{air} = 185 \times 10^{-6}$ g.cm^{-1}.s^{-1}

$\rho_{air} = 1.18 \times 10^{-3}$ g.cm^{-3}

$\lambda_{air} = 2.424 \times 10^{-4}$ J.cm^{-1}.s^{-1}.^{0}C^{-1}

$Pr_{air} = 0.74$

$Cp_{air} = 9.93 \times 10^{-2}$ J.g^{-1}.^{0}C^{-1}

CALCULATION OF THE HEAT TRANSFER COEFFICIENT, h.

The Nu for a fluid (gas) flowing across a pipe is:

$$Nu = 0.023 \times Re^{1/2} \times Pr^{2/3} \qquad (A.1)$$

but:

$$Re = \rho DU/\mu \qquad (A.2)$$

and the velocity of the fluid is:

U = Flow rate/Area

$U = (5 \text{ Nl/min})/\pi(0.125 \text{ cm})^2$

$= (83.33 \text{ cm}^3.\text{s}^{-1})/0.049 \text{ cm}^2 = 1700.68 \text{ cm.s}^{-1}$

so

$$Re = \frac{1.18\times10^{-3}\ g.cm^{-3} \times 0.312\ cm \times 1086.5\ cm.s^{-1}}{1.85\times10^{-4}\ g.cm^{-1}.s^{-1}}$$

$$Re = 2165.5$$

That is, laminar flow.

Substituting the values of Re and Pr into equation (A.1)

$$Nu = 0.023\times(2165.5)^{1/2}(0.74)^{2/3} = 0.875$$

but

$$Nu = hD/\lambda$$

therefore

$$h = Nu\lambda/D \qquad (A.3)$$

Upon substitution of Nu, λ, and D into Eq.(A.3) yields:

$$h = 0.875\times2.424\times10^{-4}\ J.cm^{-1}.s^{-1}.{}^{0}C^{-1}/0.25\ cm$$

$$h = 2.1\times10^{-4}\ J.s^{-1}.{}^{0}C^{-1}$$

CALCULATION OF THE HEAT FLOW RATE:

The heat flow rate is given by :

$$q = hA(\theta_1 - \theta_2) \qquad (A.4)$$

Average air temperature = (50 + 15)/2 = 32.5 ^{0}C

ΔT average = 50 - 32.5 = 17.5 ^{0}C

ΔT air = 50 -15 = 35 ^{0}C

The flow rate also can be expressed by:

$$q = Cp\rho(\theta_1 - \theta_2) \qquad (A.5)$$

Substituting values into Eq.(A.5) yields:

$$q = 9.93x10^{-2}\ J.g^{-1}.{}^{0}C^{-1}x1.18x10^{-3}\ g.cm^{-3}x35\ {}^{0}C$$

$$q = 0.041\ J.cm^{-3} = 41.011\ J.Nl^{-1}$$

but the maximum flow rate is 5 $Nl.min^{-1}$, thus:

$$q = 41.011\ J.Nl^{-1} \times 5\ Nl.min^{-1} = 205.055\ J.min^{-1}$$

or

$$q = 3.42\ J.s^{-1}$$

Then substituting into Eq.(A.5) yields:

$$3.42\ J.s^{-1} = h.A(\theta_1 - \theta_2)$$

so

$$A = \frac{3.42\ J.s^{-1}}{2.1x10^{-4}\ J.s^{-1}.\ ^{0}C^{-1}\ x17.5\ ^{0}C} = 926.4\ cm^{2}$$

but,

$$A = \pi.D.L$$

so

$$L = 926.4\ cm^{2}/3.1416x0.3125\ cm = 950\ cm$$

$$L \simeq 10\ m.$$

APPENDIX B: DETERMINATION OF BUOYANCY EFFECT

The calculation were carried out using data from run No.13.

Weight of CaO pellet = 3.6189 g.

Pellet diameter = 18.25 mm.

p_{H_2O} = 2.8 kPa.

Hydration temperature = 323 K

Recarbonisation temperature = 923 K

SOLUTION: Using equation reported by Zuliani[22].

$$\Delta W_b = W_s(\rho' - \rho)/\rho_s$$

The density of dry air at 323 and 923 K and 101.3 kPa is given by:

$$\rho = PM/RT$$

Thus

$$\rho_{323} = \frac{1 \text{ atm} \times 28.97 \text{ g.mol}^{-1}}{82.06 \text{ atm.cm}^3\text{.mol}^{-1}\text{.K}^{-1} \times 323 \text{ K}} = 1.093 \times 10^{-3} \text{ g.cm}^{-3}$$

$$\rho_{923} = \frac{1 \text{ atm} \times 28.97 \text{ g.mol}^{-1}}{82.06 \text{ atm.cm}^3\text{.mol}^{-1}\text{.K}^{-1} \times 923 \text{ K}} = 3.8249 \times 10^{-4}$$

and

$$\rho'_{\text{moist air}} = P\{M_{air}(1-X_{H_2O}) + M_{H_2O}.X_{H_2O}\}/RT$$

were,

$$X_{H_2O} = p_{H_2O}/P = 2.8 \text{ kPa}/101.3 \text{ kPa} = 0.0276$$

so

$$\rho'_{\text{moist air}} = \frac{1\text{atm}\{28.97\ \text{g.mol}^{-1}(1-0.0276)+18\text{x}0.0276\}}{82.06\ \text{atm.cm}^3\text{.mol-}^1\text{.K-}^1\text{x}323\ \text{K}}$$

$$= 1.0824\text{x}10^{-3}\ \text{g.cm}^{-3}$$

$$\rho'_{CO} = \frac{1\ \text{atm x}\ 44\ \text{g.mol}^{-1}}{82.06\ \text{atm.cm}^3\text{.mol-}^1\text{.K-}^1\text{x}923\ \text{K}}$$

$$= 5.8092\text{x}10^{-4}\ \text{g.cm}^{-3}$$

For hydration:

$$\Delta W_b = \frac{3.6189\ \text{g}(1.0824\text{x}10^{-3}\ \text{g.cm}^{-3}-1.093\text{x}10^{-3}\ \text{g.cm}^{-3})}{1.200\ \text{g.cm-}^3}$$

$$= -0.035\ \text{mg}$$

Switching from a more dense to a less dense gaseous species results in a negative value for ΔW_b.

For recarbonisation:

$$\Delta W_b = \frac{3.6189\ \text{g}(5.8092\text{x}10^{-4}\ \text{g.cm}^{-3}-3.8249\text{x}10^{-4}\ \text{g.cm}^{-3})}{1.200\ \text{g.cm-}^3}$$

$$= 0.598\ \text{mg}$$

APPENDIX C:

```
100 'PROGRAM TO MONITOR THE KINETICS OF CALCIUM CARBONATE
110 'THERMAL DECOMPOSITION, CALCIUM OXIDE HYDRATION AND
120 'RECARBONISATION.
130 '
140 CLS : PRINT "PRESS E TO STOP"
150 INPUT "TYPE RUN No.";NUM
155 INPUT "TYPE PELLET WEIGHT";Wo
160 INPUT "TYPE PELLET DIAMETER";D
165 INPUT "TYPE MOLECULAR WEIGHT OF SOLID REACTANT";MS
170 INPUT "TYPE MOLECULAR WEIGHT OF GASEOUS REACTANT";MG
180 INPUT "TYPE FLOW RATE";FR
190 INPUT "TYPE THERMOCOUPLE WEIGHT";C
200 INPUT "TYPE PARTIAL PRESSURE OF GASEOUS REACTANT";PP
210 INPUT "TYPE CALCINATION TEMPERATURE";T
220 INPUT "TYPE FRACTIONAL RECARBONISATION";R
230 INPUT "TYPE THICKNESS OF RECARBONATED LAYER";TRL
235 INPUT "TYPE REACTION";A$
240 LPRINT "   RUN No.";NUM
250 LPRINT "   PELLET WEIGHT =";Wo;" g"
260 LPRINT "   PELLET DIAMETER =";D;" mm"
270 LPRINT "   FLOW RATE =";FR;" Nl/Min"
280 LPRINT "   PARTIAL PRESSURE OF REACTANT=";PP;" kPa"
290 LPRINT "   CALCINATION TEMPERATURE =";T;" °C"
300 IF A$=CALCINATION OR A$=RECABONISATION GOTO 330
310 LPRINT "   FRACTIONAL RECARBONISATION =";R
320 LPRINT "   THICKNESS OF RECARBONATED LAYER =";TRL;" mm"
330 LPRINT
340 LPRINT "   ";A$
350 LPRINT "   ----------"
360 LPRINT "   TIME(Min)     TEMP( °)     WEIGHT(g)    X  "
370 LPRINT "   ----------"
380 '
390 TIME=-1
400 B$=INKEYS : IF B$="E" THEN END
410 X$=TIME$
420 LOCATE 10,20
440 PRINT X$
450 H$=MID$(X$,1,2) : M$=MID$(X$,4,2)
460 IF TIME=-1 THEN 480
470 IF H$=T$ AND M$=R$ THEN 410
480 T$=H$ : R$=M$
490 GOSUB 660
500 TEMP=502.01*V(1)+511.79     'TEMPERATURE AT TIME t
510 WEIGHT=9.1683*V(0)+2.7337-C 'WEIGHT AT TIME t
520 DELTAWt=Wo*MG/MS
540 DELTAW=WEIGHT-Wo
560 X=DELTAW/DELTAWt    'FRACTION REACTED AT TIME t
580 PRINT "TIME(Min)   TEMP( C)   WEIGHT(g)      X "
590 F$="                .      ."
600 PRINT USING F$;TIME;TEMP;WEIGHT;X
```

```
610 LPRINT USING F$;TIME;TEMP;WEIGHT;X
620 GOTO 410
630 END
640 '
650 '
660 '**** KINETICS A/D ROUTINE ****
665 '
670 TIME=TIME+1
680 V(0)=0 : V(1)=0
690 BE%=&H220
700 FOR CH%=0 TO 1          'Channel number
710 FOR I%=0 TO 99          'Readings
720 OUT BE%+10,CH%
730 OUT BE%+11,1            'Direct trigger mode A/D
740 HI=INP(BE%+5)           'High byte of lab-card
750 IF HI>=16 THEN 740
760 LO=INP(BE%+4)           'Low byte of lab-card
770 HIA=HIA+HI : LOA=LOA+LO :HI=0 :LO=0
780 NEXT I%
790 AHI=HIA/100 : ALO=LOA/100 :HIA=0 : LOA=0
800 V(CH%)=(AHI*256+ALO-2048)*2/4096
810 NEXT CH%
820 RETURN
```

APPENDIX D. EVALUATION OF THE PHYSICAL PROPERTY VALUES AND OTHERS CONSTANTS.

D.1. DIFFUSION COEFFICIENTS.

Using the equation developed by Fuller et all [123] it is possible obtain the binary diffusion coefficient. Their equation is:

$$D_{AB} = \frac{10^{-3} T^{1.75}}{P\{(v_A)1/3+(v_B)1/3\}2}\sqrt{1/M_A + 1/M_B};\ [cm^2.s^{-1}] \quad (D.1)$$

where T is the temperature in Kelvin, P the total pressure in atm, M_A and M_B the molecular weight of species A and B in g/g-mole, and v_A, v_B the diffusion volumes.

By substitution of values for water vapour and air, and taking into account that the total pressure in the reaction system was 1 atm, the following relationship is obtained which is only a function of experimental temperature.

$$D_{AB} = 1.1759x10^{-5} T^{1.75} \quad (D.2)$$

Thus the binary effective diffusion coefficient is:

$$D_{AB,eff} = 5.8595x10^{-6} \epsilon T^{1.75} \quad (D.3)$$

which is only a function of temperature and product layer

porosity, the $Ca(OH)_2$ porosity was derived using equation (3.1) and the tortuousity factor was taken equal 2. The binary effective diffusivity was calculated for each experimental conditions and reported in Table LIV.

The Knudsen coefficient can be calculated using Eq.(2.43)

$$D_{A,k} = A_o\sqrt{T/M}$$

The parameter A_o depends upon the properties of the solid and it is inversely proportional to the internal surface area of the pellet, that is, $A_o \alpha 1/S$. Then the relationship between the A_o parameter for lime and hydrated lime can be given by:

$$[A_o]_{Ca(OH)} /[A_o]_{CaO} = S_{CaO}/S_{Ca(OH)} \qquad (D.4)$$

Since the sample swells during the reaction the right hand side of Eq.(D.4) is rewritten as:

$$S_{CaO}/S_{Ca(OH)} = \{1/(1+\Phi)\}^{1/3}$$

where $\Phi = (r_o'-r_o)/r_o$ is the swelling ratio and r_o' is the pellet radius due to swelling (the average swelling was (0.23). Thus:

$$[A_o]_{Ca(OH)} = \{1/(1+\Phi)\}^{1/3} = 0.93x[A_o]_{CaO}$$

Substitution of $[A_o]_{Ca(OH)}$ value into Eq.(2.43) yields:

$$D_{A,k} = 0.93[A_o]_{CaO}\sqrt{T/M_A} \qquad (D.5)$$

The values of $[A_o]_{CaO}$ were taken from Staia and Hills[97], and reported below:

POROSITY	A_o
0.40	0.051
0.46	0.066
0.49	0.073
0.55	0.081
0.60	0.086
0.65	0.089

The values of $D_{A,k}$ were calculated in this way for each hydration experiment and reported in Table LIV.

D.2. MASS TRANSFER COEFFICIENT.

The gaseous flow can be assumed pure air, since the water concentration was very low. The viscosity can be then calculated using the equation developed by Chapman and Enskog, cited by Geiger and Poirier [124]. Their equation is:

$$\mu = 2.67\times10^{-5}\sqrt{M_B T}/\sigma^2\Omega_\mu \qquad (D.6)$$

Here σ is a characteristic diameter of the molecule in A, and Ω_μ is the collision integral of the Chapman-Enskog theory. Taking values for σ and Ω_μ from the literature [123] the following relationship is obtained:

$$\mu = 1.8672 \times 10^{-5} T^{1/2}, \quad [g.cm^{-1}.s^{-1}] \qquad (D.7)$$

The gaseous flow density can be determined using the following relationship:

$$\rho_B = PM_B/RT = 0.353/T, \quad [g.cm^{-3}] \qquad (D.8)$$

Here

$P = 1$ atm, $M_B = 28.97$ g/g-mole,

$R = 82.06$ cm^3.atm/g-mol.K,

and T is in Kelvin.

The velocity, U, of the gas stream is given by:

$$U = \text{Flow rate/Transversal surface area} \qquad (D.9)$$

substituting the experimental data into the Eq.(D.9) the value of U is obtained as 0.33 cm/s.

Upon substitution of Eqs.(D.7), (D.8) and the value for U into Eq.(2.53), the mass transfer coefficient can be obtained as a function of the binary diffusion

coefficient, experimental temperature and pellet radius,

$$\alpha = \frac{D_{AB}}{r_o} + \frac{2.52 D_{AB}^{2/3}}{T^{\frac{1}{4}} r_o^{\frac{1}{2}}} \qquad (D.10)$$

Since the sample swells r_o is substituted by $r_o(1+\Phi f)$ into the Eq.(D.10) and the Equation (D.11) is obtained:

$$\alpha = \frac{D_{AB}}{r_o(1+\Phi f)} + \frac{2.52 D_{AB}^{2/3}}{T^{\frac{1}{4}} [r_o(1+\Phi f)]^{\frac{1}{2}}} \qquad (D.11)$$

This equation shows that the mass transfer coefficient decreases as the reaction proceeds.

D.3. EQUILIBRIUM CONSTANT

The equilibrium constant of reaction (5.1)

$$CaO + H_2O = Ca(HO)_2 \quad \text{is:}$$

$$K = 1/p_{A,e} \tag{D.12}$$

but

$$\Delta G_T = -RT\ln K \tag{D.13}$$

The change of free energy was determined as a function of experimental temperature using thermochemical data tabulated by Kubaschewski and Alcock [125].

$$\Delta G_T = -25102.4 + 4.15T + 3.8\times10^{-3}T^2 + 1.5\times10^{5}T^{-1} - 6.14T\ln T$$

Then

$$K = \mathrm{Exp}(12633.3T^{-1} - 1.9\times10^{-3}T + 3.1\ln T - 2.1)$$

at T = 323 K; $K = 3.85\times10^{23}$

therefore

$$p_{A,e} = 2.6\times10^{-24} \text{ atm.}$$

Since $p_{A,e}$ is very small at low temperatures, it can be neglected and the overall rate equation may be simplified to a function of partial pressure of the water vapour in the bulk gas.